Spring 2012

Guanidinato and amidinato complexes of iridium(I): synthesis O_2 and S_8 reactivity, and (alkene)peroxo- and (alkene)persulfidoiridium(III) intermediates

Matthew Ryan Kelley
University of Iowa

GUANIDINATO AND AMIDINATO COMPLEXES OF IRIDIUM(I): SYNTHESIS, O_2 AND S_8 REACTIVITY, AND (ALKENE)PEROXO- AND (ALKENE)PERSULFIDOIRIDIUM(III) INTERMEDIATES

by

Matthew Ryan Kelley

An Abstract

Of a thesis submitted in partial fulfillment
of the requirements for the Doctor of
Philosophy degree in Chemistry
in the Graduate College of
The University of Iowa

May 2012

Thesis Supervisor: Assistant Professor Jan-Uwe Rohde

ABSTRACT

A variety of mononuclear alkene complexes, [Ir{ArNC(NR$_2$)NAr}(cod)], and dicarbonyl complexes, [Ir{ArNC(NR$_2$)NAr}(CO)$_2$] (where R = Me or Et; Ar = Ph, 4-MeC$_6$H$_4$, 4-MeOC$_6$H$_4$, 2,6-Me$_2$C$_6$H$_3$ or 2,6-^{i}Pr$_2$C$_6$H$_3$; and cod = 1,5-cyclooctadiene), were synthesized from the neutral *N*,*N*-dialkyl-*N*′,*N*″-diarylguanidines via deprotonation and transmetalation. These complexes were fully characterized by spectroscopic techniques and single-crystal X-ray diffraction. The single-crystal structure determinations show the guanidinato(1−) ligands coordinate the low valent d^8 iridium(I) center in an N,N′-chelating binding mode, and the C–N bond lengths indicate a high degree of π-electron delocalization over the CN$_3$ core. The ^{13}C NMR chemical shifts of the alkene carbon atoms in the Ir^{I}(cod) complexes and the average CO stretching frequencies for the Ir^{I}(CO)$_2$ complexes suggest that the guanidinato ligands function as stronger donors than related monoanionic, bidentate nitrogen-donor ligands.

Intermediates in the reactions of the [Ir{ArNC(NR$_2$)NAr}(cod)] complexes with O$_2$ were identified and characterized as (alkene)peroxoiridium(III) species, [Ir{ArNC(NR$_2$)NAr}(η^4-cod)(η^2-O$_2$)], using multi-dimensional NMR and IR spectroscopy. The (alkene)persulfidoiridium(III) intermediate [Ir{PhNC(NMe$_2$)NPh}(η^4-cod)(η^2-S$_2$)] was identified and characterized in the reaction of [Ir{PhNC(NMe$_2$)NPh}(cod)] with S$_8$. It was determined that these intermediates are able to transfer oxygen or sulfur to simple organic molecules such as PPh$_3$. The self-decay of the (alkene)peroxoiridium(III) intermediates leads to C–O bond formation and alkene oxidation, and upon addition of excess cod release of 4-cycloocten-1-one was observed.

In addition, a mononuclear alkene complex, [Ir{PhNC(Me)NPh}(cod)], and a dinuclear tetracarbonyl complex, [{Ir(CO)$_2$}$_2${μ-PhNC(Me)NPh-κN:$\kappa N'$}$_2$], with an amidinato ligand, were synthesized and characterized. In the reaction of the Ir^{I}(cod) complex with O$_2$, the corresponding (alkene)peroxoiridium(III) intermediate

[Ir{PhNC(Me)NPh}(η^4-cod)(η^2-O_2)] was observed. The reactivity of this intermediate and its decay products is similar to that of [Ir{ArNC(NR_2)NAr}(η^4-cod)(η^2-O_2)], with the formation of 4-cycloocten-1-one being observed upon addition of cod.

Mononuclear (alkene)rhodium(I) complexes, [Rh{PhNC(NMe_2)NPh}(cod)] and [Rh{PhNC(Me)NPh}(cod)], and a dinuclear complex, [{Rh(nbd)}$_2${μ-PhNC(NMe_2)NPh-κN:$\kappa N'$}$_2$], were synthesized and characterized (where nbd = norbornadiene or bicyclo[2.2.1]hepta-2,5-diene). Investigation of the reactivity of these complexes with O_2 show they react very slowly or not at all.

Abstract Approved: _____
Thesis Supervisor

_____
Title and Department

_____
Date

GUANIDINATO AND AMIDINATO COMPLEXES OF IRIDIUM(I): SYNTHESIS, O_2 AND S_8 REACTIVITY, AND (ALKENE)PEROXO- AND (ALKENE)PERSULFIDOIRIDIUM(III) INTERMEDIATES

by

Matthew Ryan Kelley

A thesis submitted in partial fulfillment
of the requirements for the Doctor of
Philosophy degree in Chemistry
in the Graduate College of
The University of Iowa

May 2012

Thesis Supervisor: Assistant Professor Jan-Uwe Rohde

Graduate College
The University of Iowa
Iowa City, Iowa

CERTIFICATE OF APPROVAL

_____

PH.D. THESIS

_____

This is to certify that the Ph.D. thesis of

Matthew Ryan Kelley

has been approved by the Examining Committee
for the thesis requirement for the Doctor of Philosophy
degree in Chemistry at the May 2012 graduation.

Thesis Committee: _____
Jan-Uwe Rohde, Thesis Supervisor

_____
Edward G. Gillan

_____
Julie L. P. Jessop

_____
Sarah C. Larsen

_____
F. Christopher Pigge

ACKNOWLEDGMENTS

I would first like to thank my advisor, Jan-Uwe Rohde. He has been a great help through the years and I owe him a lot of credit for the knowledge that I have obtained during my graduate career.

My wife, Kara, has been one of my biggest supporters over the years, especially during our time here in Iowa. She has always understood the long hours and hard work that were required to achieve my goals. I cannot thank her enough for everything that she has sacrificed to allow me to pursue my doctoral degree.

Next, I would like to thank my family, especially my parents, for always standing behind me in whatever endeavors I was undertaking. They have always given me encouragement to pursue whatever I wanted to do, including moving to Iowa for graduate school. They have always had the utmost confidence in me and my abilities, sometimes more than I have had in myself. I would not have gotten to this point if it was not for their love and support.

The current and past members of the Rohde group have been great help during my graduate studies. Wei-Tsung, Travis and Tony have been great co-workers and friends through this process and have always been there to discuss anything with.

I would like to thank a number of people in the chemistry department that have helped me through this entire journey. Dale Swenson for his collection of x-ray data and help with questions I had while solving crystal structures and Santhana and Robert for their help with the NMR instrumentation and their willingness to go behind just training me to use the instruments. I would like to especially thank Lynn Teesch and Vic Parcell for all their help with mass spectrometry and also for allowing me to work along with them in the mass spectrometry facility for two semesters. I gained a great deal of knowledge from both of them that will be very helpful in the future.

It has been a great experience working with all the different faculty members and Brian, Shonda and Earlene teaching undergraduate laboratories through the years. I have enjoyed working with all of you and have gained an immeasurable amount of knowledge that will help me in the future.

Lastly, I would like to thank Sharon, Janet, Jessica and Betty for all the help with the paperwork and administrative details that you have taken care of over the years. It has been great to have people willing to help with whatever situation I may have had and people that know the answer to nearly every question that I had.

ABSTRACT

A variety of mononuclear alkene complexes, [Ir{ArNC(NR$_2$)NAr}(cod)], and dicarbonyl complexes, [Ir{ArNC(NR$_2$)NAr}(CO)$_2$] (where R = Me or Et; Ar = Ph, 4-MeC$_6$H$_4$, 4-MeOC$_6$H$_4$, 2,6-Me$_2$C$_6$H$_3$ or 2,6-^{i}Pr$_2$C$_6$H$_3$; and cod = 1,5-cyclooctadiene), were synthesized from the neutral *N*,*N*-dialkyl-*N*′,*N*″-diarylguanidines via deprotonation and transmetalation. These complexes were fully characterized by spectroscopic techniques and single-crystal X-ray diffraction. The single-crystal structure determinations show the guanidinato(1−) ligands coordinate the low valent d^8 iridium(I) center in an N,N′-chelating binding mode, and the C–N bond lengths indicate a high degree of π-electron delocalization over the CN$_3$ core. The ^{13}C NMR chemical shifts of the alkene carbon atoms in the Ir^{I}(cod) complexes and the average CO stretching frequencies for the Ir^{I}(CO)$_2$ complexes suggest that the guanidinato ligands function as stronger donors than related monoanionic, bidentate nitrogen-donor ligands.

Intermediates in the reactions of the [Ir{ArNC(NR$_2$)NAr}(cod)] complexes with O$_2$ were identified and characterized as (alkene)peroxoiridium(III) species, [Ir{ArNC(NR$_2$)NAr}(η^4-cod)(η^2-O$_2$)], using multi-dimensional NMR and IR spectroscopy. The (alkene)persulfidoiridium(III) intermediate [Ir{PhNC(NMe$_2$)NPh}(η^4-cod)(η^2-S$_2$)] was identified and characterized in the reaction of [Ir{PhNC(NMe$_2$)NPh}(cod)] with S$_8$. It was determined that these intermediates are able to transfer oxygen or sulfur to simple organic molecules such as PPh$_3$. The self-decay of the (alkene)peroxoiridium(III) intermediates leads to C–O bond formation and alkene oxidation, and upon addition of excess cod release of 4-cycloocten-1-one was observed.

In addition, a mononuclear alkene complex, [Ir{PhNC(Me)NPh}(cod)], and a dinuclear tetracarbonyl complex, [{Ir(CO)$_2$}$_2${μ-PhNC(Me)NPh-κN:$\kappa N'$}$_2$], with an amidinato ligand, were synthesized and characterized. In the reaction of the Ir^{I}(cod) complex with O$_2$, the corresponding (alkene)peroxoiridium(III) intermediate [Ir{PhNC(Me)NPh}(η^4-cod)(η^2-O$_2$)] was observed. The reactivity of this intermediate

and its decay products is similar to that of [Ir{ArNC(NR_2)NAr}(η^4-cod)(η^2-O_2)], with the formation of 4-cycloocten-1-one being observed upon addition of cod.

Mononuclear (alkene)rhodium(I) complexes, [Rh{PhNC(NMe_2)NPh}(cod)] and [Rh{PhNC(Me)NPh}(cod)], and a dinuclear complex, [{Rh(nbd)}$_2${μ-PhNC(NMe_2)NPh-κN:$\kappa N'$}$_2$], were synthesized and characterized (where nbd = norbornadiene or bicyclo[2.2.1]hepta-2,5-diene). Investigation of the reactivity of these complexes with O_2 show they react very slowly or not at all.

TABLE OF CONTENTS

LIST OF TABLES

LIST OF FIGURES

LIST OF SCHEMES

CHAPTER 1

INTRODUCTION

This thesis covers the synthesis, characterization and reactivity of iridium and rhodium complexes supported by guanidinato and amidinato ligands. It has been found that the guanidinato ligands function as stronger donors than other monoanionic nitrogen-donor ligands in the literature. Results show that the iridium(I) complexes readily react with O_2 and S_8 to form metastable complexes. These intermediates and their decay products are reactive and have been able to form functionalized organic species.

Examples of catalytic and stoichiometric oxidation of alkene complexes with O_2 will be discussed in Chapter 2. The catalytic systems that are well-known industrially employ simple metal complexes but have a limited range of substrates. The ability to selectively functionalize other alkenes, such as cyclic alkenes (*i.e. cis*-cyclooctene or 1,5-cyclooctadiene), using reactive metal alkene complexes and O_2 has only been observed in selected cases in the literature. Stoichiometric oxidation of alkene complexes gives valuable insight into the mechanisms for these transformations and the examples using iridium and rhodium complexes discussed in Chapter 2 show how the catalytic systems might operate. The synthesis of these reactive metal alkene complexes is an interesting area of research and the selection of the appropriate supporting ligand is crucial. A variety of monoanionic nitrogen-donor ligands will be discussed with guanidinato ligands showing the ability to function as supporting ligands for these reactive metal complexes. Guanidinato ligands are conceptually related to ligands previously observed in this type of chemistry, but have not been used thus far.

The synthesis and characterization of $Ir^{I}(cod)$ and $Ir^{I}(CO)_2$ complexes supported by guanidinato ligands is covered in Chapter 3 (where cod = 1,5-cyclooctadiene). Investigation of the ligand donor strength of the guanidinato ligands and comparison to structurally similar examples in the literature will be discussed. The ^{13}C NMR (cod

complexes) and IR (dicarbonyl complexes) data indicate that the guanidinato ligands function as stronger donors than similar monoanionic, bidentate nitrogen-donor ligands in the literature. Finally, the reactivity of one Ir^{I}(cod) complex toward MeI and MeOTf and the formation and characterization of octahedral iridium(III) complexes will be discussed (where $TfO^{-} = CF_3SO_3^{-}$ = trifluoromethanesulfonate anion).

The reactivity of the guanidinato Ir^{I}(cod) complexes toward O_2 and S_8 will be discussed in Chapters 4 and 5 respectively. Identification and characterization of (alkene)peroxo- and (alkene)persulfidoiridium(III) intermediates by multi-dimensional NMR and IR spectroscopy has been achieved. These complexes have shown the ability to transfer an oxygen atom or sulfur atom to simple organic substrates such as PPh_3. It was shown that the (alkene)peroxoiridium(III) intermediate can undergo C−O bond formation and alkene oxidation upon self-decay. Addition of cod to the decay products causes release of 4-cycloocten-1-one.

The synthesis and characterization of a mononuclear Ir^{I}(cod) complex and a dinuclear tetracarbonyl complex supported by an amidinato ligand will be discussed in Chapter 6. These complexes were synthesized in an analogous manner as the mononuclear guanidinato cod and dicarbonyl complexes. The reactivity of the amidinato Ir^{I}(cod) complex toward O_2 is similar to that of the corresponding guanidinato complex with the formation of an (alkene)peroxoiridium(III) intermediate also being observed. This intermediate and its decay products react in a similar manner as the guanidinato species.

In Chapter 7, the synthesis and characterization of two mononuclear Rh^{I}(cod) complexes supported by guanidinato or amidinato ligands will be discussed. Also, a dinuclear nbd complex supported by a guanidinato ligand has been synthesized and will be discussed (where nbd = norbornadiene or bicyclo[2.2.1]hepta-2,5-diene). Analysis of these complexes by NMR spectroscopy and single-crystal X-ray crystallography shows that the size of the alkene ligand has a major effect on the nuclearity of the complex. The

reactivity of these rhodium(I) complexes toward O_2 will be discussed. Differences in reactivity of these complexes compared to the Ir^{I}(cod) complexes will also be covered.

CHAPTER 2

BACKGROUND

2.1 Introduction

The activation of small inert molecules and incorporation of these molecules into organic substrates is an attractive strategy for the formation of value-added organic molecules. Small inert molecules such as O_2 and S_8 are cheap, abundant and environmentally benign. The use of reactive transition metal complexes is of central importance in these transformations for the activation of O_2 or S_8. Synthesis of the appropriate reactive transition metal complex is the first step to achieve these transformations and that is what we have focused on in our approach to achieve functionalization of organic substrates.

Synthesis of the appropriate reactive metal complex involves the use of nitrogen-donor ligands that can stabilize metal centers in the +1 and +3 oxidation states and are resistant to oxidation. Guanidinato ligands are well-known for their ability to coordinate complexes of early transition metals and lanthanides in high oxidation states.[1-7] We have synthesized and characterized a variety of low-valent metal complexes (iridium(I) and rhodium(I)) and have investigated the reactivity of these complexes toward O_2 and S_8.

This chapter begins with an overview of catalytic and stoichiometric pathways for alkene oxidation with O_2 and some examples of what has been observed so far in the literature for these types of transformations. Valuable insights into how the catalytic systems might operate were obtained from studies of stoichiometric reactions using alkene complexes of iridium and rhodium. The general pathways and examples of stoichiometric oxidation of alkene complexes of iridium and rhodium with O_2 will be discussed. Finally, commonly used monoanionic nitrogen-donor ligands are discussed

and explanation of the important properties of guanidinato ligands and why they serve as good supporting ligands is discussed.

2.2 Oxidation of Alkenes with Dioxygen

2.2.1 Catalytic Oxidation of Alkenes

Catalytic oxidation of alkenes is an effective strategy for the production of value-added compounds from hydrocarbon feedstocks and for the functionalization of more complex organic molecules. The use of dioxygen (O_2) as an oxidant for these transformations is very attractive because it is readily available, cheap and environmentally friendly. There are some challenges that must be overcome when using O_2 as a reactant with the most significant challenge being that O_2 is kinetically inert.[8] The activation barrier of $^3O_2$ in reactions with diamagnetic organic substrates is high and this often causes a slow initial reaction step that is followed by many fast, uncontrollable steps, which may lead to low selectivity.[9,10,11] Therefore, reactions with O_2 usually are difficult to control and can lead to many products. Because of this, transition metal complexes must be used to activate O_2 and control the reactivity of O_2.

Two main catalytic systems used industrially for the oxidation of alkenes with O_2 are palladium complexes and silver.[10-19] The Wacker oxidation process uses palladium and copper catalysts for homogeneous alkene oxidation. The overall reaction in the Wacker process is the oxidation of terminal alkenes to methyl ketones using O_2 with $PdCl_2$ and $CuCl_2$ catalysts, as shown in Scheme 1. In this system, O_2 is actually used for reformation of the copper catalyst, and the oxygen atom that is incorporated into the substrate comes from water.[12-15]

Scheme 1. Formation of Methyl Ketones by the Wacker Oxidation Process

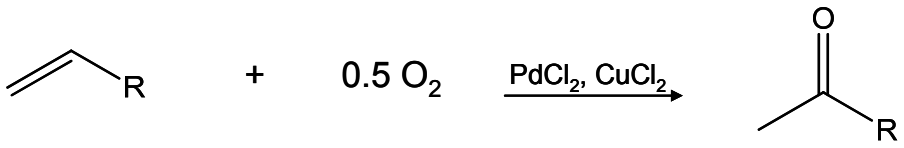

Wacker Oxidation Reactions

$$C_2H_4 + PdCl_2 + H_2O \rightarrow CH_3CHO + Pd(0) + 2\ HCl$$

$$Pd(0) + 2\ CuCl_2 \rightarrow PdCl_2 + 2\ CuCl$$

$$2\ CuCl + 2\ HCl + ½\ O_2 \rightarrow 2\ CuCl_2 + H_2O$$

Ag has seen extensive use industrially for heterogeneous alkene oxidation.[16-19] Alumina-supported Ag has shown the ability to catalyze the epoxidation of alkenes to epoxides, with one example shown in Scheme 2. In this example, ethene is oxidized to ethene oxide which is used widely as a starting material in industrial processes.[18] Both of these types of catalytic systems ($PdCl_2/CuCl_2$ and Ag) work very well, but only for a limited range of substrates.

Scheme 2. Formation of Ethylene Oxide Catalyzed by Supported Ag

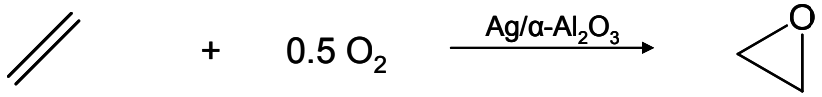

Catalytic oxidation of alkenes using simple iridium and rhodium catalysts has also been described in the literature.[20-24] A number of examples were reported for oxidation of terminal alkenes to methyl ketones, with one example shown in Scheme 3, using $RhCl_3$ and a Cu^{II} co-catalyst for the formation of 2-hexanone from 1-hexene.[22] Commonly, this method is applicable to terminal alkenes, but a few examples of oxidation of a cyclic alkene have been reported as well, with one example shown in Scheme 4.[20,21,23] Here,

[{Ir(coe)$_2$}$_2$(μ-Cl)$_2$] is used as the catalyst for oxidation of coe to 4-cycloocten-1-one (coe = *cis*-cyclooctene).[20,21] Mechanisms for these reactions have been proposed, but are not always well known and to better understand how these catalytic systems work, stoichiometric reactions of well-defined alkene complexes of iridium and rhodium have been investigated.

Scheme 3. Catalytic Oxidation of Terminal Alkenes using $RhCl_3$

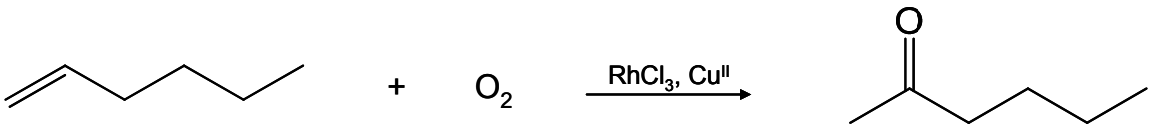

Scheme 4. Catalytic Oxidation of a Cyclic Alkene using [{Ir(coe)$_2$}$_2$(μ-Cl)$_2$]

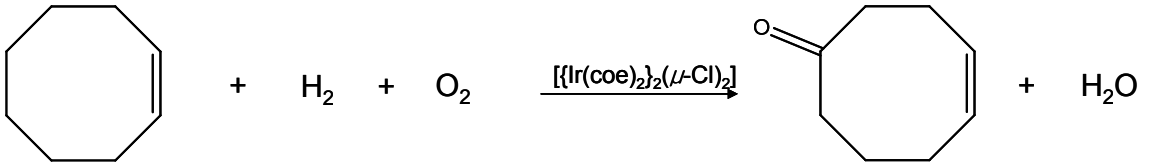

2.2.2 Stoichiometric Oxidation of Alkene Complexes of Iridium and Rhodium

In general, there are few examples in the literature of stoichiometric oxidation of alkene complexes of iridium(I) or rhodium(I) using O_2.[9,11] The examples that are known for these complexes can be categorized into four major pathways, as shown in Scheme 5. These pathways include (*i*) formation of a peroxo complex under loss of alkene, (*ii*) oxidation of the coordinated alkene by a radical-based autoxidation mechanism, (*iii*) formation of a metallaoxetane, and (*iv*) formation of a metalladioxolane. All of these

pathways begin with a metal alkene complex reacting with O_2 to form an oxidized species. Scheme 5 shows alkene complexes with ethene and cod as the coordinated alkenes, but the use of other alkene ligands such as propene has also been observed in these reactions.

Scheme 5. Pathways for the O_2 Oxidation of Alkene Complexes

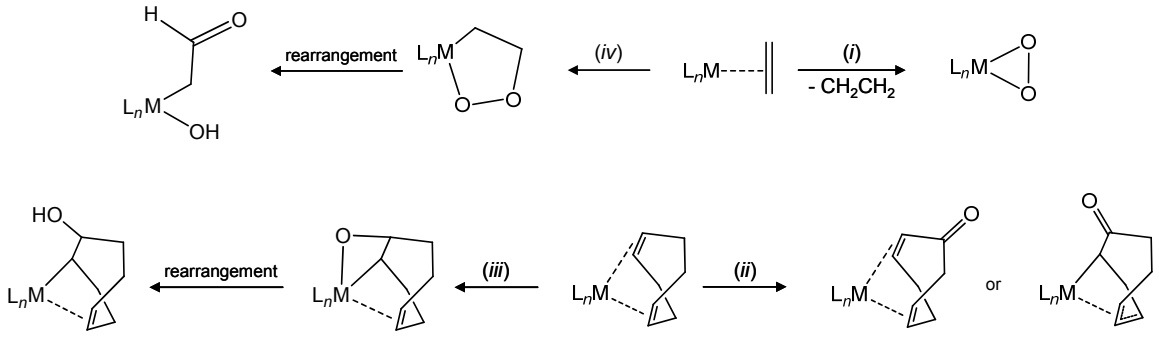

L_n = supporting ligand; M = Ir, Rh; *i* – *iv*, see text.

Formation of peroxo complexes under concomitant alkene dissociation may occur when a mono-alkene is not tightly bound to the metal center (*i*, Scheme 5).[9,25] One example of this type of reaction is an (ethene)rhodium(I) complex, $[Rh(Me_3\text{-}tpa)(CH_2CH_2)]^+$ (where Me_3-tpa = tris((6-methyl-2-pyridyl)methyl)amine), that reacted with O_2 at 20 °C to form the (η^2-peroxo)rhodium(III) complex, $[Rh(Me_3\text{-}tpa)(\eta^2\text{-}O_2)]^+$, and free ethene.[25] In general, this pathway is unproductive for alkene oxidation because the alkene dissociates from the metal center prior to C–O bond formation.

Autoxidation (*ii*, Scheme 5) is another pathway that has been described in the literature. For this transformation, oxidation of the alkene occurs by a radical chain mechanism possibly without involvement of the metal center. One example of this oxidation is the reaction of [Ir(Cp′)(cod)] (where Cp′ = 1,3-$C_5H_3(SiMe_3)_2$) with O_2 at 75

°C in the presence of 1,1,2,2-tetrachloroethane (TCE).[29] The TCE acts as a radical initiator and formation of a mixture of oxo-η^4-cyclooctadiene and oxo-η^3-cyclooctenediyl species was observed.

Scheme 6. Metallaoxetane Formation and Rearrangement

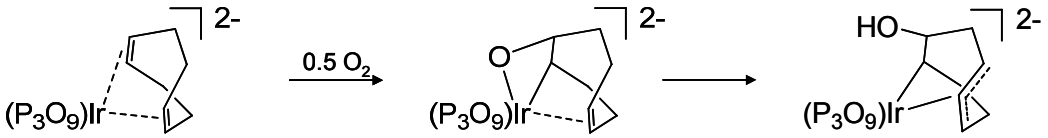

The third pathway *(iii*, Scheme 5) is the formation of metallaoxetane complexes upon reaction with O_2. These metallaoxetane species (Scheme 6) have the potential for release of the oxidized organic species from the metal center, but usually rearrangement of the metallaoxetane is observed which precludes the release of the organic fragment.[9] There are two examples that form metallaoxetane species in solution by an atom-economic (both atoms of O_2 are incorporated) reaction with O_2.[26,27] The first example, as shown in Scheme 6, is an anionic iridium(I) complex supported by a trimetaphosphate ligand, $[Ir(P_3O_9)(cod)]^{2-}$, that reacts with 0.5 equiv of O_2 to form the metallaoxetane species, $[Ir(P_3O_9)(C_8H_{12}O)]^{2-}$.[26] The metallaoxetane species is unstable in solution and rearranges to a hydroxycyclooctenediyl complex, $[Ir(P_3O_9)(C_8H_{11}OH)]^{2-}$. The second example, a (triazenide)rhodium(I) complex [Rh(1,3-PhN$_3$Ph)(cod)], reacts with O_2 to form the bis(rhodaoxetane) complex $[\{Rh(1,3\text{-}PhN_3Ph)(C_8H_{12}O)\}_2]$.[27] Similar to $[Ir(P_3O_9)(C_8H_{12}O)]^{2-}$, rearrangement and formation of the hydroxycyclooctenediyl complex was observed. However, the bis(rhodaoxetane) is somewhat more interesting than the iridaoxetane, because upon addition of excess PMe_3 or CO prior to rearrangement the oxidized organic fragment, 4-cycloocten-1-one, was released.[27,28]

Unfortunately, because the release of 4-cycloocten-1-one only occurs with the addition of PMe_3 or CO, reformation of the starting material [Rh(1,3-PhN_3Ph)(cod)] does not occur.

Scheme 7. Metalladioxolane Formation and Rearrangement

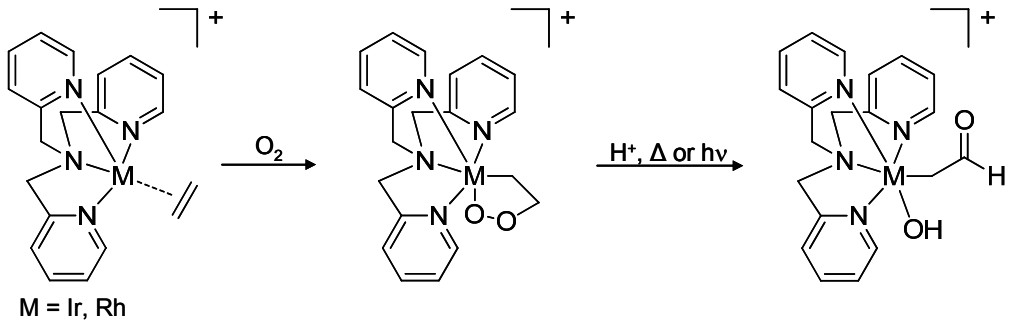

The final pathway (*iv*, Scheme 5) is related to the formation of metallaoxetanes, but in this pathway both oxygen atoms are incorporated into the same metal complex to form a metalladioxolane. Examples of this pathway for analogous iridium(I) and rhodium(I) complexes, [M(tpa)(cod)] (where M = Ir or Rh; tpa = tris((2-pyridyl)methyl)amine), are shown in Scheme 7.[30,31] Similar to the metallaoxetanes, rearrangement of the metalladioxolanes was observed and release of the oxidized organic substrate did not occur. In general, only few examples exist for the formation of metallaoxetanes and metalladioxolanes from the reaction of metal alkene complexes with O_2. It is also important to note that these species are the first complexes observed in these reactions. Activation of O_2 and C–O bond formation has already occurred, and the formation of any intermediates before the metallaoxetanes or metalladioxolanes has not been observed.[9,10,32] Complexes that are commonly invoked as intermediates in these reactions are (alkene)peroxo complexes where a peroxide ligand and an alkene ligand are bound to the metal center at the same time.

Even though (alkene)peroxoiridium and (alkene)peroxorhodium complexes have not been observed in the formation of metallaoxetanes and metalladioxolanes, there are a

few examples that have been prepared previously. Shown in Scheme 8 are the examples of characterized (alkene)peroxo complexes reported in the literature for iridium and rhodium.[25,33-38] The first example, a rhodium(I) hydride species, is an interesting complex because it has an internal alkene that is part of the phosphine supporting ligand. Two of the (alkene)peroxo complexes are supported by nitrogen-donor ligands, with one of them bearing cod and the other one ethene as the alkene ligand. The last example is a simple bis(triphenylphosphine) iridium(I) complex with an ethene ligand bound to the metal center. These examples show that the metal center can be coordinated to an alkene and a peroxide ligand at the same time, but in most of these cases alkene oxidation has not been observed.

Scheme 8. (Alkene)peroxoiridium(III) and (Alkene)peroxorhodium(III) Complexes

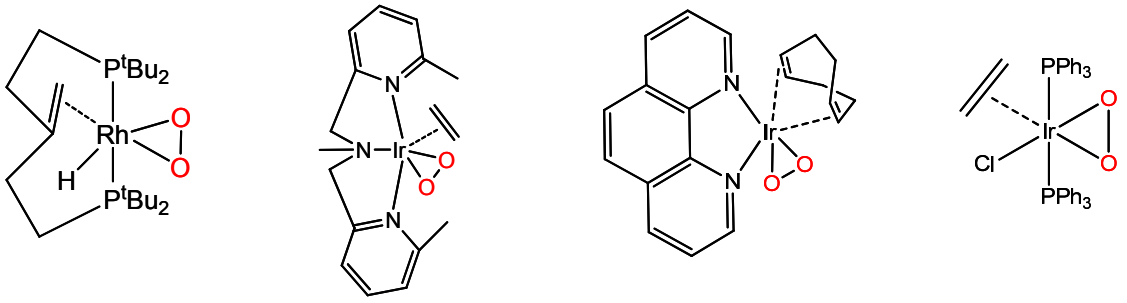

Of these four (alkene)peroxo complexes, only one has been reported to oxidize the coordinated alkene.[38] The bis(triphenylphosphine) iridium(I) complex has been able to oxidize the ethene ligand to acetaldehyde but co-oxidation of the PPh_3 ligand to $OPPh_3$ occurred, as shown in Scheme 9. Consequently, the iridium complex disintegrates due to the oxidation of the PPh_3 ligand. To avoid oxidation of the supporting ligands, researchers have focused on ligands that resist oxidation, and a common group of ligands that have been explored are nitrogen-donor ligands.

Scheme 9. Alkene Oxidation from an (Alkene)peroxoiridium(III) Complex

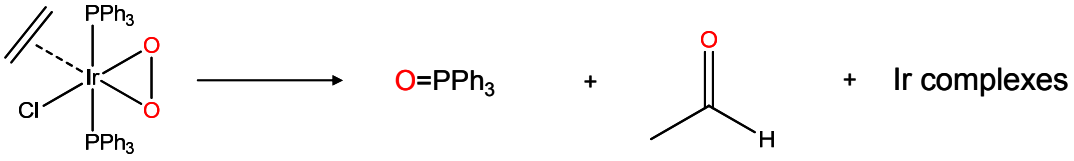

2.3 Monoanionic Nitrogen-donor Ligands

There is a variety of nitrogen-donor ligands in the literature that are used as supporting ligands for transition metal centers. Monoanionic nitrogen-donor ligands represent an important class of supporting ligands and have been widely used in the coordination chemistry of transition metals to impart diverse properties and reactivity. Prominent examples include poly(1-pyrazolyl)borate,[39,40] *β*-diiminate,[41] aminotroponiminate,[42] amidinate,[43,44] and triazenide[45,46] ligands (Schemes 10 and 11).

Scheme 10. Monoanionic Nitrogen-donor Ligands

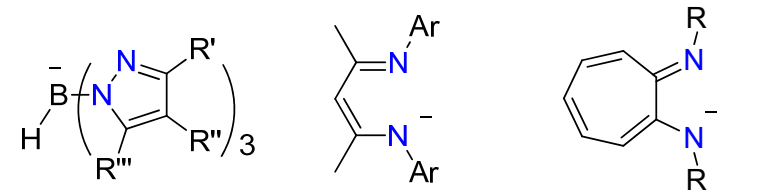

Because guanidinates are conceptually related to amidinates and triazenides, they may also be expected to serve as good supporting ligands for reactive transition metal centers (Scheme 11). Guanidinate complexes are well known for a variety of metal centers, particularly for early transition metals and lanthanides in mid- to high-valent oxidation states.[1-7] Stabilization of electron-deficient metal centers by guanidinato ligands can be attributed to the ability of the NR_2 group to donate its lone-pair into the CN_3 core

of the ligand. When significant lone-pair donation occurs, a major contribution from the iminium/diamide resonance structure can be observed, Structure **II** in Scheme 12.

Scheme 11. Guanidinate, Amidinate, and Triazenide Anions

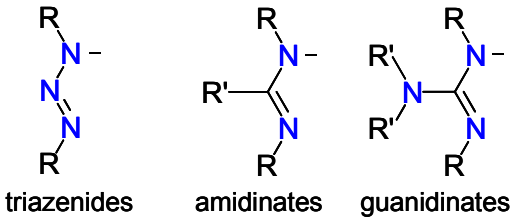

Scheme 12. Resonance Structures of the Guanidinate Monoanion

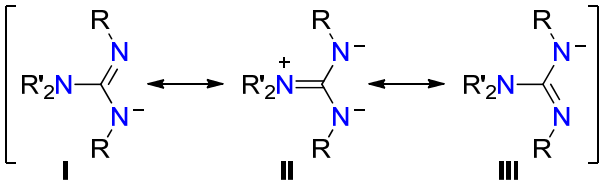

This places more electron density on the two donor atoms available for metal coordination, thereby making this class of ligands stronger donors than the closely related amidinate and triazenide ligands, Scheme 11. When guanidinate ligands are coordinated to a lower-valent metal center, they confer greater oxidizability on the metal, which can be observed from the redox potentials of $[Mo^{II}_2(\mu\text{-}L)_4]$ complexes.[47-49] There are some examples of low-valent metal complexes, mostly di- and tetranuclear complexes of the coinage metals[1,49-53] and a few more recent examples of iridium(I) and rhodium(I) complexes, [Ir{^{i}PrNC(N^{i}Pr$_2$)N^{i}Pr}(cod)] and [Rh{(2,6-^{i}Pr$_2$C$_6$H$_3$)NC(NR$_2$)N(2,6-^{i}Pr$_2$C$_6$H$_3$)}(cod)] (where R = ^{i}Pr or C$_6$H$_{11}$).[54,55]

2.4 Conclusion

Oxidation of alkenes to value-added organic species is a very important industrial process. In order to use O_2 and broaden the substrate range, reactive transition metal complexes are required. These reactive transition metal complexes must be able to activate O_2 and control the oxidation of the coordinated alkene without significant decomposition. Selection and design of the supporting ligand is very important, because it must stabilize the metal center in more than one oxidation state and be resistant to oxidation. The interesting properties of electron-donating guanidinato ligands have directed us to investigate their ability in supporting low-valent iridium(I) and rhodium(I) metal centers. Guanidinato ligands have shown the ability to support a range of oxidation states[1,49-57] and when coordinated to low-valent iridium and rhodium may provide a pathway to controlled catalytic alkene oxidation with O_2. Mechanistic studies on stoichiometric alkene oxidation with O_2 may provide insights into the mechanisms of these reactions. We have prepared these complexes and have used them in the activation of small inert molecules and have observed the formation of interesting metal complexes (Chapters 3, 4, 5 and 7).

CHAPTER 3
SYNTHESIS AND CHARACTERIZATION OF IRIDIUM(I) COMPLEXES SUPPORTED BY GUANIDINATO(1−) LIGANDS

3.1 Introduction

This chapter includes the synthesis and characterization of mononuclear Ir^{I}(cod) and $Ir^{I}(CO)_2$ complexes supported by *N*,*N*-dialkyl-*N*′,*N*″-diarylguanidinato ligands(1−). Two methods have been used for the synthesis of the neutral guanidines with the corresponding lithium guanidinate salts being prepared by deprotonation of the free guanidines. The Ir^{I}(cod) complexes were also synthesized by two different methods. In the first method, the guanidinato iridium(I) complexes were synthesized by transmetallation of the lithium salts with [{Ir(cod)}$_2$(μ-Cl)$_2$] under an inert atmosphere. The second method employs the neutral ligands in the reaction with [{Ir(cod)}$_2$(μ-OMe)$_2$] under an inert atmosphere. In this method, MeO^- functions as an internal base, for *in situ* deprotonation of the neutral ligand. These complexes have been characterized by nuclear magnetic resonance (NMR) and infrared (IR) spectroscopy, electron impact mass spectrometry (EI MS), and elemental analysis. As determined by spectroscopic methods and single-crystal X-ray diffraction, the guanidinato(1−) ligands coordinate the low-valent d^8 iridium(I) center in an N,N′-chelating binding mode. The bond lengths and angles obtained from several single-crystal structure determinations indicate a significant contribution of the iminium/diamide resonance structure, Structure **II** in Scheme 11. The synthesis and characterization of a subset of the guanidinato ligands and iridium(I) complexes was published in 2008.[58]

The dicarbonyl complexes were synthesized by a ligand substitution reaction from the corresponding cod complexes. These complexes have been characterized by NMR and IR spectroscopy, EI MS, and elemental analysis. The single-crystal structure

determination of one of the complexes shows that they are analogous to the cod complexes with the guanidinato ligand binding in an N,N′-chelating binding mode and two terminal CO ligands. IR analysis of the dicarbonyl complexes and ^{13}C NMR analysis of the cod complexes have shown that these guanidinato ligands function as stronger donor ligands than other monoanionic bidentate nitrogen-donors in the literature.

To explore the accessibility of iridium(III) in the (guanidinato)(alkene) ligand environment, the reactivity of one complex toward MeI and MeOTf has been investigated. Formation of octahedral iridium(III) complexes has been observed through oxidative addition reactions under mild conditions. These complexes have been characterized by ^{1}H NMR spectroscopy and EI MS.

3.2 Experimental Section

3.2.1 Materials and Methods

Materials. All reagents and solvents were purchased from commercial sources and were used as received, unless noted otherwise. Diethyl ether and toluene were deoxygenated by sparging with N_2 and purified by passage through two packed columns of molecular sieves under an N_2 pressure (MBraun solvent purification system). *n*-Pentane was dried over Na and distilled under N_2 prior to use.[59] Preparation and handling of air- and moisture-sensitive materials were carried out under an inert gas atmosphere by using either standard Schlenk and vacuum line techniques or a glovebox. The guanidines PhN=C(NMe$_2$)NHPh,[60,61] PhN=C(NEt$_2$)NHPh,[61-63] and (4-MeC$_6$H$_4$)N=C(NMe$_2$)NH(4-MeC$_6$H$_4$)[60] were briefly mentioned in the literature but were only sparsely characterized. [{Ir(cod)}$_2$(μ-Cl)$_2$] was synthesized according to a published procedure (cod = 1,5-cyclooctadiene).[64] [{Ir(cod)}$_2$(μ-OMe)$_2$][65] was prepared from [{Ir(cod)}$_2$(μ-Cl)$_2$] and sodium methoxide in dichloromethane,[66] isolated by filtration and removal of the

volatiles and used without further purification. Elemental analyses were performed by Atlantic Microlab, Inc., Norcross, GA, USA.

Physical Methods. NMR spectra were recorded on a Bruker Avance MicroBay 300 or Avance DPX 300 spectrometer at ambient temperature, unless noted otherwise. ^{1}H, ^{13}C and ^{19}F chemical shifts are reported in parts per million (ppm) and were referenced to residual solvent peaks (for ^{1}H and ^{13}C NMR spectra) or an external standard [$CFCl_3$ ($\delta = 0$ ppm) for ^{19}F NMR spectra]. IR spectra were recorded on a Bruker Vertex 70 Fourier-transform IR spectrometer using solutions of the compounds in *n*-pentane (5−15 mM) or solid samples. Solid samples were prepared by grinding the solid compound with KBr and pressing the mixture into a disk. Mass spectral data were acquired on a quadrupole ion trap ThermoFinnigan LCQ Deca mass spectrometer using an electrospray ionization source or on a single quadrupole ThermoFinnigan Voyager mass spectrometer using an electron impact ionization source (equipped with a solids probe). UV–Visible spectra were recorded on an HP 8453A diode array spectrophotometer (Agilent Technologies).

3.2.2 Preparation of Guanidines

***N,N*-Dimethyl-*N′,N″*-diphenylguanidine, PhN=C(NMe$_2$)NHPh (a).** A total of 9.0 mL of a dimethylamine solution (2.0 M in THF; 18 mmol) was added to a solution of 2.01 g (8.80 mmol) of *N*,*N*′-diphenylthiourea in 15 mL of tetrahydrofuran at 0 °C. Over a period of 15 min, 2.73 g (8.77 mmol) of benzyltriethylammoniun permanganate[67] was added to the solution under stirring, resulting in the formation of a brown precipitate, and the mixture was stirred for an additional 15 min. The precipitate was separated by filtration through a celite pad and washed with tetrahydrofuran. The volatiles of the combined filtrates were removed under reduced pressure to afford a yellow oil. The guanidine was extracted from the oil with 30 mL of diethyl ether and, after evaporation of

the solvent, isolated as a colorless powder. The product was recrystallized from hot hexanes and dried *in vacuo*. Yield: 1.49 g (71%). Anal. Calcd for $C_{15}H_{17}N_3$: C, 75.28; H, 7.16; N, 17.56. Found: C, 75.29; H, 7.06; N, 17.59. ^{1}H NMR (300 MHz, $CDCl_3$, δ): 7.25 (t, J = 7.5 Hz, 4H, Ar H), 6.99 (t, J = 7.4 Hz, 2H, Ar H), 6.86 (d, J = 8.5 Hz, 4H, Ar H), 5.5 (br s, 1H, NH), 2.91 (s, 6H, NCH_3). $^{13}C\{^1H\}$ NMR (75.5 MHz, $CDCl_3$, δ): 151.4, 129.2, 121.9, and 120.1 (Ar), 38.1 (NCH_3). EIMS (70 eV) m/z: $M^{+\bullet}$ calcd for $C_{15}H_{17}N_3$, 239.14; found, 239.1.

***N,N*-Diethyl-*N′,N″*-diphenylguanidine, PhN=C(NEt$_2$)NHPh (b).** A total of 1.51 mL of diethylamine (1.07 g, 14.6 mmol) was added to a solution of 1.62 g (7.10 mmol) of *N*,*N*′-diphenylthiourea in 15 mL of tetrahydrofuran at 0 °C. Over a period of 15 min, 2.23 g (7.16 mmol) of benzyltriethylammoniun permanganate[67] was added to the solution under stirring, resulting in the formation of a brown precipitate, and the mixture was stirred for an additional 15 min. The precipitate was separated by filtration through a celite pad and washed with tetrahydrofuran. The volatiles of the combined filtrates were removed under reduced pressure to afford a yellow oil. The guanidine was extracted from the oil with diethyl ether (2 x 50 mL) and, after evaporation of the solvent, isolated as a colorless powder. The product was recrystallized from hot hexanes and dried *in vacuo*. Yield: 1.52 g (80%). Anal. Calcd for $C_{17}H_{21}N_3$: C, 76.37; H, 7.92; N, 15.72. Found: C, 76.07; H, 7.79; N, 15.66. ^{1}H NMR (300 MHz, $CDCl_3$, δ): 7.12 (t, J = 8.0 Hz, 4H, Ar H), 6.86–6.77 (m, 6H, Ar H), 5.31 (br s, 1H, NH), 3.23 (q, J = 7.1 Hz, 4H, NCH_2CH_3), 1.07 (t, J = 7.1 Hz, 6H, NCH_2CH_3). $^{13}C\{^1H\}$ NMR (75.5 MHz, $CDCl_3$, δ): 150.0, 129.1, 121.8, and 118.3 (Ar), 41.9 (NCH_2CH_3), 12.8 (NCH_2CH_3). EIMS (70 eV) m/z: $M^{+\bullet}$ calcd for $C_{17}H_{21}N_3$, 267.17; found, 267.0.

***N,N*-Dimethyl-*N′,N″*-bis(4-methylphenyl)guanidine, (4-MeC$_6$H$_4$)N=C(NMe$_2$)-NH(4-MeC$_6$H$_4$) (c).** The procedure for the synthesis of the corresponding guanidinium iodide was adapted from a method previously described for other guanidinium iodides.[68] A solution of 0.50 g (1.95 mmol) of *N*,*N*′-bis(4-methylphenyl)thiourea and 1.22 mL (2.78

g, 19.5 mmol) of iodomethane in 12 mL of methanol was heated under reflux for 2 h. After the solution was cooled to room temperature, the volatiles, including unconsumed iodomethane, were removed under reduced pressure, affording *S*-methyl-*N*,*N*′-bis(4-methylphenyl)isothiourea hydroiodide in quantitative yield (0.78 g). To a solution of this product in 5 mL of methanol was added 1.06 mL of a dimethylamine solution (5.6 M in EtOH; 5.94 mmol). The resulting solution was heated in a sealed flask for 7 h at 70 °C. (*Caution:* Due to the formation of methanethiol, which is a gas under the reaction conditions, the pressure in the flask may increase substantially. A shield should be used for protection.) The solution was then cooled to room temperature, and methanethiol was carefully removed in a stream of N_2. (MeSH was trapped by routing the gas stream through concentrated HNO_3.) Upon evaporation of the solvents, *N*,*N*-dimethyl-*N*′,*N*″-bis(4-methylphenyl)guanidinium iodide was obtained as a colorless solid (0.73 g).

This salt was dissolved in 20 mL of diethyl ether and treated with 50 mL of a saturated aqueous Na_2CO_3 solution. The biphasic mixture was vigorously stirred for 1 h, before the organic phase was separated and dried over $MgSO_4$ and the volatiles were removed under reduced pressure. The crude product was purified by column chromatography on silica gel using a solution of 1% NEt_3 in diethyl ether as the eluent. Yield: 0.34 g (65%). Alternatively, the product could be recrystallized from hot hexanes and dried *in vacuo*. Anal. Calcd for $C_{17}H_{21}N_3$: C, 76.37; H, 7.92; N, 15.72. Found: C, 76.53; H, 8.07; N, 15.74. ^{1}H NMR (300 MHz, $CDCl_3$, δ): 7.05 (d, J = 8.4 Hz, 4H, Ar H), 6.79 (d, J = 8.4 Hz, 4H, Ar H), 5.44 (br, 1H, NH), 2.89 (s, 6H, NCH_3), 2.29 (s, 6H, $C_6H_4CH_3$). $^{13}C\{^1H\}$ NMR (75.5 MHz, $CDCl_3$, δ): 152.1, 131.4, 129.9, and 120.5 (Ar), 38.2 (NCH_3), 20.8 ($C_6H_4CH_3$). EIMS (70 eV) *m*/*z*: $M^{+\bullet}$ calcd for $C_{17}H_{21}N_3$, 267.17; found, 267.3.

***N*,*N*-Diethyl-*N*′,*N*″-bis(4-methylphenyl)guanidine, (4-MeC$_6$H$_4$)N=C(NEt$_2$)-NH(4-MeC$_6$H$_4$) (d).** A solution of 2.00 g (7.80 mmol) of *N*,*N*′-bis(4-methylphenyl)thiourea and 4.90 mL (11.17 g, 78.71 mmol) of iodomethane in 15 mL of

methanol was heated under reflux for 2 h. After the solution was cooled to room temperature, the volatiles, including excess iodomethane, were removed under reduced pressure to afford *S*-methyl-*N*,*N*′-bis(4-methylphenyl)isothiourea hydroiodide as a yellow solid. Yield: 3.00 g (97%). ^{1}H NMR (300 MHz, $(CD_3)_2SO$, δ): 10.81 (br, 2H, NH), 7.28 (br, 8H, Ar H), 2.65 (s, 3H, SCH_3), 2.32 (s, 6H, $C_6H_4CH_3$). ESI(+)MS (CH_3CN) *m*/*z*: $\{M - I\}^+$ calcd for $C_{16}H_{19}IN_2S$, 271.1; found, 271.2.

A solution of 3.00 g (7.53 mmol) of *S*-methyl-*N*,*N*′-bis(4-methylphenyl)isothiourea hydroiodide and 3.10 mL (2.19 g, 29.97 mmol) of diethylamine in 15 mL of methanol was heated in a sealed flask for 7 h at 70 °C. (*Caution:* Due to the formation of methanethiol, which is a gas under the reaction conditions, the pressure in the flask may increase substantially. A shield should be used for protection.) The solution was cooled to room temperature, and methanethiol was carefully removed with a stream of N_2. (MeSH was trapped by routing the gas stream through concentrated HNO_3). Upon evaporation of the solvents, *N*,*N*-diethyl-*N*′,*N*″-bis(4-methylphenyl)guanidinium iodide was obtained as a yellow solid. Yield: 3.05 g (96%). ^{1}H NMR (300 MHz, $CDCl_3$, δ): 7.12 (d, J = 8.6 Hz, 4H, Ar H), 7.02 (d, J = 8.4 Hz, 4H, Ar H), 5.49 (br, 2H, NH), 2.95 (q, J = 7.3 Hz, 4H, NCH_2CH_3), 2.32 (s, 3H, $C_6H_4CH_3$), 2.31 (s, 3H, $C_6H_4CH_3$), and 1.40 (t, J = 7.3 Hz, 6H, NCH_2CH_3). ESI(+)MS (CH_3CN) *m*/*z*: $\{M - I\}^+$ calcd for $C_{19}H_{26}IN_3$, 296.2; found, 296.2.

A solution of 3.05 g (7.20 mmol) of *N*,*N*-diethyl-*N*′,*N*″-bis(4-methylphenyl)guanidinium iodide in 20 mL of diethyl ether was treated with 50 mL of a saturated aqueous solution of Na_2CO_3. The biphasic mixture was vigorously stirred for 1 h, after which the organic phase was separated and dried over $MgSO_4$ and the volatiles were removed under reduced pressure. The crude product was purified by column chromatography on silica gel using a solution of 3% NEt_3 in diethyl ether as the eluent affording a colorless solid. Yield: 1.45 g (68%). Anal. Calcd for $C_{19}H_{25}N_3$: C, 77.25; H, 8.53; N, 14.22. Found: C, 77.45; H, 8.52; N, 13.95. ^{1}H NMR (300 MHz, $CDCl_3$, δ): 7.04

(d, J = 8.0 Hz, 4H, Ar H), 6.80 (d, J = 7.5 Hz, 4H, Ar H), 5.35 (br, 1H, NH), 3.33 (q, J = 7.1 Hz, 4H, NCH_2CH$_3$), 2.29 (s, 6H, C$_6$H$_4$CH_3), 1.16 (t, J = 7.1 Hz, 6H, NCH$_2$CH_3). ^{13}C{^{1}H} NMR (75.5 MHz, CDCl$_3$, δ): 150.8, 131.4, 129.9, 122.2, and 118.7 (Ar), 42.1 (NCH$_2$CH$_3$), 20.8 (C$_6$H$_4$$CH_3$), 13.0 (NCH$_2$$CH_3$). EIMS (70 eV) m/z: M$^{+\bullet}$ calcd for C$_{19}$H$_{25}$N$_3$, 295.2; found, 295.3.

***N*,*N*′-Bis(4-methoxyphenyl)thiourea, (4-MeOC$_6$H$_4$NH)$_2$C=S.** This compound[69] was synthesized using conditions reported for the synthesis of a closely related *N*,*N*′-diarylthiourea.[70] A solution of 1.12 mL (1.31 g, 7.95 mmol) of 4-methoxyphenyl isothiocyanate and 1.00 g (8.12 mmol) of 4-methoxyaniline in 10 mL of toluene was prepared and heated under reflux for 24 h, during which a purple solid was formed. The reaction mixture was cooled to room temperature, and the solid was separated by filtration, washed with cold toluene (3 x 5 mL) and dried *in vacuo*. Yield: 1.94 g (85%). ^{1}H NMR (300 MHz, (CD$_3$)$_2$SO, δ): 9.41 (s, 2H, NH), 7.30 (d, J = 8.9 Hz, 4H, Ar H), 6.88 (d, J = 8.9 Hz, 4H, Ar H), 3.73 (s, 6H, C$_6$H$_4$OCH_3). EIMS (70 eV) m/z: M$^{+\bullet}$ calcd for C$_{15}$H$_{16}$N$_2$S, 256.1; found, 255.9.

***N*,*N*-Dimethyl-*N*′,*N*″-bis(4-methoxyphenyl)guanidine, (4-MeOC$_6$H$_4$)N=C-(NMe$_2$)NH(4-MeOC$_6$H$_4$) (e).** A solution of 0.60 g (2.08 mmol) of *N*,*N*′-bis(4-methoxyphenyl)thiourea and 1.28 mL (2.92 g, 20.56 mmol) of iodomethane in 15 mL of methanol was heated under reflux for 2 h. After the solution was cooled to room temperature, the volatiles, including excess iodomethane, were removed under reduced pressure to afford *S*-methyl-*N*,*N*′-bis(4-methoxyphenyl)isothiourea hydroiodide as a yellow solid. Yield: 0.85 g (95%). ^{1}H NMR (300 MHz, (CD$_3$)$_2$SO, δ): 10.68 (br, 2H, NH), 7.33 (br, 4H, Ar H), 7.03 (br, 4H, Ar H), 3.77 (s, 6H, C$_6$H$_4$OCH_3), 2.66 (s, 3H, SCH$_3$). ESI(+)MS (CH$_3$CN) m/z: {M – I}$^+$ calcd for C$_{16}$H$_{19}$IN$_2$O$_2$S, 303.1; found, 303.1.

A solution of 0.75 g (1.74 mmol) of *S*-methyl-*N*,*N*′-bis(4-methoxyphenyl)isothiourea hydroiodide and 3.67 mL of a dimethylamine solution (5.6 M in EtOH; 20.55 mmol) in 15 mL of methanol was heated in a sealed flask for 7 h at 70

°C. (*Caution:* Due to the formation of methanethiol, which is a gas under the reaction conditions, the pressure in the flask may increase substantially. A shield should be used for protection.) The solution was cooled to room temperature, and methanethiol was carefully removed with a stream of N_2. (MeSH was trapped by routing the gas stream through concentrated HNO_3). Upon evaporation of the solvents, *N,N*-dimethyl-*N′,N″*-bis(4-methoxyphenyl)guanidinium iodide was obtained as a yellow solid. Yield: 0.68 g (91%). ^{1}H NMR (300 MHz, $(CD_3)_2SO$, δ): 9.28 (br, 2H, NH), 7.02 (d, J = 8.9 Hz, 4H, Ar H), 6.87 (d, J = 9.0 Hz, 4H, Ar H), 3.70 (s, 6H, $C_6H_4OCH_3$), 2.99 (s, 6H, NCH_3). ESI(+)MS (CH_3CN) m/z: $\{M - I\}^+$ calcd for $C_{17}H_{22}IN_3O_2$, 300.2; found, 300.2.

A solution of 0.45 g (1.05 mmol) of *N,N*-dimethyl-*N′,N″*-bis(4-methoxyphenyl)guanidinium iodide in 20 mL of diethyl ether was treated with 50 mL of a saturated aqueous solution of Na_2CO_3. The biphasic mixture was vigorously stirred for 1 h, after which the organic phase was separated and dried over $MgSO_4$ and the volatiles were removed under reduced pressure. The crude product was purified by column chromatography on silica gel using a solution of 5% NEt_3 in diethyl ether as the eluent affording an off-white solid. Yield: 0.15 g (47%). Anal. Calcd for $C_{17}H_{21}N_3O_2$: C, 68.20; H, 7.07; N, 14.04. Found: C, 67.73; H, 7.11; N, 13.75. ^{1}H NMR (300 MHz, $CDCl_3$, δ): 6.84–6.76 (m, 8H, Ar H), 4.82 (br, 1H, NH), 3.74 (s, 6H, $C_6H_4OCH_3$), 2.83 (s, 6H, NCH_3). $^{13}C\{^1H\}$ NMR (75.5 MHz, $CDCl_3$, δ): 155.2, 153.0, 122.1, and 114.8 (Ar), 55.6 ($C_6H_4OCH_3$), 38.3 (NCH_3). EIMS (70 eV) m/z: $M^{+\bullet}$ calcd for $C_{17}H_{21}N_3O_2$, 299.2; found, 299.4.

***N,N′*-Bis(2,6-dimethylphenyl)thiourea, $(2,6\text{-}Me_2C_6H_3NH)_2C{=}S$.** This compound was synthesized according to a method for *N,N′*-bis(2,4,6-trimethylphenyl)thiourea.[70] A solution of 1.0 mL (1.09 g, 6.65 mmol) of 2,6-dimethylphenyl isothiocyanate and 1.2 mL (1.18 g, 9.74 mmol) of 2,6-dimethylaniline in 10 mL of toluene was prepared and heated under reflux for 24 h, during which a colorless solid was formed. After the reaction mixture was cooled to room temperature, the solid

was separated by filtration, washed three times with 5 mL of cold toluene and dried *in vacuo*. Yield: 1.60 g (85%). Anal. Calcd for $C_{17}H_{20}N_2S$: C, 71.79; H, 7.09, N, 9.85; S, 11.27. Found: C, 71.96; H, 7.07; N, 9.82; S, 11.28. ^{1}H NMR (300 MHz, $CDCl_3$, δ): 8.26 (s, 1H, NH), 7.26–7.18 (m, 3H, Ar H), 7.14–7.04 (m, 3H, Ar H), 6.51 (s, 1H, NH), 2.46 (s, 6H, $C_6H_3(CH_3)_2$), 2.25 (s, 6H, $C_6H_3(CH_3)_2$). $^{13}C\{^1H\}$ NMR (75.5 MHz, $CDCl_3$, δ): 181.1 (N_2CS), 137.8, 136.7, 135.8, 133.4, 129.5, 129.3, 128.5, and 128.3 (Ar), 18.8 and 18.4 ($C_6H_3(CH_3)_2$). EIMS (70 eV) *m*/*z*: $M^{+\bullet}$ calcd for $C_{17}H_{20}N_2S$, 284.13; found, 284.2.

***N*,*N*-Dimethyl-*N*′,*N*″-bis(2,6-dimethylphenyl)guanidine, (2,6-Me$_2$C$_6$H$_3$)N=C(NMe$_2$)NH(2,6-Me$_2$C$_6$H$_3$) (f).** A solution of 0.50 g (1.76 mmol) of *N*,*N*′-bis(2,6-dimethylphenyl)thiourea and 1.1 mL (2.51 g, 17.7 mmol) of iodomethane in 15 mL of methanol was heated under reflux for 2 h. After the solution was cooled to room temperature, the volatiles, including unconsumed iodomethane, were removed under reduced pressure, affording *S*-methyl-*N*,*N*′-bis(2,6-dimethylphenyl)isothiourea hydroiodide in quantitative yield (0.75 g). To a solution of this product in 5 mL of methanol was added 0.65 mL of a dimethylamine solution (5.6 M in EtOH; 3.64 mmol). The resulting solution was heated in a sealed flask for 7 h at 70 °C. (*Caution:* Due to the formation of methanethiol, which is a gas under the reaction conditions, the pressure in the flask may increase substantially. A shield should be used for protection.) The solution was then cooled to room temperature and methanethiol was carefully removed in a stream of N_2. (MeSH was trapped by routing the gas stream through concentrated HNO_3.) Upon evaporation of the solvents, *N*,*N*-dimethyl-*N*′,*N*″-bis(2,6-dimethylphenyl)guanidinium iodide was obtained as a colorless solid (0.67 g).

This salt was dissolved in 20 mL of diethyl ether and treated with 50 mL of a saturated aqueous Na_2CO_3 solution. The biphasic mixture was vigorously stirred for 1 h, before the organic phase was separated and the volatiles were removed under reduced pressure. The remaining colorless powder was recrystallized from hot hexanes and dried *in vacuo*. Yield: 0.39 g (75%). Anal. Calcd for $C_{19}H_{25}N_3$: C, 77.25; H, 8.53; N, 14.22.

Found: C, 77.38; H, 8.69; N, 14.12. ^{1}H NMR (300 MHz, $CDCl_3$, δ): 7.02–6.88 (br, 6H, Ar H), 5.06 (br, 1H, NH), 2.66 (s, 6H, NCH_3), 2.28–2.24 (br, 12H, $C_6H_3(CH_3)_2$). $^{13}C\{^{1}H\}$ NMR (75.5 MHz, $CDCl_3$, δ): 151.4, 133.9, 130.1, 128.5, 125.4, and 122.1 (Ar), 38.7 (NCH_3), 18.9 and 18.2 ($C_6H_3(CH_3)_2$). EIMS (70 eV) *m*/*z*: $M^{+\bullet}$ calcd for $C_{19}H_{25}N_3$, 295.20; found, 295.3.

3.2.3 Preparation of (Cyclooctadiene)iridium(I) Complexes

General Procedure for the Synthesis of [Ir{ArNC(NR$_2$)NAr}(cod)] Complexes (1a–1g). Method A. In a typical procedure, 1.20 mmol of the *N*,*N*-dialkyl-*N*′,*N*″-diarylguanidine was dissolved in 15 mL of degassed diethyl ether. The solution was cooled to –40 °C and 1.1 equiv of methyllithium (1.6 M in Et_2O) was added under stirring. The resulting solution was allowed to warm to 20 °C and stirred for 1 h. Upon removal of the volatiles under reduced pressure, the Li^+ salt of the *N*,*N*-dialkyl-*N*′,*N*″-diarylguanidinate anion, ($Li\{ArNC(NR_2)NAr\}\cdot Et_2O$), was isolated as a colorless powder and stored under rigorous exclusion of moisture. The powder could also be recrystallized from a concentrated *n*-pentane solution at –30 °C to afford a microcrystalline solid.

In an N_2 atmosphere, a solution of 0.300 mmol of lithium guanidinate in 10 mL of diethyl ether was added to a suspension of 100 mg (0.149 mmol) of $[\{Ir(cod)\}_2(\mu\text{-}Cl)_2]$ in 5 mL of diethyl ether under stirring at 20 °C. The color of the reaction mixture changed from orange to yellow, accompanied by precipitation of a colorless solid. After 3 h, the solution was filtered and the solvent was removed under reduced pressure. The residue was recrystallized from *n*-pentane by preparing a concentrated solution at 20 °C and storing it at –30 °C. Yellow single crystals of X-ray diffraction quality were typically obtained within two days.

Method B. In an N_2 atmosphere, a solution of 0.300 mmol of the *N*,*N*-dialkyl-*N*′,*N*″-diarylguanidine in 15 mL of diethyl ether was added to a suspension of 0.149

mmol of [{Ir(cod)}$_2$(μ-OMe)$_2$] in 5 mL of diethyl ether under stirring. The dark–orange mixture turned into a yellow–orange solution. After 3 h, the volatiles were removed under reduced pressure to afford a yellow–orange oil. The residue was recrystallized as described above (Method A).

[Ir{PhNC(NMe$_2$)NPh}(cod)] (1a). Yield (Method A): 102 mg (64%). Anal. Calcd for $C_{23}H_{28}IrN_3$: C, 51.28; H, 5.24; N, 7.80. Found: C, 51.51; H, 5.31; N, 7.90. ^{1}H NMR (300 MHz, $CDCl_3$, δ): 7.22 (t, J = 7.6 Hz, 4H, Ar H), 6.91 (t, J = 7.4 Hz, 2H, Ar H), 6.79 (d, J = 7.3 Hz, 4H, Ar H), 3.66 (m, 4H, =C*H*CH$_2$–), 2.52 (s, 6H, NCH$_3$), 2.18 (m, 4H, =CHC*H*$_2$–), 1.43 (m, 4H, =CHC*H*$_2$–). ^{13}C{^{1}H} NMR (75.5 MHz, $CDCl_3$, δ): 147.3, 128.6, 122.3, and 121.8 (Ar), 61.0 (=*C*HCH$_2$–), 39.0 (NCH$_3$), 31.8 (=CH*C*H$_2$–). EIMS (70 eV) m/z: $M^{+\bullet}$ calcd for $C_{23}H_{28}IrN_3$, 539.19; found, 539.4. UV–Vis (toluene) λ_{max}, nm (ε): 417 (1600), 470 (300). This complex was also synthesized using Method B. Yield: 67%. The ^{1}H NMR spectrum of this batch was identical to that of the product obtained from Method A.

[Ir{PhNC(NEt$_2$)NPh}(cod)] (1b). Yield (Method A): 116 mg (69%). Anal. Calcd for $C_{25}H_{32}IrN_3$: C, 52.98; H, 5.69; N, 7.41. Found: C, 52.93; H, 5.71; N, 7.33. ^{1}H NMR (300 MHz, $CDCl_3$, δ): 7.21 (t, J = 7.8 Hz, 4H, Ar H), 6.90 (t, J = 7.4 Hz, 2H, Ar H), 6.83 (d, J = 7.3 Hz, 4H, Ar H), 3.61 (m, 4H, =C*H*CH$_2$–), 2.87 (q, J = 7.2 Hz, 4H, NC*H*$_2$CH$_3$), 2.18 (m, 4H, =CHC*H*$_2$–), 1.43 (m, 4H, =CHC*H*$_2$–), 1.03 (t, J = 7.2 Hz, 6H, NCH$_2$C*H*$_3$). ^{13}C{^{1}H} NMR (75.5 MHz, $CDCl_3$, δ): 147.8, 128.7, 122.2, and 121.9 (Ar), 60.8 (=*C*HCH$_2$–), 41.2 (N*C*H$_2$CH$_3$), 31.8 (=CH*C*H$_2$–), 12.0 (NCH$_2$*C*H$_3$). EIMS (70 eV) m/z: $M^{+\bullet}$ calcd for $C_{25}H_{32}IrN_3$, 567.22; found, 567.4. UV–Vis (toluene) λ_{max}, nm (ε): 418 (1600), 470 (300). This complex was also synthesized using Method B. Yield: 70%. The ^{1}H NMR spectrum of this batch was identical to that of the product obtained from Method A.

[Ir{(4-MeC$_6$H$_4$)NC(NMe$_2$)N(4-MeC$_6$H$_4$)}(cod)] (1c). Yield: 84 mg (50%). Anal. Calcd for $C_{25}H_{32}IrN_3$: C, 52.98; H, 5.69; N, 7.41. Found: C, 52.91; H, 5.72; N, 7.17. ^{1}H

NMR (300 MHz, $CDCl_3$, δ): 7.02 (d, J = 8.5 Hz, 4H, Ar H), 6.68 (d, J = 8.2 Hz, 4H, Ar H), 3.64 (m, 4H, =C*H*CH_2–), 2.51 (s, 6H, NCH_3), 2.29 (s, 6H, $C_6H_4CH_3$), 2.18 (m, 4H, =CHC*H*$_2$–), 1.44 (m, 4H, =CHC*H*$_2$–). $^{13}C\{^1H\}$ NMR (75.5 MHz, $CDCl_3$, δ): 144.7, 131.1, 129.2, and 122.2 (Ar), 60.8 (=*C*HCH_2–), 39.0 (NCH_3), 31.8 (=CH*C*H$_2$–), 20.8 ($C_6H_4CH_3$). EIMS (70 eV) m/z: $M^{+\bullet}$ calcd for $C_{25}H_{32}IrN_3$, 567.22; found, 567.4. UV–Vis (toluene) λ_{max}, nm (ε): 370 (sh), 418 (1700), 470 (300).

[Ir{(4-MeC$_6$H$_4$)NC(NEt$_2$)N(4-MeC$_6$H$_4$)}(cod)] (1d). Yield (Method A): 114 mg (64%). Anal. Calcd for $C_{27}H_{36}IrN_3$: C, 54.52; H, 6.10; N, 7.06. Found: C, 54.81; H, 6.01; N, 7.02. ^1H NMR (300 MHz, $CDCl_3$, δ): 7.00 (d, J = 8.6 Hz, 4H, Ar H), 6.72 (d, J = 8.2 Hz, 4H, Ar H), 3.60 (br m, 4H, =C*H*CH_2–), 2.86 (q, J = 7.1 Hz, 4H, NC*H*$_2$CH$_3$), 2.29 (s, 6H, $C_6H_4CH_3$), 2.18 (br m, 4H, =CHC*H*$_2$–), 1.43 (m, 4H, =CHC*H*$_2$–), 1.02 (t, J = 7.1 Hz, 6H, NCH_2CH_3). $^{13}C\{^1H\}$ NMR (75.5 MHz, $CDCl_3$, δ): 145.2, 131.1, 129.2, and 121.8 (Ar), 60.7 (=*C*HCH_2–), 41.0 (N*C*H$_2$CH$_3$), 31.8 (=CH*C*H$_2$–), 20.8 ($C_6H_4CH_3$), 12.0 (NCH_2CH_3). EIMS (70 eV) m/z: $M^{+\bullet}$ calcd for $C_{27}H_{36}IrN_3$, 595.3; found, 595.2. UV-Vis (toluene) λ_{max}, nm (ε): 370 (sh), 419 (1700), 471 (300). This complex was also synthesized using Method B. Yield: 58%. The UV–Vis spectrum of this batch was identical to that of the product obtained from Method A.

[Ir{(4-MeOC$_6$H$_4$)NC(NMe$_2$)N(4-MeOC$_6$H$_4$)}(cod)] (1e). Yield (Method B): 116 mg (65%). Anal. Calcd for $C_{25}H_{32}IrN_3O_2$: C, 50.15; H, 5.39; N, 7.02. Found: C, 50.40; H, 5.58; N, 6.94. ^1H NMR (300 MHz, $CDCl_3$, δ): 6.79–6.71 (m, J = 9.2 Hz, 8H, Ar H), 3.77 (s, 6H, $C_6H_4OCH_3$), 3.63 (br m, 4H, =C*H*CH_2–), 2.49 (s, 6H, NCH_3), 2.19 (br m, 4H, =CHC*H*$_2$–), 1.44 (m, 4H, =CHC*H*$_2$–). $^{13}C\{^1H\}$ NMR (75.5 MHz, $CDCl_3$, δ): 174.5 (CN_3), 154.7, 140.8, 123.3, and 113.9 (Ar), 60.7 (=*C*HCH_2–), 55.4 ($C_6H_4OCH_3$), 38.9 (NCH_3), 31.8 (=CH*C*H$_2$–). EIMS (70 eV) m/z: $M^{+\bullet}$ calcd for $C_{25}H_{32}IrN_3O_2$, 599.2; found, 599.2. UV-Vis (toluene) λ_{max}, nm (ε): 370 (sh), 419 (1600), 471 (300).

[Ir{(2,6-Me$_2$C$_6$H$_3$)NC(NMe$_2$)N(2,6-Me$_2$C$_6$H$_3$)}(cod)] (1f). Yield: 89 mg (50%). Anal. Calcd for $C_{27}H_{36}IrN_3$: C, 54.52; H, 6.10; N, 7.06. Found: C, 54.81; H, 6.40; N,

6.76. ^{1}H NMR (300 MHz, $CDCl_3$, δ): 6.98 (d, J = 7.4 Hz, 4H, Ar H), 6.82 (t, J = 7.4 Hz, 2H, Ar H), 3.27 (m, 4H, =C*H*CH_2–), 2.47 (s, 12H, $C_6H_3(CH_3)_2$), 2.23 (s, 6H, NCH_3), 2.06 (m, 4H, =CHC*H*$_2$–), 1.31 (m, 4H, =CHC*H*$_2$–). ^{13}C{^{1}H} NMR (75.5 MHz, $CDCl_3$, δ): 144.9, 133.0, 127.7, and 123.2 (Ar), 58.8 (=*C*HCH_2–), 36.7 (NCH_3), 32.0 (=CH*C*H$_2$–), 18.9 ($C_6H_3(CH_3)_2$). EIMS (70 eV) m/z: $M^{+\bullet}$ calcd for $C_{27}H_{36}IrN_3$, 595.25; found, 595.5. UV–Vis (toluene) λ_{max}, nm (ε): 370 (950), 423 (950), 480 (300).

[Ir{(2,6-^{i}Pr$_2$C$_6$H$_3$)NC(NMe$_2$)N(2,6-^{i}Pr$_2$C$_6$H$_3$)}(cod)] (1g). This compound was synthesized from Li{(2,6-^{i}Pr$_2$C$_6$H$_3$)NC(NMe$_2$)N(2,6-^{i}Pr$_2$C$_6$H$_3$)} (prepared *in situ* as described elsewhere[71,72]) and [{Ir(cod)}$_2$(μ-Cl)$_2$] according to the general procedure described above (Method A). Yield: 110 mg (52%). Anal. Calcd for $C_{35}H_{52}IrN_3$: C, 59.46; H, 7.41; N, 5.94. Found: C, 59.88; H, 7.30; N, 6.14. ^{1}H NMR (300 MHz, $CDCl_3$, δ): 7.09–6.98 (m, 6H, Ar H), 3.77 (sept, J = 6.8 Hz, 4H, Ar C*H*$(CH_3)_2$), 3.36 (br m, 4H, =C*H*CH_2–), 2.23 (s, 6H, NCH_3), 2.04 (br m, 4H, =CHC*H*$_2$–), 1.37 (d, J = 6.8 Hz, 12H, Ar CH(C*H*$_3$)$_2$), 1.32 (m, 4H, =CHC*H*$_2$–), 1.21 (d, J = 6.9 Hz, 12H, Ar CH(C*H*$_3$)$_2$). ^{13}C{^{1}H} NMR (75.5 MHz, $CDCl_3$, δ): 175.4 (CN_3), 143.9, 141.7, 124.0, and 123.1 (Ar), 58.7 (=*C*HCH_2–), 38.5 (NCH_3), 31.8 (=CH*C*H$_2$–), 27.1 (Ar *C*H$(CH_3)_2$, 25.3 and 23.4 (Ar CH(*C*H$_3$)$_2$). EIMS (70 eV) m/z: $M^{+\bullet}$ calcd for $C_{35}H_{52}IrN_3$, 707.4; found, 707.6. UV-Vis (toluene) λ_{max}, nm (ε): 370 (900), 423 (900), 476 (300).

3.2.4 Preparation of Dicarbonyliridium(I) Complexes

[Ir{PhNC(NMe$_2$)NPh}(CO)$_2$] (2a). A steady stream of CO(g) was purged through a solution of 100 mg (0.186 mmol) of [Ir{PhNC(NMe$_2$)NPh}(cod)] in 15 mL of diethyl ether for 15 min at 20 °C. The yellow solution gradually turned purple over the first five minutes. Subsequently, the volatiles were removed under reduced pressure to afford a purple solid. Due to the low solubility of the solid in *n*-pentane, the preparation of a saturated solution suitable for growing single crystals required about a day. After

separation of undissolved solid, the solution was stored at –30 °C. Formation of yellow single crystals typically occurred within two days. Yield: 61 mg (68%). Anal. Calcd for $C_{17}H_{16}IrN_3O_2$: C, 41.97; H, 3.31; N, 8.64. Found: C, 42.09; H, 3.20; N, 8.59. ^{1}H NMR (300 MHz, C_6D_6, δ): 7.06 (t, J = 8.1 Hz, 4H, Ar H), 6.85 (d, J = 8.1 Hz, 4H, Ar H), 6.81 (t, J = 7.3 Hz, 2H, Ar H), 1.82 (s, 6H, NCH_3). $^{13}C\{^1H\}$ NMR (75.5 MHz, C_6D_6, δ): 175.6 (IrCO), 171.1 (CN_3), 148.2, 129.3, 123.3, and 123.0 (Ar), 38.0 (NCH_3). EIMS (70 eV) m/z: $M^{+\bullet}$ calcd for $C_{17}H_{16}IrN_3O_2$, 487.1; found, 487.1. IR (n-pentane, cm^{-1}): 2055 and 1983 (ν_{CO}). IR (KBr, cm^{-1}): 2042 and 1956 (ν_{CO}). UV-Vis (toluene) λ_{max}, nm: 355 (sh). It should be noted that solutions of **2a** in n-pentane, benzene-d_6 and diethyl ether slowly turned pink upon standing for several hours. No changes, however, were observed in the IR (n-C_5H_{12}, C_6D_6 and Et_2O) and ^{1}H NMR spectra (C_6D_6) of these solutions. Upon standing at 20 °C, **2a** was recovered from the n-pentane solution as a yellow microcrystalline solid.

Synthesis and Characterization of [Ir{ArNC(NR$_2$)NAr}(CO)$_2$] Complexes 2b–2g. The iridium dicarbonyls **2b**–**2g** were synthesized in a manner analogous to **2a**. The reaction solutions turned purple (**2b** and **2c**), yellow–orange (**2d**, **2f** and **2g**) or green (**2e**) over a similar time frame as observed for **2a**. Between 50 and 100 mg of the Ir^I(cod) complexes was used, and the corresponding $Ir^I(CO)_2$ complexes were obtained as yellow solids in yields of 65–80% (**2b**–**2f**, after recrystallization) and 48% (**2g**).

[Ir{PhNC(NEt$_2$)NPh}(CO)$_2$] (2b). Anal. Calcd for $C_{19}H_{20}IrN_3O_2$: C, 44.35; H, 3.92; N, 8.17. Found: C, 44.64; H, 3.87; N, 8.20. ^{1}H NMR (300 MHz, C_6D_6, δ): 7.11–7.01 (m, 8H, Ar H), 6.82 (t, J = 7.1 Hz, 2H, Ar H), 2.45 (q, J = 7.2, Hz, 4H, NCH_2CH_3), 0.43 (t, J = 7.2 Hz, 6H, NCH_2CH_3). EIMS (70 eV) m/z: $M^{+\bullet}$ calcd for $C_{19}H_{20}IrN_3O_2$, 515.1; found, 515.2. IR (n-pentane, cm^{-1}): 2055 and 1982 (ν_{CO}). IR (KBr, cm^{-1}): 2051 and 1963 (ν_{CO}). UV-Vis (toluene) λ_{max}, nm: 355 (sh).

[Ir{(4-MeC$_6$H$_4$)NC(NMe$_2$)N(4-MeC$_6$H$_4$)}(CO)$_2$] (2c). Anal. Calcd for $C_{19}H_{20}IrN_3O_2$: C, 44.35; H, 3.92; N, 8.17. Found: C, 44.28; H, 3.87; N, 8.08. ^{1}H NMR

(300 MHz, C_6D_6, δ): 6.90 (d, J = 8.1 Hz, 4H, Ar H), 6.82 (d, J = 8.5 Hz, 4H, Ar H), 2.11 (s, 6H, NCH_3), 1.89 (s, 6H, $C_6H_4CH_3$). EIMS (70 eV) m/z: $M^{+\bullet}$ calcd for $C_{19}H_{20}IrN_3O_2$, 515.1; found, 515.1. IR (n-pentane, cm^{-1}): 2054 and 1981 (ν_{CO}). IR (KBr, cm^{-1}): 2044 and 1970 (ν_{CO}). UV-Vis (toluene) λ_{max}, nm: 355 (sh).

[Ir{(4-MeC$_6$H$_4$)NC(NEt$_2$)N(4-MeC$_6$H$_4$)}(CO)$_2$] (2d). Anal. Calcd for $C_{21}H_{24}IrN_3O_2$: C, 46.48; H, 4.46; N, 7.74. Found: C, 46.48; H, 4.52; N, 7.69. ^{1}H NMR (300 MHz, C_6D_6, δ): 6.98 (d, J = 8.4 Hz, 4H, Ar H), 6.89 (d, J = 8.0 Hz, 4H, Ar H), 2.52 (q, J = 7.1 Hz, 4H, NCH_2CH_3), 2.10 (s, 6H, $C_6H_4CH_3$), 0.49 (t, J = 7.1 Hz, 6H, NCH_2CH_3). EIMS (70 eV) m/z: $M^{+\bullet}$ calcd for $C_{21}H_{24}IrN_3O_2$, 543.2; found, 543.3. IR (n-pentane, cm^{-1}): 2053 and 1980 (ν_{CO}). IR (KBr, cm^{-1}): 2053 and 1978 (ν_{CO}). UV-Vis (toluene) λ_{max}, nm: 355 (sh).

[Ir{(4-MeOC$_6$H$_4$)NC(NMe$_2$)N(4-MeOC$_6$H$_4$)}(CO)$_2$] (2e). Anal. Calcd for $C_{20}H_{22.5}IrN_3O_{4.25}$ (**16**·0.25Et_2O): C, 42.51; H, 4.01; N, 7.44. Found: C, 42.31; H, 3.73; N, 7.54. ^{1}H NMR (300 MHz, C_6D_6, δ): 6.82 (d, J = 9.0 Hz, 4H, Ar H), 6.69 (d, J = 9.0 Hz, 4H, Ar H), 3.32 (s, 6H, $C_6H_4OCH_3$), 1.93 (s, 6H, NCH_3). EIMS (70 eV) m/z: $M^{+\bullet}$ calcd for $C_{19}H_{20}IrN_3O_4$, 547.1; found, 547.3. IR (n-pentane, cm^{-1}): 2053 and 1980 (ν_{CO}). IR (KBr, cm^{-1}): 2041 and 1962 (ν_{CO}). UV-Vis (toluene) λ_{max}, nm: 355 (sh).

[Ir{(2,6-Me$_2$C$_6$H$_3$)NC(NMe$_2$)N(2,6-Me$_2$C$_6$H$_3$)}(CO)$_2$] (2f). Anal. Calcd for $C_{21}H_{24}IrN_3O_2$: C, 46.48; H, 4.46; N, 7.74. Found: C, 46.63; H, 4.40; N, 7.68. ^{1}H NMR (300 MHz, C_6D_6, δ): 6.93 (d, J = 7.8 Hz, 4H, Ar H), 6.85 and 6.83 (dd, J = 7.1 and 6.4 Hz, 2H, Ar H), 2.40 (s, 12H, $C_6H_3(CH_3)_2$), 1.69 (s, 6H, NCH_3). EIMS (70 eV) m/z: $M^{+\bullet}$ calcd for $C_{21}H_{24}IrN_3O_2$, 543.2; found, 543.3. IR (n-pentane, cm^{-1}): 2053 and 1980 (ν_{CO}). IR (KBr, cm^{-1}): 2044 and 1977 (ν_{CO}). UV-Vis (toluene) λ_{max}, nm (ε): 353 (2400), 380 (sh), 410 (sh).

[Ir{(2,6-^{i}Pr$_2$C$_6$H$_3$)NC(NMe$_2$)N(2,6-^{i}Pr$_2$C$_6$H$_3$)}(CO)$_2$] (2g). Anal. Calcd for $C_{29}H_{40}IrN_3O_2$: C, 53.19; H, 6.16; N, 6.42. Found: C, 53.39; H, 6.27; N, 6.41. ^{1}H NMR (300 MHz, C_6D_6, δ): 7.06–7.03 (m, 6H, Ar H), 3.85 (sept, J = 6.8 Hz, 4H, Ar $CH(CH_3)_2$),

1.88 (s, 6H, NCH_3), 1.46 (d, J = 6.8 Hz, 12H, Ar CH(CH_3)$_2$), 1.21 (d, J = 6.9 Hz, 12H, Ar CH(CH_3)$_2$). EIMS (70 eV) m/z: $M^{+\bullet}$ calcd for $C_{29}H_{40}IrN_3O_2$, 655.3; found, 655.5. IR (n-pentane, cm^{-1}): 2052 and 1980 (ν_{CO}). IR (KBr, cm^{-1}): 2041 and 1966 (ν_{CO}). UV-Vis (toluene) λ_{max}, nm (ε): 353 (2300), 380 (sh), 410 (sh).

3.2.5 Preparation of Iridium(III) Complexes

[Ir{PhNC(NMe$_2$)NPh}(cod)(Me)I] (3a). To a 17.0 mM solution of [Ir{PhNC(NMe$_2$)NPh}(cod)] (4.6 mg, 0.0085 mmol) in 0.5 mL of C_6D_6 was added 0.011 mL of a methyl iodide solution in C_6D_6 (1.2 mg, 0.009 mmol). The resulting solution was allowed to stand for 5 h at 20 °C, while it turned pale yellow from bright yellow. The progress of the reaction was monitored by ^{1}H NMR spectroscopy. ^{1}H NMR (300 MHz, C_6D_6, δ): 7.15–7.08 (m, Ar H; this signal partially overlap with the residual solvent peak), 6.97 (d, J = 7.3 Hz, 4 H, Ar H), 6.90 (t, J = 7.3 Hz, 2H, Ar H), 5.05–4.98 (m, 2H, =C*H*CH$_2$–), 3.83–3.76 (m, 2H, =C*H*CH$_2$–), 3.02–2.97 (m, 2H, =CHC*H*$_2$–), 2.51 (s, 3H, IrCH$_3$), 2.05 (s, 6H, NCH_3), 1.85–1.79 (m, 2H, =CHC*H*$_2$–), 1.72–1.65 (m, 2H, =CHC*H*$_2$–), 1.08–1.01 (m, 2H, =CHC*H*$_2$–). EIMS (70 eV) m/z: $M^{+\bullet}$ calcd for $C_{24}H_{31}IIrN_3$, 681.1; found, 681.2.

[Ir{PhNC(NMe$_2$)NPh}(cod)(Me)(OTf)] (4a). To a 18.0 mM solution of [Ir{PhNC(NMe$_2$)NPh}(cod)] (4.9 mg, 0.009 mmol) in 0.5 mL C_6D_6, 0.0011 mL of methyl trifluoromethanesulfonate (1.4 mg, 0.009 mmol). The resulting solution was allowed to stand for 30 min at 20 °C, while it turned pale yellow from bright yellow. The progress of the reaction was monitored by ^{1}H NMR spectroscopy. ^{1}H NMR (300 MHz, C_6D_6, δ): 7.30–7.05 (m, Ar H; these signals partially overlap with the residual solvent peak), 6.92–6.86 (m, 3H, Ar H), 5.26–5.12 (m, 2H, =C*H*CH$_2$–), 4.09–3.93 (m, 2H, =C*H*CH$_2$–), 2.57–2.52 (m, 2H, =CHC*H*$_2$–), 2.25 (s, 3H, IrCH$_3$), 2.15 (s, 6H, NCH_3), 1.65–1.53 (m, 2H, =CHC*H*$_2$–), 1.28–1.16 (m, 2H, =CHC*H*$_2$–), 1.10–1.00 (m, 2H,

=CHCH_2–). ^{19}F NMR (282.4 MHz, C_6D_6, δ): −78.7 ($IrOS(O)_2CF_3$). EIMS (70 eV) *m/z*: $M^{+\bullet}$ calcd for $C_{25}F_3H_{31}IrN_3O_3S$, 703.2; found, 703.4.

3.2.6 Single-crystal X-ray Crystallography

X-ray Crystallographic Analyses. A single crystal of each compound was coated with Paratone N oil and mounted on a glass capillary for data collection at 209(2) (**1b**), 210(2) (**1d**), 190(2) (**1f**) or 190(2) (**2b**) K on a Nonius KappaCCD diffractometer using Mo *Kα* radiation (graphite monochromator). The temperature was controlled by an Oxford Cryostream Cooler (700 series, N_2 gas). Data collection, data reduction, and absorption correction were carried out following standard CCD techniques using the software packages Collect and HKL-2000.[73,74] Final cell constants were calculated from 10100 (**1b**), 5525 (**1d**), 10584 (**1f**) or 8035 (**2b**) reflections from the complete data set. The space groups $P2_1/n$ (**1b**), $P\bar{1}$ (**1d**), $P2_1/c$ (**1f**) and $P\bar{4}n2$ (**2b**) were determined based on systematic absences and intensity statistics. The structures were solved by direct methods and refined by full-matrix least-squares minimization and difference Fourier methods (SHELXTL v.6.12).[75,76] All non-hydrogen atoms were refined with anisotropic displacement parameters. All hydrogen atoms were placed in ideal positions and refined as riding atoms with relative isotropic displacement parameters, with the exception of the alkene hydrogen atoms (=C*H*), which were located in the difference Fourier map and refined with a restrained C–H distance (1.00 Å) and relative isotropic displacement parameters (1.2 times the equivalent isotropic value of the bonded carbon atom). For **1b**, the final full-matrix least-squares refinement converged to $R1$ = 0.0371 and $wR2$ = 0.0505 (F^2, all data). For **1d**, the final full-matrix least-squares refinement converged to $R1$ = 0.0264 and $wR2$ = 0.0531 (F^2, all data). For **1f**, the final full-matrix least-squares refinement converged to $R1$ = 0.0332 and $wR2$ = 0.0468 (F^2, all data). For **2b**, the final full-matrix least-squares refinement converged to $R1$ = 0.0308 and $wR2$ = 0.0873 (F^2, all

data). Tables 2 and 6 contain additional crystal and refinement information. Selected distances and angles are summarized in Tables 3–5 and 7–9.

3.3 Results and Discussion

3.3.1 Synthesis and Characterization of Guanidines

The six neutral *N*,*N*-dialkyl-*N*′,*N*″-diarylguanidines, ArN=C(NR_2)NHAr (where R = Me, Ar = Ph, **a**; R = Et, Ar = Ph, **b**; R = Me, Ar = 4-MeC_6H_4, **c**; R = Et, Ar = 4-MeC_6H_4, **d**; R = Me, Ar = 4-$MeOC_6H_4$, **e**; R = Me, Ar = 2,6-MeC_6H_3, **f**), used as ligand precursors for the iridium(I) complexes were obtained from *N*,*N*′-diarylthiourea and *N*,*N*-dialkylamine building blocks (Scheme 13). While the thioureas ArHNC(S)NHAr with Ar = Ph and 4-MeC_6H_4 are commercially available, those with Ar = 4-$MeOC_6H_4$[69] and 2,6-$Me_2C_6H_3$[69] were synthesized by addition of the appropriate aniline, $ArNH_2$, to the corresponding arylisothiocyanate, ArNCS, under conditions reported for the closely related *N*,*N*′-bis(2,4,6-trimethylphenyl)thiourea.[70]

The diphenyl-substituted guanidines **a** and **b** (PhN=C(NMe_2)NHPh[58] and PhN=C(NEt_2)NHPh[58,62]) were prepared in a convenient one-pot procedure by oxidation of *N*,*N*′-diphenylthiourea with benzyltriethylammonium permanganate[67] in the presence of a two-fold excess of *N*,*N*-dialkylamine and obtained in yields of 70–80% after recrystallization (Scheme 13). Other procedures reported for the desulfurization of *N*,*N*′-diphenylthioureas to produce guanidines involved reaction with $CuSO_4$, SiO_2 and NEt_3 or oxidation with $NaClO_2$ or $NaIO_4$.[61,63]

For guanidines with substituted aryl groups (**c**–**f**), a different method[58,68] has proven more successful. The appropriate thiourea is first converted into the *S*-methyl-*N*,*N*′-diarylisothiourea hydroiodide in a reaction with MeI. The *S*-methyl-*N*,*N*′-

diarylisothiourea hydroiodide is then reacted with the appropriate dialkylamine to afford the *N*,*N*-dialkyl-*N*′,*N*″-diarylguanidinium iodide.

Scheme 13. Synthesis of Guanidines **a**–**f**

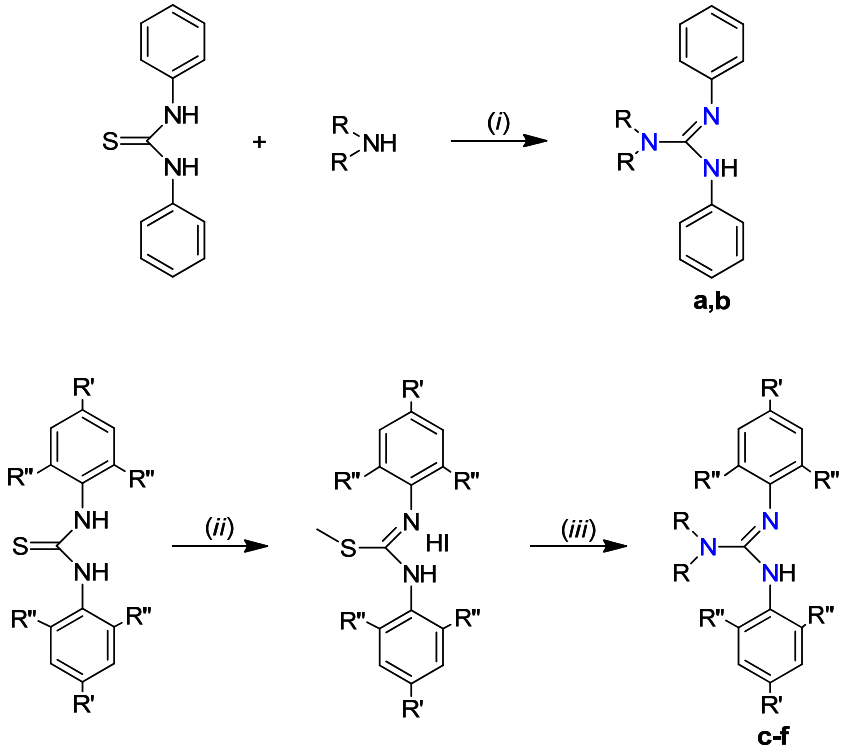

(*i*) $NBzEt_3[MnO_4]$, 0 °C, THF; (*ii*) CH_3I, 70 °C, EtOH; (*iii*) 1. R_2NH, 70 °C, EtOH, 2. Na_2CO_3, 20 °C, H_2O/diethyl ether

a, R = Me; **b**, R = Et; **c**, R = Me, R′ = Me, R″ = H; **d**, R = Et, R′ = Me, R″ = H; **e**, R = Me, R′ = MeO, R″ = H; **f**, R = Me, R′ = H, R″ = Me

Deprotonation of the *N*,*N*-dialkyl-*N*′,*N*″-diarylguanidinium iodide with Na_2CO_3 gave the guanidine in good overall yield (45–75%, after column chromatography or recrystallization; Scheme 13). It should be noted that some of the guanidines in this study are also accessible from diarylcarbodiimides and *N*,*N*-dimethylamine [*i.e.*, $ArN{=}C(NR_2)NHAr$ where R = Me and Ar = Ph, 4-MeC_6H_4 or 4-$MeOC_6H_4$].[60] In various

other cases, the preparation of tetra-substituted lithium guanidinates from carbodiimides and lithium amides has been the method of choice.[54,71,72] But, considering the cost, lower stability and limited availability of carbodiimides, the routes *via* thioureas appeared to be more practical and generally applicable for the targeted range of substitution patterns. The six guanidines described here were characterized by elemental analysis, ^{1}H and ^{13}C NMR spectroscopy, and EI MS.[58]

3.3.2 Synthesis and Characterization of (Cyclooctadiene)iridium(I) Complexes

Two different methods were employed for the synthesis of the air-sensitive Ir^{I}(cod) complexes of the anionic guanidinates, [Ir{ArNC(NR$_2$)NAr}(cod)], **1a**–**g** (Scheme 14). In one method, the guanidine was deprotonated with MeLi at low temperature, followed by reaction of the resulting lithium salt with [{Ir(cod)}$_2$(μ-Cl)$_2$] to yield the yellow iridium(I) complex of the guanidinato(1–) ligand. Alternatively, [{Ir(cod)}$_2$(μ-OMe)$_2$] reacted cleanly with the guanidine to give the desired complex under elimination of methanol (the bridging MeO$^-$ ligands act as an internal base for deprotonation of the guanidines). While the deprotonation–transmetalation route allowed the preparation of the diphenyl, bis(4-methylphenyl) and bis(2,6-dimethylphenyl) derivatives **1a**–**d** and **1f**, it only gave an impure product in poor yield in case of the bis(4-methoxyphenyl) derivative **1e**. This compound was instead directly synthesized from the guanidine using [{Ir(cod)}$_2$(μ-OMe)$_2$]. The second method has also been used to synthesize some of the other complexes and produced results comparable to the initially used deprotonation–transmetalation method.

Scheme 14. Synthesis of the (Cyclooctadiene)iridium(I) Complexes **1a**–**1g**

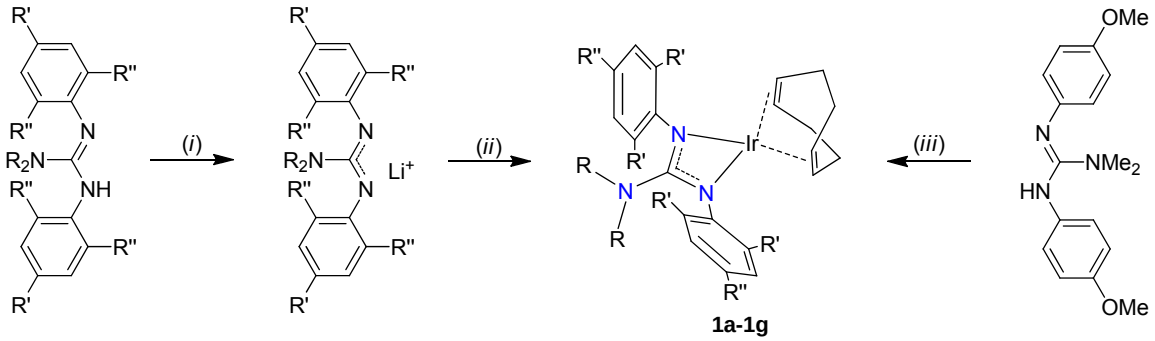

(*i*) MeLi, –40 °C → 20 °C, diethyl ether; (*ii*) [{Ir(cod)}$_2$(μ-Cl)$_2$], 20 °C, diethyl ether; [{Ir(cod)}$_2$(μ-OMe)$_2$], 20 °C, diethyl ether

1a, R = Me, R′, R″ = H; **1b**, R = Et, R′, R″ = H; **1c**, R = Me, R′ = Me, R″ = H; **1d**, R = Et, R′ = Me, R″ = H; **1e**, R = Me, R′ = MeO, R″ = H; **1f**, R = Me, R′ = H, R″ = Me; **1g**, R = Me, R′ = H, R″ = ^{i}Pr

Overall, we found the second method to be more reliable and this method produced good yields more consistently, presumably because it avoids the lithiation step. Complex **1g** (where R = Me and Ar = 2,6-^{i}Pr$_2$C$_6$H$_3$) was prepared from the reaction of [{Ir(cod)}$_2$(μ-Cl)$_2$] and the corresponding lithium guanidinate which was synthesized *in situ* from a known literature procedure.[71,72] The seven guanidinato complexes are well soluble in organic solvents of low-polarity, such as toluene, diethyl ether and *n*-pentane, but only sparingly soluble in acetonitrile. They can be recrystallized from *n*-pentane and were obtained as analytically pure solids in good yields.

All complexes were characterized by ^{1}H and ^{13}C NMR spectroscopy (Figures 1 and 2 for **1a**), mass spectrometry, and UV–Vis spectroscopy, and three complexes (**1b**, **1d**, and **1f**) were also characterized by X-ray crystallography (discussed in Section 3.3.4). Each of the ^{1}H NMR spectra of **1a**–**f** exhibits only four or five resonance signals attributable to the guanidinato-κ^2N,N' ligand and three to the η^4-cod ligand. While the molecules **1b**, **1d**, and **1f** have nearly C_2 symmetry in the solid state, the NMR spectra

indicate fluxional behavior in solution with only one set of resonance signals for the *ortho* (or *ortho* methyl protons in **1f**), *meta* and alkene protons as well as two signals for the cod CH_2 protons.

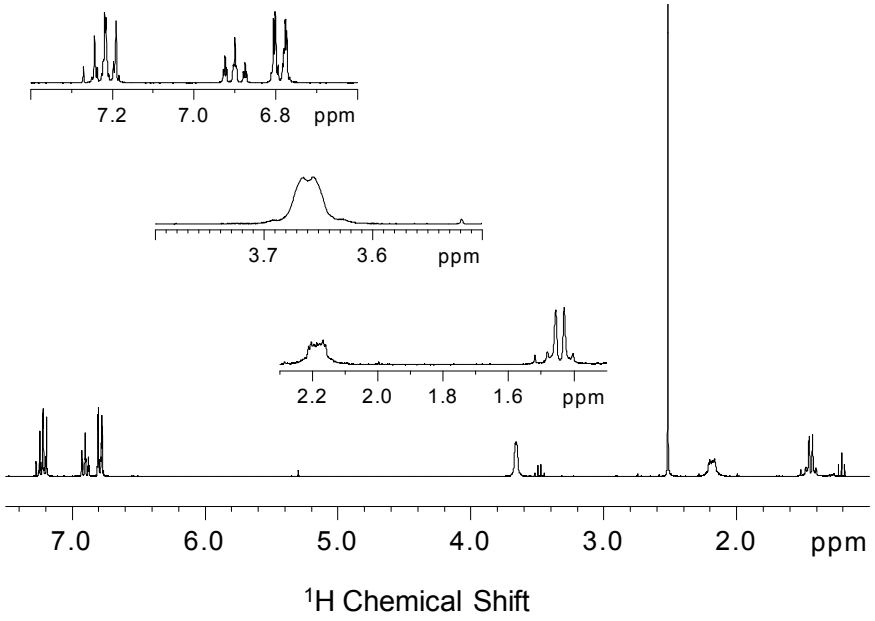

Figure 1. ^{1}H NMR spectrum of (cyclooctadiene)iridium(I) complex **1a** in $CDCl_3$.

The energy barrier for the dynamic process that renders these protons equivalent must be low, because no significant changes were observed in variable-temperature ^{1}H NMR measurements for **1a** and the bulkier **1f** between 20 and –80 °C. Coordination of the guanidinato ligand to the iridium center (**1a**–**g**) is most clearly discerned from the diagnostic peak of the *N*-methyl or *N*-methylene protons, which undergoes an upfield shift of 0.3–0.6 ppm relative to the neutral guanidine. As expected, the $\delta(^1H_{C=CH})$ and $\delta(^{13}C_{C=C})$ values for the cod ligands in **1a**–**g** are significantly lower than those for the free alkene.

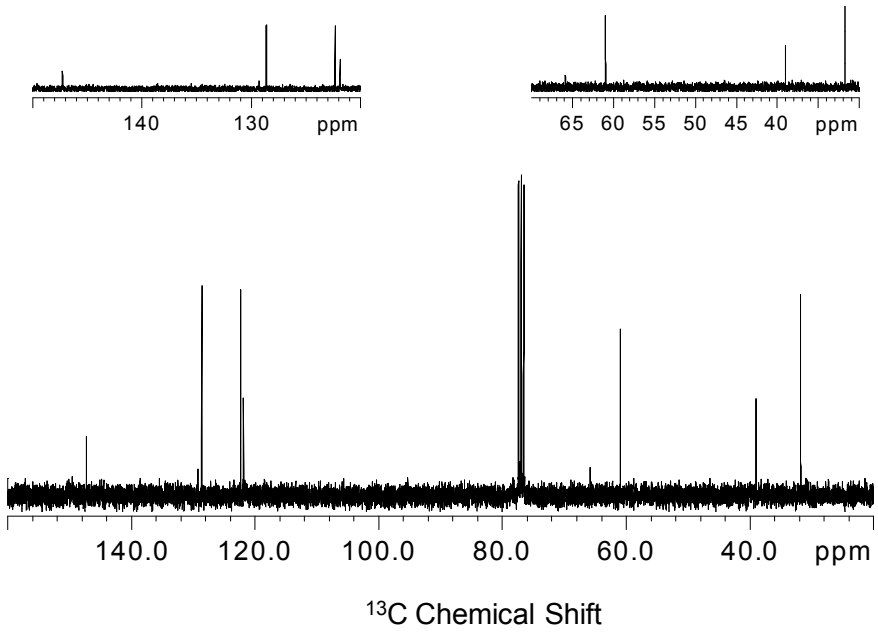

Figure 2. ^{13}C NMR spectrum of (cyclooctadiene)iridium(I) complex **1a** in $CDCl_3$.

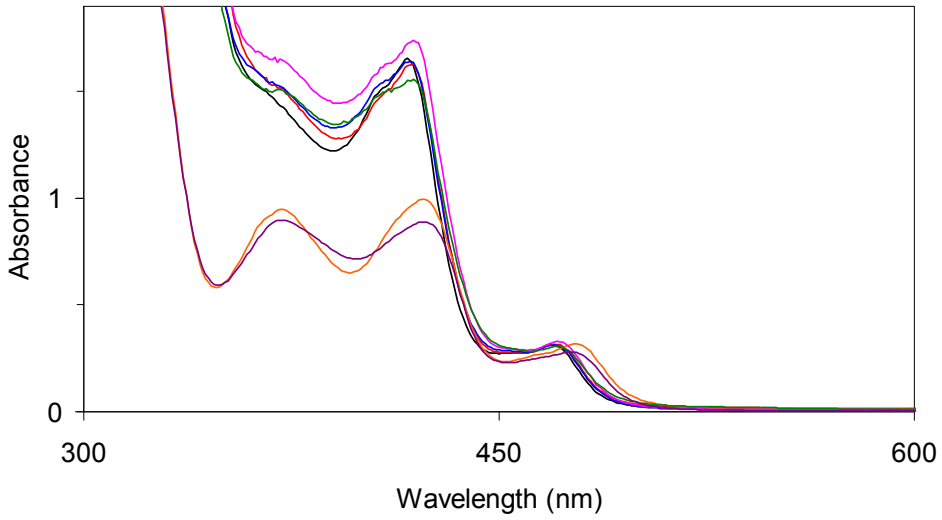

Figure 3. UV−Vis spectra of cyclooctadiene complexes **1a**–**1g** in toluene.

1a, 2.0 mM, black; **1b**, 2.0 mM, red; **1c**, 2.0 mM, blue; **1d**, 2.0 mM, pink; **1e**, 2.0 mM, green; **1f**, 2.0 mM orange; **1g**, 2.0 mM, purple

The UV–Vis spectra of the guanidinato complexes exhibit absorption features near 370, 420 and 470 nm (Figure 3). According to the appearance of the bands below 450 nm, the complexes can be divided into two groups. Complexes **1a**–**e** each display one absorption maximum and a shoulder, whereas the 2,6-dialkylphenyl-substituted complexes **1f** and **1g** show two maxima, each with about half the extinction coefficient observed for **1a**–**e**.

3.3.3 Synthesis and Characterization of Dicarbonyliridium(I) Complexes

As shown in Scheme 15, the reaction of **1a**–**1g** with an excess of CO produced the dicarbonyl complexes [Ir{ArNC(NR$_2$)NAr}(CO)$_2$], **2a**–**2g**. Although the substitution reactions were accompanied by conspicuous color changes, the isolated dicarbonyls appear yellow after recrystallization from *n*-pentane solutions.

Scheme 15. Synthesis of the Dicarbonyliridium(I) Complexes **2a**–**2g**

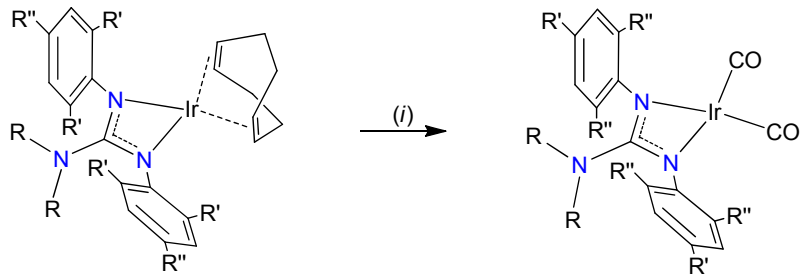

1a-1g **2a-2g**

(*i*) CO(*g*), 20 °C, diethyl ether

2a, R = Me, R′, R″ = H; **2b**, R = Et, R′, R″ = H; **2c**, R = Me, R′ = Me, R″ = H; **2d**, R = Et, R′ = Me, R″ = H; **2e**, R = Me, R′ = MeO, R″ = H; **2f**, R = Me, R′ = H, R″ = Me; **2g**, R = Me, R′ = H, R″ = ^{i}Pr

The ^{1}H NMR spectra of **2a**–**2g** and the solid-state structure of **2b** demonstrate that these complexes are structurally analogous to **1a**–**1g** in that the guanidinato(1–) ligands coordinate the iridium center in a symmetric N,N'-chelating binding mode and the complexes are mononuclear (^{1}H and ^{13}C NMR spectra of **2a** are shown in Figures 4 and 5).

The UV-Vis analysis of these complexes, Figure 6, shows that they can be divided into two groups similar to the cod complexes. Complexes **2a**–**2e** have a shoulder at approximately 355 nm, while **2f** and **2g** each have a peak observed at 353 nm and two broad shoulders at 380 and 410 nm.

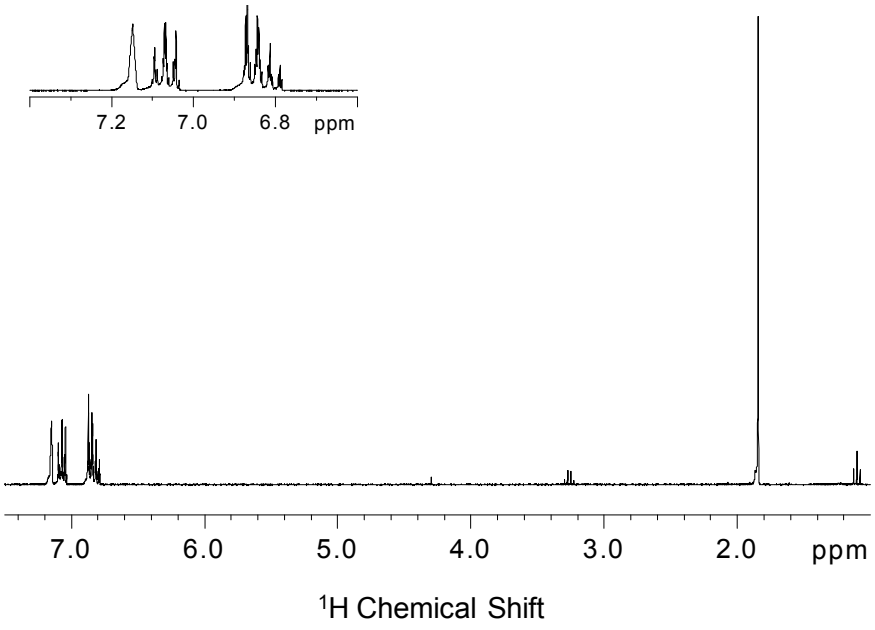

Figure 4. ^{1}H NMR spectrum of dicarbonyliridium(I) complex **2a** in benzene-d_6.

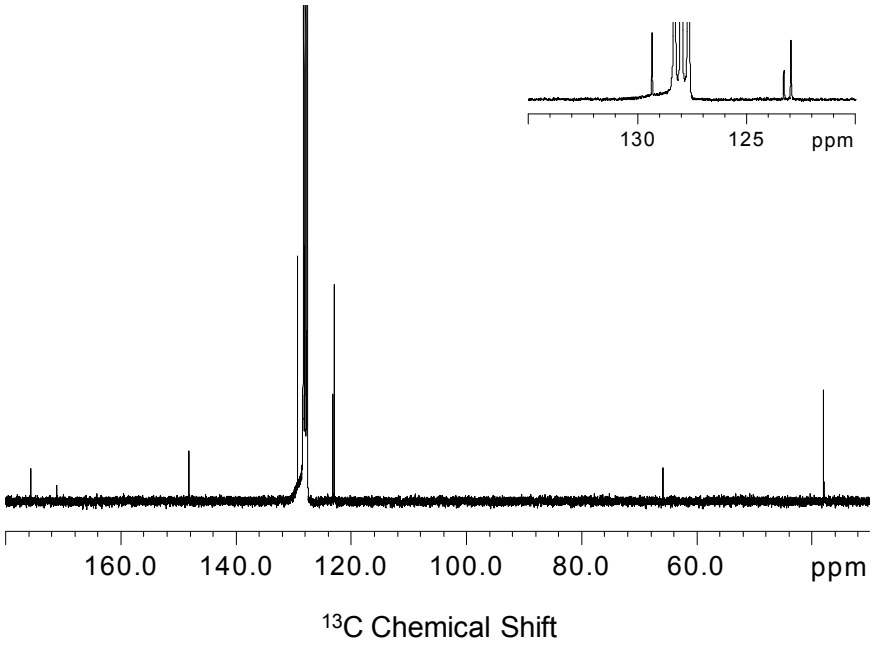

Figure 5. ^{13}C NMR spectrum of dicarbonyliridium(I) complex **2a** in benzene-d_6.

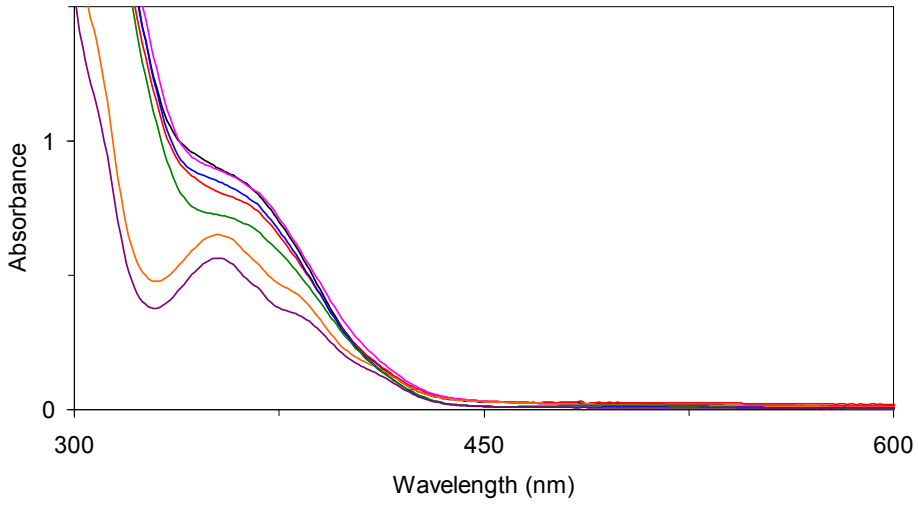

Figure 6. UV–Vis spectra of Dicarbonyliridium(I) complexes **2a**–**2g** in toluene.

2a, 0.52 mM, black; **2b**, 0.50 mM, red; **2c**, 0.52 mM, blue; **2d**, 0.50 mM, pink; **2e**, 0.48 mM, green; **2f**, 0.54 mM orange; **2g**, 0.50 mM, purple

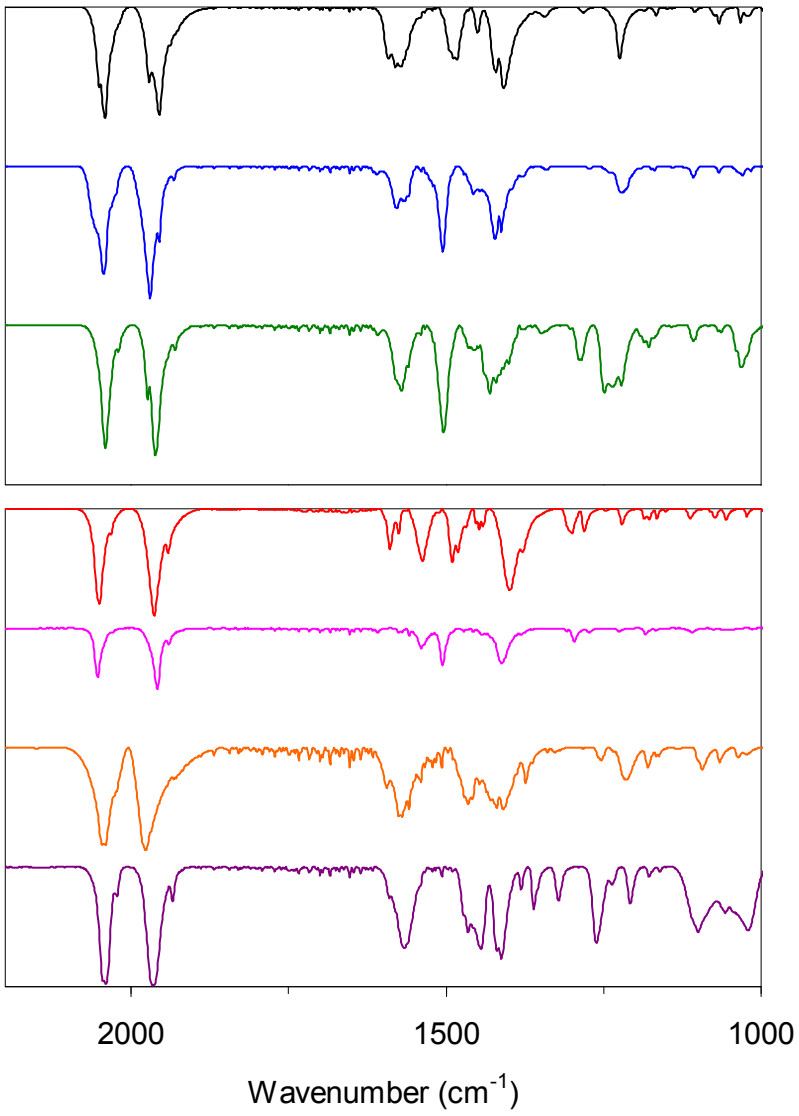

Figure 7. Solid-state IR (KBr) spectra of dicarbonyl complexes **2a**–**2g**.

Top: **2a**, black; **2c**, blue; **2e**, green; Bottom: **2b**, red; **2d**, pink; **2f**, orange; **2g**, purple

Consistent with the presence of two *cis*-coordinated CO ligands, two intense bands were observed in the CO stretching region (ν_{CO}) of the IR spectra of **2a**–**2g** (Figure 7). In *n*-pentane solution, the energies of these bands fall in the ranges of 1980–1983 and 2053–2055 cm^{-1} (*A* and *B* modes), and these data are further discussed in Section 3.3.5 (Table 1). Bands between 1400 and 1600 cm^{-1}, where CN stretching vibrations of the

guanidinato CN_3 core are expected, could be observed in the IR spectra of solid samples. The spectra of the *N*,*N*-dimethyl derivatives **2a**, **2c** and **2e** (R = Me and Ar = Ph, 4-MeC_6H_4, or 4-$MeOC_6H_4$) agree strikingly well and each exhibit three principal features at ca. 1420, 1500 and 1580 cm^{-1} (Figure 7, top). Two of the three guanidinato ν_{CN} modes may be expected to fall into this region. In addition, arene CC stretching (likely at 1500 and 1580 cm^{-1}) and alkyl CH deformation vibrations (<1480 cm^{-1}) may give rise to absorptions in this region. Similarities in the 1400–1600 cm^{-1} region were also observed for the *N*,*N*-diethyl derivatives **2b** and **2d** (R = Et and Ar = Ph or 4-MeC_6H_4) as well as the *N*,*N*′-bis(2,6-dialkylphenyl) derivatives **2f** and **2g** (R = Me and Ar = 2,6-$Me_2C_6H_3$ or 2,6-$^{i}Pr_2C_6H_3$).

Table 1. CO Stretching Frequencies of Dicarbonyl Complexes **2a**–**2g**.

	IR Stretching Frequencies
2a	2052, 1956, 1592, 1580, 1572, 1489, 1483, 1450, 1421, 1409, 1225, 1167, 1067, 1033
2b	2051, 1963, 1589, 1575, 1538, 1490, 1481, 1448, 1399, 1379, 1300, 1281, 1221, 1177, 1165, 1113, 1073, 1056, 1023
2c	2044, 1970, 1578, 1565, 1506, 1422, 1413, 1222, 1107, 1029
2d	2053, 1958, 1540, 1506, 1412, 1297, 1273, 1226, 1184, 1109
2e	2041, 1962, 1581, 1571, 1561, 1504, 1430, 1422, 1401, 1285, 1249, 1236, 1222, 1178, 1108, 1032
2f	2044, 1977, 1594, 1570, 1559, 1465, 1420, 1409, 1374, 1254, 1214, 1180, 1094, 1066, 1037
2g	2041, 1966, 1591, 1566, 1507, 1465, 1445, 1420, 1412, 1381, 1361, 1322, 1262, 1208, 1100, 1021

3.3.4 Crystal Structures

Yellow single crystals of **1b**, **1d**, **1f** and **2b** were grown from concentrated *n*-pentane solutions upon standing at –30 °C. The solid-state molecular structures of these

compounds were determined from crystallographic analyses and confirmed the mononuclear nature of **1b**, **1d**, **1f** and **2b** (Figures 8 and 9 and Tables 2-5 and 6-9).[77-79]

For the cod complexes **1b**, **1d** and **1f**, the Ir–N and Ir–C distances are in the ranges of 2.069(2)–2.099(2) Å and 2.095(3)–2.122(3) Å, respectively, which agree well with values of related complexes.[78-81] Due to the acute bite angles of the chelating guanidinato ligands (N1–Ir–N2, 63.68(9)° for **1b**, 63.76(9)° for **1d** and 63.72(9)° for **1f**), the metal centers adopt a distorted square-planar coordination geometry. The structural analysis also revealed important intra-ligand parameters that provide insight into the bonding of the guanidinato ligands.

Remarkably, the C–N distances in the planar CN_3 core of each complex are nearly identical, 1.346(4)–1.361(4) Å for **1b**, 1.347(4)–1.359(4) Å for **1d** and 1.335(4)–1.354(4) Å for **1f**. These parameters indicate a high degree of π electron delocalization over the CN_3 core, implicating a significant contribution of the iminium / diamide resonance structure (Scheme 11, structure **II**). In accord with the sp^2 hybridization expected for efficient lone-pair donation into the CN_3 unit, the N3 atoms adopt a trigonal-planar geometry with bond angle sums of 359.9(5)° (**1b**), 359.9(5) (**1d**), and 359.8(4)° (**1f**). In contrast, the N1 and N2 atoms are more pyramidalized with bond angle sums ranging from 346.0(3) to 352.5(3)°. Although the C–N3–C and N1–C1–N2 planes are slightly twisted with respect to each other (25.6(1)° for **1b**, 33.9(2)° for **1d** and 18.7(3)° for **1f**), presumably due to minor steric interactions between the NR_2 alkyl and the NAr aryl groups, the conjugation of N3 and C1 *p* orbitals is apparently not disrupted.

Table 2. Crystallographic data and structure refinement for [Ir{PhNC(NEt_2)NPh}(cod)], **1b**, and [Ir{(4-MeC_6H_4)NC(NEt_2)N(4-MeC_6H_4)}(cod)], **1d**.

	1b	**1d**
Empirical formula	$C_{25}H_{32}IrN_3$	$C_{27}H_{36}IrN_3$
Formula weight	566.74	594.79
Crystal habit, color	blade, yellow	prism, yellow
Crystal size	0.17 x 0.08 x 0.03 mm^3	0.27 x 0.17 x 0.16 mm^3
Temperature, T	209(2) K	210(2) K
Wavelength, λ	0.71073 Å	0.71073 Å
Crystal system	monoclinic	triclinic
Space group	$P2_1/n$	$P\bar{1}$
Unit cell dimensions	a = 10.2528(11) Å	a = 9.5336(11) Å
	b = 17.8077(19) Å	b = 9.6634(11) Å
	c = 12.6997(14) Å	c = 13.6109(15) Å
		α = 87.444(5)°
	β = 107.034(5)°	β = 89.343(5)°
		γ = 74.719(5)°
Volume, V	2217.0(4) $Å^3$	1208.4(2) $Å^3$
Z	4	2
Calculated density	1.698 $Mg \cdot m^{-3}$	1.635 $Mg \cdot m^{-3}$
Absorption coefficient, μ	6.038 mm^{-1}	5.543 mm^{-1}
F(000)	1120	592
θ range for data collection	3.03 to 27.89°	3.00 to 27.87°
Limiting indices	$-13 \le h \le 13, -23 \le k \le 23, -16 \le l \le 15$	$-12 \le h \le 12, -12 \le k \le 12, -17 \le l \le 17$
Reflections collected / unique	19485 / 5287 [R(int) = 0.0388]	10816 / 5740 [R(int) = 0.0166]
Completeness to θ	99.8 % (θ = 27.89°)	99.4 % (θ = 27.87°)
Max. and min. transmission	0.8637 and 0.4267	0.4708 and 0.3160
Refinement method	Full-matrix least-squares on F^2	Full-matrix least-squares on F^2
Data / restraints / parameters	5287 / 4 / 276	5740 / 4 / 296
Goodness-of-fit on F^2	1.035	1.118
Final R indices [I>2sigma(I)]	R1 = 0.0246, wR2 = 0.0472	R1 = 0.0225, wR2 = 0.0516
R indices (all data)	R1 = 0.0371, wR2 = 0.0505	R1 = 0.0264, wR2 = 0.0531
Largest diff. peak and hole	0.922 and –0.707 $e \cdot A^{-3}$	1.108 and –1.175 $e \cdot A^{-3}$

Table 3. Selected interatomic distances (Å) for [Ir{PhNC(NEt$_2$)NPh}(cod)], **1b**, and [Ir{(4-MeC$_6$H$_4$)NC(NEt$_2$)N{(4-MeC$_6$H$_4$)}(cod)], **1d**.[a]

1b		**1d**	
Ir–N1	2.069(2)	Ir–N1	2.078(2)
Ir–N2	2.085(2)	Ir–N2	2.087(2)
Ir–C18	2.095(3)	Ir–C20	2.115(3)
Ir–C19	2.120(3)	Ir–C21	2.107(3)
Ir–C22	2.112(3)	Ir–C24	2.111(3)
Ir–C23	2.119(3)	Ir–C25	2.104(3)
N1–C1	1.361(4)	N1–C1	1.347(4)
N1–C2	1.420(4)	N1–C2	1.412(4)
N2–C1	1.348(4)	N2–C1	1.350(4)
N2–C8	1.417(4)	N2–C9	1.411(4)
N3–C1	1.346(4)	N3–C1	1.359(4)
N3–C14	1.469(4)	N3–C16	1.457(4)
N3–C16	1.470(4)	N3–C18	1.472(4)
C18–C19	1.408(5)	C20–C21	1.417(5)
C22–C23	1.408(4)	C24–C25	1.419(5)

[a] Numbers in parentheses are standard uncertainties in the last significant figures. Atoms are labeled as indicated in Figure 8.

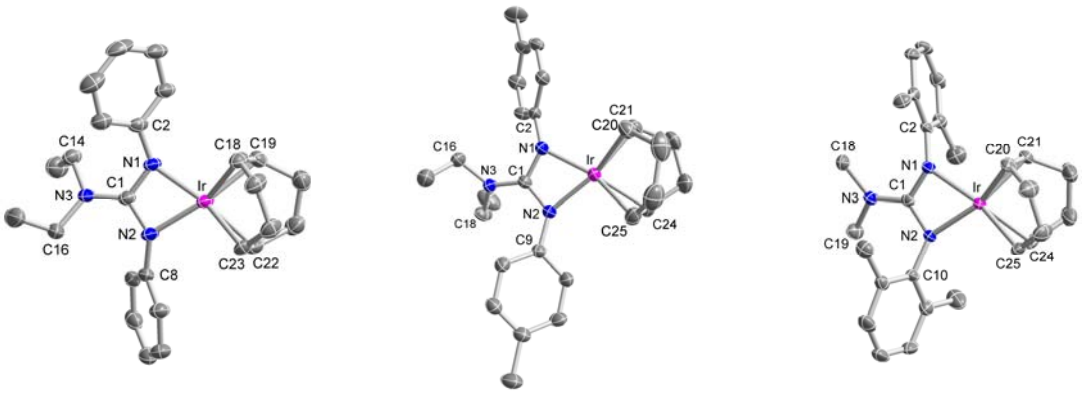

1b **1d** **1f**

Figure 8. Molecular structures of [Ir{PhNC(NEt$_2$)NPh}(cod)], **1b**, [Ir{(4-MeC$_6$H$_4$)NC(NEt$_2$)N{(4-MeC$_6$H$_4$)}(cod)], **1d**, and [Ir{(2,6-MeC$_6$H$_3$)NC(NMe$_2$)N(2,6-MeC$_6$H$_3$)}(cod)], **1f**. Displacement ellipsoids are drawn at the 50% probability level; hydrogen atoms have been omitted for clarity.

Table 4. Selected angles (°) for [Ir{PhNC(NEt_2)NPh}(cod)], **1b**, and [Ir{(4-MeC_6H_4)NC(NEt_2)N{(4-MeC_6H_4)}(cod)], **1d**.[a]

1b		**1d**	
N1–Ir–N2	63.68(9)	N1–Ir–N2	63.76(9)
N1–Ir–C18	101.03(11)	N1–Ir–C20	104.93(11)
N1–Ir–C19	104.94(12)	N1–Ir–C21	101.46(11)
N1–Ir–C22	155.68(12)	N1–Ir–C24	159.33(13)
N1–Ir–C23	159.76(12)	N1–Ir–C25	155.22(12)
N2–Ir–C22	102.75(11)	N2–Ir–C24	105.58(11)
N2–Ir–C23	105.74(11)	N2–Ir–C25	101.77(12)
N2–Ir–C18	153.63(12)	N2–Ir–C20	158.32(12)
N2–Ir–C19	160.38(12)	N2–Ir–C21	155.78(12)
C18–Ir–C19	39.04(13)	C21–Ir–C20	39.21(13)
C22–Ir–C23	38.87(12)	C25–Ir–C24	39.35(13)
C18–Ir–C22	98.44(13)	C24–Ir–C20	90.50(13)
C18–Ir–C23	81.39(13)	C25–Ir–C20	81.34(14)
C22–Ir–C19	81.50(13)	C21–Ir–C24	81.71(13)
C23–Ir–C19	89.67(13)	C25–Ir–C21	98.25(13)
C1–N1–C2	126.5(3)	C1–N1–C2	125.7(2)
C1–N1–Ir	94.32(17)	C1–N1–Ir	93.71(17)
C2–N1–Ir	129.09(19)	C2–N1–Ir	133.00(18)
C1–N2–C8	128.4(3)	C1–N2–C9	126.4(2)
C1–N2–Ir	94.03(18)	C1–N2–Ir	93.23(17)
C8–N2–Ir	129.93(19)	C9–N2–Ir	132.86(18)
C1–N3–C14	120.5(3)	C1–N3–C16	121.4(3)
C1–N3–C16	121.3(3)	C1–N3–C18	121.0(2)
C14–N3–C16	118.1(2)	C16–N3–C18	117.5(3)
N2–C1–N1	108.0(3)	N1–C1–N2	109.3(2)
N3–C1–N1	125.3(3)	N1–C1–N3	125.4(2)
N3–C1–N2	126.8(3)	N2–C1–N3	125.3(3)

[a] Numbers in parentheses are standard uncertainties in the last significant figures. Atoms are labeled as indicated in Figure 8.

Table 5. Selected dihedral angles (°) for [Ir{PhNC(NEt_2)NPh}(cod)], **1b**, and [Ir{(4-MeC_6H_4)NC(NEt_2)N{(4-MeC_6H_4)}(cod)], **1d**.[a]

1b		**1d**	
N1–C1–N2 / N1–Ir–N2	1.3(2)	N1–C1–N2 / N1–Ir–N2	1.6(3)
N1–Ir–N2 / C18–Ir–C19	84.8(2)	N1–Ir–N2 / C20–Ir–C21	84.9(2)
N1–Ir–N2 / C22–Ir–C23	85.9(2)	N1–Ir–N2 / C24–Ir–C25	84.7(2)
C18–Ir–C19 / C22–Ir–C23	86.7(1)	C20–Ir–C21 / C24–Ir–C25	87.1(2)
C14–N3–C16 / N1–C1–N2	25.6(1)	C16–N3–C18 / N1–C1–N2	33.9(2)
(N1,C1,N2,N3) / (C2→C7)[b]	54.5(1)	(N1,C1,N2,N3) / (C2→C7)[b]	48.0(1)
(N1,C1,N2,N3) / (C8→C13)[b]	51.7(1)	(N1,C1,N2,N3) / (C9→C14)[b]	46.1(1)

[a] Numbers in parentheses are standard uncertainties in the last significant figures. Atoms are labeled as indicated in Figure 8. [b] Angle between the least-squares planes of the guanidinate atoms (N1, C1, N2, and N3) and the aryl ring atoms (*e.g.*, C2, C3, C4, C5, C6, and C7).

In the dicarbonyl complex **2b**, the Ir–N and Ir–C distances are 2.069(2) Å and 1.832(9) Å, respectively, which agree well with values of related dicarbonyl complexes.[82,83] Other structural features for **2b** are similar to the Ir^{I}(cod) complexes **1b**, **1d** and **1f**. The bite angle for **2b** is 63.8(3)° and the metal center adopts a distorted square-planar coordination geometry. Considering the standard uncertainties, the C–N distances in the planar CN_3 core of this complex are also nearly identical, 1.338(11) Å and 1.359(8) Å. The N3 atoms adopt a trigonal-planar geometry with bond angle sum of 360.0(7)° while the N2 atom is more pyramidalized with bond angle sum of 354.5(6)°. The C–N2–C and N–C1–N planes are still slightly twisted with respect to each other (39.6(6)°).

Table 6. Crystallographic data and structure refinement for [Ir{(2,6-$Me_2C_6H_3$)NC(NMe_2)N(2,6-$Me_2C_6H_3$)}(cod)], **1f**, and [Ir{PhNC(NEt_2)NPh}$(CO)_2$], **2b**.

	1f	**2b**
Empirical formula	$C_{27}H_{36}IrN_3$	$C_{19}H_{20}IrN_3O_2$
Formula weight	594.79	514.58
Crystal habit, color	needle, yellow	rod, colorless
Crystal size	0.38 x 0.05 x 0.03 mm^3	0.36 x 0.08 x 0.08 mm^3
Temperature, T	190(2) K	190(2) K
Wavelength, λ	0.71073 Å	0.71073 Å
Crystal system	monoclinic	tetragonal
Space group	$P2_1/c$	$P\bar{4}n2$
Unit cell dimensions	a = 15.1915(16) Å	a = 17.3359(18) Å
	b = 7.6661(9) Å	
	c = 20.783(3) Å	c = 6.1770(7) Å
	β = 94.776(5)°	
Volume, V	2412.0(5) $Å^3$	1856.4(3) $Å^3$
Z	4	4
Calculated density	1.638 $Mg \cdot m^{-3}$	1.841 $Mg \cdot m^{-3}$
Absorption coefficient, μ	5.554 mm^{-1}	7.209 mm^{-1}
F(000)	1184	992
θ range for data collection	2.83 to 27.49°	3.32 to 27.87°
Limiting indices	$-19 \le h \le 19$, $-9 \le k \le 9$, $-26 \le l \le 26$	$-22 \le h \le 19$, $-22 \le k \le 22$, $-8 \le l \le 8$
Reflections collected / unique	19363 / 5510 [R(int) = 0.0369]	11591 / 2215 [R(int) = 0.0253]
Completeness to θ	99.9 % (θ = 27.49°)	99.8 % (θ = 27.87°)
Max. and min. transmission	0.8736 and 0.2267	0.5963 and 0.1812
Refinement method	Full-matrix least-squares on F^2	Full-matrix least-squares on F^2
Data / restraints / parameters	5510 / 4 / 298	2215 / 0 / 117
Goodness-of-fit on F^2	1.029	1.210
Final R indices [I>2sigma(I)]	R1 = 0.0224, wR2 = 0.0437	R1 = 0.0275, wR2 = 0.0857
R indices (all data)	R1 = 0.0332, wR2 = 0.0468	R1 = 0.0308, wR2 = 0.0873
Absolute structure parameter		0.08(2)
Largest diff. peak and hole	1.386 and –0.775 $e \cdot A^{-3}$	1.281 and –0.571 $e \cdot A^{-3}$

Table 7. Selected interatomic distances (Å) for [Ir{(2,6-$Me_2C_6H_3$)NC(NMe_2)N(2,6-$Me_2C_6H_3$)}(cod)], **1f**, and [Ir{PhNC(NEt_2)NPh}$(CO)_2$], **2b**.[a]

1f		**2b**	
Ir–N1	2.075(2)	Ir–N1	2.069(6)
Ir–N2	2.099(2)	Ir–C10	1.832(9)
Ir–C20	2.101(3)		
Ir–C21	2.119(3)		
Ir–C24	2.102(3)		
Ir–C25	2.122(3)		
N1–C1	1.351(3)	N1–C1	1.359(8)
N1–C2	1.426(4)	N1–C2	1.419(9)
N2–C1	1.335(4)	N2–C1	1.338(11)
N2–C10	1.423(4)	N2–C8	1.480(7)
N3–C1	1.354(4)		
N3–C18	1.457(4)		
N3–C19	1.458(4)		
C20–C21	1.416(5)	C10–O	1.171(11)
C24–C25	1.401(5)		

[a] Numbers in parentheses are standard uncertainties in the last significant figures. Atoms are labeled as indicated in Figure 9.

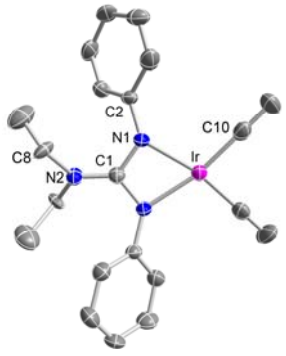

2b

Figure 9. Molecular structure of [Ir{PhNC(NEt_2)NPh}$(CO)_2$], **2b**. Displacement ellipsoids are drawn at 50% probability level; hydrogen atoms have been omitted for clarity.

Table 8. Selected angles (°) for [Ir{(2,6-$Me_2C_6H_3$)NC(NMe_2)N(2,6-$Me_2C_6H_3$)}(cod)], **1f**, and [Ir{PhNC(NEt_2)NPh}($CO)_2$], **2b**.[a]

1f		**2b**	
N1–Ir–N2	63.72(9)	N1–Ir–N1#1	63.8(3)
N1–Ir–C20	101.35(11)	C10–Ir–N1	103.9(3)
N1–Ir–C21	101.61(11)	C10#1–Ir–N1	167.5(3)
N1–Ir–C24	154.07(12)		
N1–Ir–C25	162.77(12)		
N2–Ir–C24	103.83(11)		
N2–Ir–C25	107.23(11)		
N2–Ir–C20	155.05(11)		
N2–Ir–C21	156.98(12)		
C20–Ir–C21	39.21(13)	C10#1–Ir–C10	88.5(5)
C24–Ir–C25	38.73(13)		
C20–Ir–C24	97.30(13)		
C20–Ir–C25	81.31(13)		
C24–Ir–C21	81.80(13)		
C21–Ir–C25	91.22(13)		
C1–N1–C2	123.2(2)	C1–N1–C2	126.0(6)
C1–N1–Ir	93.26(17)	C1–N1–Ir	94.5(4)
C2–N1–Ir	129.56(18)	C2–N1–Ir	133.7(5)
C1–N2–C10	124.5(2)		
C1–N2–Ir	92.69(17)		
C10–N2–Ir	135.27(19)		
C1–N3–C18	121.6(2)	C1–N2–C8	120.9(4)
C1–N3–C19	122.4(3)	C8#1–N2–C8	118.2(7)
C18–N3–C19	115.8(2)		
N2–C1–N1	110.2(2)	N1#1–C1–N1	107.2(8)
N1–C1–N3	124.1(3)	N2–C1–N1	126.4(4)
N2–C1–N3	125.6(3)		

[a] Numbers in parentheses are standard uncertainties in the last significant figures. Atoms are labeled as indicated in Figure 9. Symmetry operations: #1, –y+3/2, –x+3/2, –z+3/2.

Table 9. Selected dihedral angles (°) for [Ir{(2,6-$Me_2C_6H_3$)NC(NMe_2)N(2,6-$Me_2C_6H_3$)}(cod)], **1f**, and [Ir{PhNC(NEt_2)NPh}$(CO)_2$], **2b**.[a]

1f		**2b**	
N1–C1–N2 / N1–Ir–N2	3.5(3)	N1–C1–N1#1 / N1–Ir–N1#1	0
N1–Ir–N2 / C20–Ir–C21	89.9(2)		
N1–Ir–N2 / C24–Ir–C25	86.1(2)		
C20–Ir–C21 / C24–Ir–C25	87.3(1)		
C18–N3–C19 / N1–C1–N2	18.7(3)	C8–N2–C8#1 / N1–C1–N1#1	39.6(6)
(N1,C1,N2,N3) / (C2→C7)[b]	78.6(1)	(N1,C1,N1#1,N2) / (C2→C7)[b]	44.7(3)
(N1,C1,N2,N3) / (C10→C15)[b]	74.1(1)		

[a] Numbers in parentheses are standard uncertainties in the last significant figures. Atoms are labeled as indicated in Figure 9. Symmetry operations: #1, –y+3/2, –x+3/2, –z+3/2. [b] Angle between the least-squares planes of the guanidinate atoms (N1, C1, N2, and N3) and the aryl ring atoms (*e.g.*, C2, C3, C4, C5, C6, and C7).

The intra-ligand structural features of **1b**, **1d**, **1f** and **2b** are unusual, because complexes of guanidinato(1–) ligands typically display more localized bonding with a longer C–N bond to the non-coordinated nitrogen atom and shorter ones to the metal-coordinated nitrogen atoms.[1,7,47,48,50-53,84,85] Thus, the bonding in those guanidinate systems is best described by a relatively larger contribution of the amine / amidinate resonance structures (**I** and **III**, Scheme 11). On the other hand, the greater extent of delocalization observed for **1b**, **1d**, **1f** and **2b** is precedent in complexes of Ti^{IV},[86,87] Zr^{IV},[4] and Nb^{V}.[5] It has been argued that significant involvement of the lone pair of the NR_2 nitrogen atom is due to the ligands' coordination to an electron-deficient metal center. In this context, the observations made here for low-valent d^8 iridium(I) complexes may seem surprising. Presumably, the π-acceptor alkene ligand enhances the electron-releasing character of the guanidinato ligand and thus facilitates participation of the NR_2 lone pair in CN_3 π bonding.

3.3.5 Investigation of Ligand Donor Strength

To assess the donor strength of the guanidinato ligands **a**–**g**, we initially turned to the ^{13}C NMR spectroscopy of **1a**–**1g** to gauge the extent of Ir-to-cod π back-bonding. Complexes **1a**–**1g** exhibit ^{13}C resonance signals for the alkene carbon atoms in the range of 58.7–61.0 ppm (Table 10). A subtle trend was observed within our guanidinato cod complexes. The $\delta(^{13}C_{C=C})$ values consistently decrease with more electron donating substituents (**1a** → **1f**) on the guanidinato ligand. This indicates higher π back-donation to the cod ligands and thus an increase in ligand donor strength. These values are upfield-shifted compared to corresponding signals in Ir^{I}(cod) complexes of tris(1-pyrazolyl)borate-κ^2 (Tp) and β-diketiminate ligands, which appear in the range of 63.2–66.7 ppm.[80,81] Lower $\delta(^{13}C_{C=C})$ values reflect increased π back-donation into the alkene π^* orbitals caused by increased electron density at the metal center. Therefore, the dialkyldiarylguanidinates may be considered stronger donors than κ^2-binding tris(1-pyrazolyl)borates and β-diketiminates. They are still weaker donors than tris(1-pyrazolyl)borate-κ^3 and cyclopentadienyl ligands (54.1 and 45.5–53.1 ppm).[80,88]

Table 10. ^{13}C Chemical Shifts, δ(ppm), of Cyclooctadiene Complexes **1a**–**1g** and CO Stretching Frequencies, ν(cm^{-1}), of Dicarbonyl Complexes **2a**–**2g**.

	$\delta(^{13}C_{C=C})$		ν_{CO}	Average ν_{CO}
1a	61.0	**2a**	2055, 1983	2019.0
1b	60.8	**2b**	2055, 1982	2018.5
1c	60.8	**2c**	2054, 1981	2017.5
1d	60.7	**2d**	2053, 1980	2016.5
1e	60.7	**2e**	2053, 1980	2016.5
1f	58.8	**2f**	2053, 1980	2016.5
1g	58.7	**2g**	2052, 1980	2016.0

We also investigated the ligand donor strength of the guanidinato ligands by analysis of the IR spectroscopic data for the dicarbonyl complexes, **2a**–**2g**. A similar relationship exists for the CO stretching frequencies as for the ^{13}C NMR peaks of the alkene complexes, lower ν_{CO} values reflect increased π back-donation into the CO π^* orbitals caused by increased electron density at the metal center. Complexes **2a**–**2g** show average CO stretching frequencies in the solution IR spectrum (*n*-pentane) in the range of 2016–2019 cm^{-1} (Table 10). A subtle trend was also observed within our guanidinato dicarbonyl complexes. The ν_{CO} values consistently decrease with more electron donating substituents (**2a** → **2f**) on the guanidinato ligand. These values are observed at lower energies compared to corresponding signals in $Ir^{I}(CO)_2$ complexes of tris(1-pyrazolyl)borate-κ^2 and β-diketiminate ligands, which appear in the range of 2020–2045 cm^{-1} (average values).[81,89] The tris(1-pyrazolyl)borate-κ^3 and cyclopentadienyl ligands (average ν_{CO}, 2011 and 1997 cm^{-1}) are still stronger donating ligands than the guanidinato ligands.[89,90] The IR data for the dicarbonyl complexes confirm the data observed for the cod complexes and show that the guanidinato ligands are stronger donors than other bidentate nitrogen-donor ligands.

3.3.6 Formation of Iridium(III) Complexes from Oxidative Addition of MeI and MeOTf

The iridium(I) complexes have been synthesized and fully characterized as discussed above. Here, the reaction of **1a** with MeI and MeOTf will be discussed along with the observation of six-coordinate iridium(III) complexes as products from these reactions (Scheme 16). Oxidative addition reactions using iridium and rhodium complexes are well-known in the literature because of the ability of these metal centers to be supported in the +1 and +3 oxidation states.[91-93] Reactions with MeI and MeOTf may

be good test reactions to probe the accessibility of iridium complexes from the [Ir(L)(cod)] complexes.

Scheme 16. Generation of [Ir{PhNC(NMe$_2$)NPh}(cod)(Me)I], **3a**, and [Ir{PhNC(NMe$_2$)NPh}(cod)(Me)(OTf)], **4a**

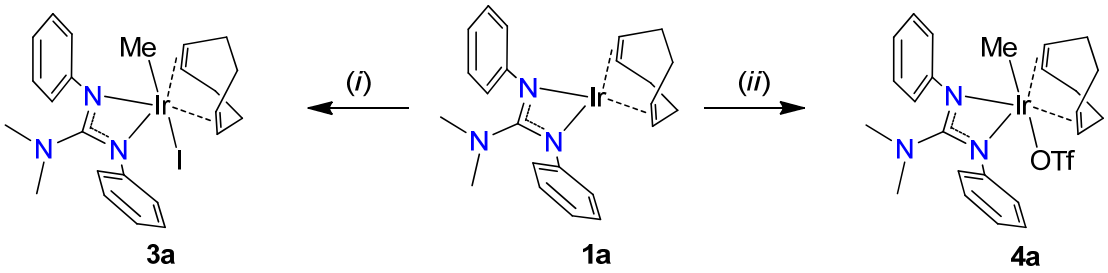

3a **1a** **4a**

(*i*) 1 or 10 equiv of MeI, 20 °C, benzene-d_6 or toluene; (*ii*) 1 or 10 equiv of MeOTf, 20 °C, benzene-d_6 or toluene

The reaction of a 2 mM solution of **1a** with 10 equiv of MeI occurs at 20 °C with a $t_{1/2}$ of ca. 1650 s as observed by UV-Vis spectroscopy. The reaction profile, shown in Figure 10, shows the peaks from the starting material decaying after addition of MeI to form a product with a featureless spectrum over approximately 4 h. Following the decay of **1a** (inset of Figure 10), only a small increase of the absorbance at 417 nm was observed over another 12 h indicating that the product is fairly stable under these reaction conditions. This reaction was also investigated by ^{1}H NMR spectroscopy. The ^{1}H NMR experiment was carried out with the addition of 1 equiv of MeI to a 17 mM solution of **1a** in benzene-d_6 at 20 °C. The solution turned pale yellow from bright yellow over 5 h, and during the same time period the ^{1}H NMR peaks of **1a** disappeared while new peaks were formed. The ^{1}H NMR spectrum of **3a** has three peaks for the aromatic protons, two broad multiplets for the alkene protons and four multiplets for the CH_2 groups of the cod ligand and two sharp singlets for the NCH_3 and $IrCH_3$ protons. The presence of two sets of

resonances for the cod ligand indicates that the product of this reaction, **3a**, has lower symmetry than **1a**. The ^{1}H NMR spectrum is consistent with the presence of the Me and OTf ligands *trans* to one another. If these ligands were in a *cis* configuration, the product would have even lower symmetry and thus a larger number of peaks in the ^{1}H NMR spectrum. The EI MS analysis of the products has a peak at m/z = 681 with the expected isotope pattern for a mononuclear iridium complex, and this peak is assigned to the octahedral iridium(III) complex, [Ir{PhNC(NMe$_2$)NPh}(cod)(Me)I] (**3a**), shown in Scheme 16. The cationic complex [Ir{PhNC(NMe$_2$)NPh}(cod)(Me)]$^+$ that would arise from loss of I$^-$ from **3a** was not detected by electrospray ioniziation mass spectrometry (ESI MS). This complex is fairly stable for at least 5 d in solution at 20 °C with only minor decay occurring. The yield of **3a** was determined by addition of 1,2-dichloroethane (5 equiv) as an internal standard. Comparison of the alkene protons to that of the internal standard indicates **3a** accumulates in ca. 65% yield.

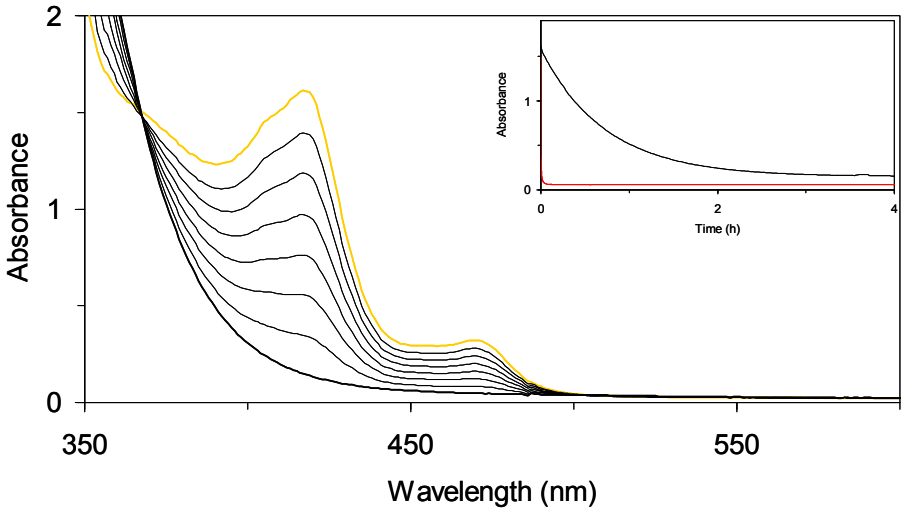

Figure 10. Reaction of **1a** with 10 equiv of MeI at 20 °C in toluene as monitored by UV-Vis spectroscopy. Inset: Time courses of the reactions of **1a** with MeI [λ = 417 nm (—, black)] and MeOTf [λ = 417 nm (—, red)].

When 10 equiv of MeOTf was added to a 2 mM solution of **1a** at 20 °C, a nearly immediate reaction was observed by UV-Vis spectroscopy. The time course of this reaction, shown in the inset of Figure 10, reaches a minimum at ca. 300 s ($t_{1/2}$ of <10 s) with no observable increase over at least 4 h. The color of the solution turned pale yellow from bright yellow over this time. An NMR experiment was done with 1 equiv of MeOTf being added to an 18 mM solution of **1a** in benzene-d_6 at 20 °C. Within 30 min after addition of MeOTf, new resonance signals were observed that could be assigned to an octahedral iridium(III) species, [Ir{PhNC(NMe$_2$)NPh}(cod)(Me)(OTf)], **4a**, (Scheme 16). This complex is stable for at least 5 d in solution, with only minor decay of the newly formed species occurring. The ^{1}H NMR spectrum of **4a** is nearly identical to that of **3a**, and the ^{19}F NMR spectrum shows a signal at −78.7 ppm for the fluorine atoms of the TfO$^-$ ligand (IrOTf). EI MS analysis of a nearly analogous experiment (1.1 equiv MeOTf added in benzene-d_6 at 20 °C) was performed with the observation of a peak at m/z = 703 which is assigned to **4a**. Similar to **3a**, no peaks can be assigned to complex **4a** in the ESI MS analysis of the reaction mixture. The yield of **4a** was determined by addition of 1,2-dichloroethane (5 equiv) as an internal standard. Comparison of the alkene protons to that of the internal standard indicates **4a** accumulates in ca. 61% yield.

When comparing the half-lives of these two reactions, one major difference is recognized. The reaction with MeOTf ($t_{1/2}$ of <10 s by UV-Vis spectroscopy) is significantly faster than that of MeI ($t_{1/2}$ of ca. 1650 s) under the same reaction conditions (Figure 10). The faster reaction observed for MeOTf compared to MeI may be explained based on the leaving ability of the anion. The TfO$^-$ anion is a better leaving group than I$^-$ and this may cause the differences observed in the reaction of these substrates. Because of this trend (i.e. MeOTf > MeI) the mechanism likely involves nucleophilic attack of the iridium(I) center on the methyl carbon of MeI or MeOTf rather than a radical-based pathway.

3.4 Conclusion

The synthesis and characterization of Ir^{I}(cod) and $Ir^{I}(CO)_2$ complexes supported by guanidinato(1−) ligands has been described in this chapter. These complexes have been characterized by NMR spectroscopy, EI MS and elemental analysis. Some of the complexes have also been characterized by single-crystal X-ray diffraction and the analysis shows that these newly synthesized species are mononuclear iridium(I) complexes with the guanidinato ligand coordinating in an N,N′-chelating binding mode. The ^{13}C NMR and IR analysis of these complexes indicate that the guanidinato ligands function as more strongly donating ligands than other monoanionic bidentate nitrogen-donor ligands. Finally, it was shown that one of the cod complexes reacts with MeI and MeOTf to form stable octahedral iridium(III) complexes by oxidative addition reactions.

CHAPTER 4
IDENTIFICATION AND CHARACTERIZATION OF REACTIVE (ALKENE)PEROXOIRIDIUM(III) INTERMEDIATES

4.1 Introduction

In this chapter, the reaction of the (alkene)(guanidinato)iridium(I) complexes [Ir{ArNC(NR_2)NAr}(cod)], **1a**−**1g**, with O_2 will be discussed. We have observed using UV−Vis spectroscopy that the substituents of the guanidinato ligands have a significant effect on the half-lives of these reactions. Increasing the electron donating ability of the ligand further destabilizes the metal center and decreases the $t_{1/2}$ of the reaction. Sterics of the guanidinato ligand also play a role in the reactions with O_2. It was observed from UV-Vis spectroscopy that substitution in the *ortho* position of the aryl ring has a decelerating affect on the reaction with O_2. We have determined by multi-dimensional NMR spectroscopy and IR that intermediates are formed in the reaction of the Ir^I(cod) complexes with O_2. Identification and characterization of the (alkene)peroxoiridium(III) intermediates will be discussed. These intermediates are reactive, and have shown the ability to transfer oxygen to PPh_3 to form $OPPh_3$ and also react with CO(*g*) to release unmodified cod. Finally, it has been observed that these intermediates decay through a mechanism where oxidation of the alkene occurs. Upon addition of cod to the decay products, formation of an oxidized organic species, 4-cycloocten-1-one, and reformation of some of the starting material, **1a**−**1g**, occurs. Part of this chapter was published in 2012.[57]

4.2 Experimental Section

4.2.1 Material and Methods

Materials. All reagents and solvents were purchased from commercial sources and were used as received, unless noted otherwise. Diethyl ether and toluene were deoxygenated by sparging with N_2 and purified by passage through two packed columns of molecular sieves under an N_2 pressure (MBraun solvent purification system). *n*-Pentane was dried over Na and distilled under N_2 prior to use.[59] Preparation and handling of air- and moisture-sensitive materials were carried out under an inert gas atmosphere by using either standard Schlenk and vacuum line techniques or a glovebox. Dioxygen was dried by passage through a short column of Drierite. Isotope-enriched $^{18}O_2$ (97% ^{18}O) was purchased from Cambridge Isotope Laboratories, Andover, MA, USA.

Physical Methods. NMR spectra were recorded on a Bruker Avance MicroBay 300, Avance DPX 300, Avance 400 or Avance 500 spectrometer at ambient temperature, unless noted otherwise. ^1H, ^{13}C and ^{31}P chemical shifts are reported in parts per million (ppm) and were referenced to residual solvent peaks (for ^1H and ^{13}C NMR spectra) or an external standard [H_3PO_4 (85%, δ = 0 ppm) for ^{31}P NMR spectra]. Two-dimensional correlated spectroscopy (COSY) and heteronuclear single-quantum coherence (HSQC) experiments were carried out on a Bruker Avance 500 spectrometer at 25 °C using the gradient versions of the COSY and HSQC pulse sequences, and the data were processed using the TopSpin 2.1 software package. For $^1H,^1H$ COSY, typical measurement parameters were as follows: time domain data points (TD), 2048 for TD and 512 for TD1; number of scans (NS), 8; and number of dummy scans (DS), 32. The data were processed with zero-filling to 4096 (TD) and 512 (TD1). For $^1H,^{13}C$ HSQC, typical measurement parameters were as follows: 2048 for TD and 200 for TD1; NS, 16; and DS, 16. The data were processed with zero-filling to 2048 (TD) and 1024 (TD1). Self-

diffusion coefficients (*D*) were determined from stimulated-echo experiments using bipolar gradients acquired in two-dimensional mode (stebpgp1s). These experiments were performed on a Bruker Avance 400 spectrometer at 25 °C. Prior to each experiment, the diffusion time (delay between the midpoints of the gradients, Δ) and gradient length (δ) were optimized using the one-dimensional version of the pulse sequence (stebpgp1s1d). The data acquisition for each diffusion experiment took approximately 30 min. Data processing and analysis to determine *D* were carried out within the TopSpin 2.1 software package.

IR spectra were recorded on a Bruker Vertex 70 Fourier-transform IR spectrometer with solid samples prepared by grinding the solid compound with KBr and pressing the mixture into a disk. Low-resolution mass spectral data were acquired on a quadrupole ion trap ThermoFinnigan LCQ Deca mass spectrometer using an electrospray ionization source or on a single quadrupole ThermoFinnigan Voyager mass spectrometer using an electron impact ionization source (equipped with a solids probe). High-resolution mass spectral data were acquired on a time-of-flight Waters GCT Premier mass spectrometer using an electron impact ionization source (equipped with a solids probe). UV–Vis spectra were recorded on an HP 8453A diode array spectrophotometer (Agilent Technologies) with samples maintained at low temperature using a cryostat from Unisoku Scientific Instruments, Japan.

4.2.2 Reactions of (Cyclooctadiene)iridium(I) Complexes with O_2

Reactions of [Ir{ArNC(NR$_2$)NAr}(cod)] Complexes with O_2. A 2 mM solution of the [Ir{ArNC(NR$_2$)NAr}(cod)] (**1a**–**1g**) complex (0.002 mmol) in 1 mL of toluene was placed in a 0.5-cm UV–Vis cuvette, precooled to 0 °C and purged with O_2 (40 s).

Generation and Characterization of [Ir{ArNC(NR$_2$)NAr}(η^4-cod)(η^2-O$_2$)] Complexes 5a–5e. In a typical experiment, a 15–20 mM solution of **1a**–**1e** (0.0075–0.010 mmol) in 0.5 mL of C_6D_6 was placed in an NMR tube and purged with O_2(*g*) at 20 °C for 40 s. The progress of the reaction was monitored by ^{1}H NMR spectroscopy. Under these conditions, **1a**–**1e** (bright yellow solutions) converted into the corresponding intermediates, **5a**–**5e** (pale yellow), in about 2–3 h, and the intermediates were typically decayed (dark green solution) within 20 h after the addition of O_2. For quantification, 5 equiv of 1,2-dichloroethane (3.0–3.9 μL, 3.8–4.9 mg, 0.038–0.050 mmol) was added to the solution of **5a**, and the yield was estimated by comparing the integrations of the 1,2-dichloroethane (δ, 2.90 ppm) and alkene proton signals (ca. 75%). For IR spectroscopy, 0.15 mL of a solution of **5a**–**5e** was mixed with KBr. The mixture was evaporated to dryness (20 °C, *in vacuo*) and pressed into a disk. For labeling experiments, 5 mL (ca. 0.2 mmol) of $^{18}O_2$ (97% ^{18}O) was added to a 15–20 mM solution of **1a** (0.0075–0.010 mmol) in 0.5 mL of C_6D_6.

[Ir{PhNC(NMe$_2$)NPh}(η^4-cod)(η^2-O$_2$)] (5a). ^{1}H NMR (500 MHz, C_6D_6, δ): 7.35 (br d, 2H, Ar H), 7.30 (d, J = 8.1 Hz, 2H, Ar H), 7.15 (Ar H; this signal partially overlaps with the residual solvent peak), 7.09 (t, J = 7.7 Hz, 2H, Ar H), 6.96 (t, J = 7.2 Hz, 1H, Ar H), 6.88 (t, J = 7.7 Hz, 1H, Ar H), 4.74 (br dt, 1H, =C*H*CH$_2$–), 4.55 (br dt, 1H, =C*H*CH$_2$–), 4.14 (br dt, 1H, =C*H*CH$_2$–), 4.01 (br dt, 1H, =C*H*CH$_2$–), 2.34–2.19 (m, 3H, =CHC*H*$_2$–), 2.17–2.09 (m, 1H, =CHC*H*$_2$–), 2.06–1.98 (m, 1H, =CHC*H*$_2$–), 2.03 (s, 6H, NCH$_3$), 1.94–1.88 (m, 1H, =CHC*H*$_2$–), 1.70–1.60 (m, 2H, =CHC*H*$_2$–). ^{1}H NMR (300 MHz, $CDCl_3$, δ): 7.35 (br d, 4H, Ar H), 7.23–7.15 (m, 3H, Ar H), 7.11–7.08 (m, 2H, Ar H), 6.97 (t, J = 7.1 Hz, 1H, Ar H), 4.59–4.56 (m, 1H, =C*H*CH$_2$–), 4.53–4.48 (m, 1H, =C*H*CH$_2$–), 4.12–4.06 (m, 1H, =C*H*CH$_2$–), 3.93–3.86 (m, 1H, =C*H*CH$_2$–), 2.68–2.61 (m, 2H, =CHC*H*$_2$–), 2.56 (s, 6H, NCH$_3$), 2.55–2.29 (m, 4H, =CHC*H*$_2$–), 2.15–2.07 (m, 2H, =CHC*H*$_2$–). IR (KBr, cm^{-1}): 865 (ν_{OO}), 575 and 459 (ν_{IrO}). IR for **5a**-$^{18}O_2$ (KBr, cm^{-1}): 813 (ν_{OO}), 550 (sh) and 442 (ν_{IrO}).

[Ir{PhNC(NEt$_2$)NPh}(η^4-cod)(η^2-O$_2$)] (5b). ^{1}H NMR (300 MHz, C_6D_6, δ): 7.44 (d, J = 7.3 Hz, 4H, Ar H), 7.18–7.09 (m, Ar H; these signals partically overlap with the residual solvent peak), 6.96 (t, J = 7.4 Hz, 1H, Ar H), 6.89 (t, J = 7.3 Hz, 1H, Ar H), 4.76–4.67 (br m, 1H, =C*H*CH$_2$–), 4.55–4.46 (br m, 1H, =C*H*CH$_2$–), 4.18–4.00 (br m, 2H, =C*H*CH$_2$–), 2.83 (sext, J = 7.1 Hz, 2H, NC*H*$_2$CH$_3$), 2.39–1.86 (br m, 6H, =CHC*H*$_2$–), 2.33 (sext, J = 7.2 Hz, 2H, NC*H*$_2$CH$_3$), 1.71–1.55 (br m, 2H, =CHC*H*$_2$–), 0.62 (t, J = 7.1 Hz, 6H, NCH$_2$C*H*$_3$). IR (KBr, cm^{-1}): 865 (ν_{OO}), 576 and 459 (ν_{IrO}).

[Ir{(4-MeC$_6$H$_4$)NC(NMe$_2$)N(4-MeC$_6$H$_4$)}(η^4-cod)(η^2-O$_2$)] (5c). ^{1}H NMR (300 MHz, C_6D_6, δ): 7.30 (d, J = 7.9 Hz, 2H, Ar H), 7.25 (d, J = 8.3 Hz, 2H, Ar H), 6.98 (d, J = 7.9 Hz, 2H, Ar H), 6.93 (d, J = 8.0 Hz, 2H, Ar H), 4.80–4.70 (br m, 1H, =C*H*CH$_2$–), 4.64–4.53 (br m, 1H, =C*H*CH$_2$–), 4.20–4.10 (br m, 1H, =C*H*CH$_2$–), 4.10–4.00 (br m, 1H, =C*H*CH$_2$–), 2.42–1.95 (br m, 6H, =CHC*H*$_2$–), 2.12 (s, 3H, C$_6$H$_4$C*H*$_3$), 2.11 (s, 3H, C$_6$H$_4$C*H*$_3$), 2.09 (s, 6H, NCH$_3$), 1.77–1.58 (br m, 2H, =CHC*H*$_2$–). IR (KBr, cm^{-1}): 862 (ν_{OO}), 575 and 459 (ν_{IrO}).

[Ir{(4-MeC$_6$H$_4$)NC(NEt$_2$)N(4-MeC$_6$H$_4$)}(η^4-cod)(η^2-O$_2$)] (5d). ^{1}H NMR (300 MHz, C_6D_6, δ): 7.38 (d, J = 8.3 Hz, 4H, Ar H), 6.99 (d, J = 8.4 Hz, 2H, Ar H), 6.95 (d, J = 8.1 Hz, 2H, Ar H), 4.78–4.72 (br m, 1H, =C*H*CH$_2$–), 4.61–4.53 (br m, 1H, =C*H*CH$_2$–), 4.20–4.06 (br m, 2H, =C*H*CH$_2$–), 2.91 (sext, J = 7.1 Hz, 2H, NC*H*$_2$CH$_3$), 2.38 (sext, J = 7.1 Hz, 2H, NC*H*$_2$CH$_3$), 2.30–1.96 (br m, 6H, =CHC*H*$_2$–), 2.11 (s, 3H, C$_6$H$_4$C*H*$_3$), 2.10 (s, 3H, C$_6$H$_4$C*H*$_3$), 1.76–1.61 (br m, 2H, =CHC*H*$_2$–), 0.67 (t, J = 7.1 Hz, 6H, NCH$_2$C*H*$_3$). IR (KBr, cm^{-1}): 862 (ν_{OO}), 575 and 458 (ν_{IrO}).

[Ir{(4-MeOC$_6$H$_4$)NC(NMe$_2$)N(4-MeOC$_6$H$_4$)}(η^4-cod)(η^2-O$_2$)] (5e). ^{1}H NMR (300 MHz, C_6D_6, δ): 7.32 (d, J = 8.8 Hz, 2H, Ar H), 7.26 (d, J = 8.6 Hz, 2H, Ar H), 6.78 (d, J = 8.9 Hz, 2H, Ar H), 6.73 (d, J = 8.7 Hz, 2H, Ar H), 4.78–4.67 (br m, 1H, =C*H*CH$_2$–), 4.66–4.58 (br m, 1H, =C*H*CH$_2$–), 4.22–4.13 (br m, 1H, =C*H*CH$_2$–), 4.08–3.99 (br m, 1H, =C*H*CH$_2$–), 3.34 (s, 3H, C$_6$H$_4$OC*H*$_3$), 3.32 (s, 3H, C$_6$H$_4$OC*H*$_3$), 2.40–2.15

(br m, 4H, =CHCH_2–), 2.15–1.97 (br m, 2H, =CHCH_2–), 2.12 (s, 6H, NCH_3) 1.82–1.57 (br m, 2H, =CHCH_2–). IR (KBr, cm^{-1}): 857 (ν_{OO}), 573 and 457 (ν_{IrO}).

4.2.3 Reactions of (Alkene)peroxoiridium(III) Intermediates and Their Decay Products

Reaction of 5a with Triphenylphosphine. A solution of **5a** in C_6D_6 was prepared as described above (ca. 3 h for the formation of **5a**) and then purged with Ar for 5 min to remove excess O_2. A solution of 0.075–0.100 mmol of PPh_3 (10 equiv with respect to Ir) in 0.2 mL of C_6D_6 was added to the solution of **5a**, and the progress of the reaction was monitored by ^{31}P NMR spectroscopy. The intermediate was fully decayed within 4 h (pale orange solution). $^{31}P\{^1H\}$ NMR (121.5 MHz, C_6D_6, δ): 25.5 (s, $OPPh_3$), –4.4 (s, PPh_3), –9.1 (s).

Reaction of 5a with CO. A solution of **5a** in C_6D_6 was prepared as described above, then purged with CO(*g*) for 10 min and kept at 20 °C for 1 d. Complex **2a** and free cod were identified as products by ^1H NMR spectroscopy (quantification against 1,2-dichloroethane as a standard) and **2a** also by IR spectroscopy. ^1H NMR (300 MHz, C_6D_6, δ): 7.07 (m, 4H, Ar H), 6.87–6.79 (m, 6H, Ar H), 5.56 (br m, 4H, =C*H*CH_2–, free cod), 2.20 (br m, 4H, =CHCH_2–, free cod), 1.83 (s, 6H, NCH_3). IR (C_6D_6, cm^{-1}): 2068 (ν_{CO}), 2051 (ν_{CO}, **2a**), 2012 (ν_{CO}), 1976 (ν_{CO}, **2a**).

Reaction of the Decay Products of 5a with 1,5-Cyclooctadiene. A 15–20 mM solution of **1a** in C_6D_6 was purged with O_2 as described above, allowed to stand for at least 16 h, and then purged with Ar for 5 min to remove excess O_2. Alternatively, the solution was evaporated to dryness (20 °C, *in vacuo*), and the residue was dissolved in deoxygenated C_6D_6. After addition of 0.015–0.020 or 0.075–0.100 mmol of cod (2 or 10 equiv with respect to Ir), the solution was kept at 20 °C for 1 d and then heated at 70 °C for 1 d (NMR tube equipped with a J. Young valve). During this time the color of the

solution changed from dark green to orange. 4-Cycloocten-1-one[23,94] and **1a** were identified as products by ^{1}H NMR spectroscopy (quantified against 1,2-dichloroethane as a standard) and EIMS. Quantifications (against 1,2-dichloroethane as a standard) were performed in triplicate. The average yields were 0.88 (±0.13) equiv of 4-cycloocten-1-one and 0.30 (±0.05) equiv of **1a**. Data for 4-cycloocten-1-one were as follows: ^{1}H NMR (300 MHz, C_6D_6, δ): 5.65 (m, 1H, =C*H*CH_2–), 5.37 (m, 1H, =C*H*CH_2–), 2.66 (m, 1H, =CHC*H*$_2$–), 2.24 (m, 3H, =CHC*H*$_2$–), 2.10 (m, 2H, =CHC*H*$_2$–), 1.40–1.31 (m, 4H, =CHC*H*$_2$–). EIMS (70 eV) *m/z*: $M^{+\bullet}$ calcd for $C_8H_{12}O$, 124.1; found, 124.3 (the expected fragmentation pattern[95] was observed as follows: 109.3, 96.3, 81.3, 67.2, 54.2). For the reaction carried out using $^{18}O_2$, EIMS (70 eV) *m*/*z*: 126.3 ($M^{+\bullet}$; fragmentation pattern: 111.3, 96.3, 81.3, 67.2, 54.2).

Recovery of *N,N*-Dimethyl-*N′,N″*-diphenylguanidine, PhN=C(NMe$_2$)NHPh from the Decay Products of 5a. A solution of 9.8 mg (0.018 mmol) of **1a** in 3 mL of toluene was purged with O_2 (40 s) at 20 °C. After 16 h, 3.0 μL (3.6 mg, 0.036 mmol) of concentrated HCl and 3 mL of water were added to the resulting green solution. The biphasic mixture was vigorously stirred for 1 h. The aqueous phase was separated and combined with 5 mL of diethyl ether and 15 mL of a saturated Na_2CO_3 solution. The biphasic mixture was vigorously stirred for 1 h, after which the organic phase was separated and dried over $MgSO_4$ and the volatiles were removed under reduced pressure. Yield: 2.9 mg (67%). The ^{1}H NMR and ESI(+)MS data were indistinguishable from those of the guanidine ligand precursor[58] and did not reveal any other products. ^{1}H NMR (300 MHz, $CDCl_3$, δ): 7.20 (t, J = 6.8 Hz, 4H, Ar H), 7.01 (t, J = 7.4 Hz, 2H, Ar H), 6.92 (d, J = 7.6 Hz, 4H, Ar H), 2.86 (s, 6H, NCH_3). ESI(+)MS (CH_3CN) *m*/*z*: $\{M + H\}^+$ calcd for $C_{15}H_{17}N_3$, 240.2; found, 240.2.

4.3 Results and Discussion

4.3.1 Reactivity of(Cyclooctadiene)iridium(I) Complexes toward O_2

In solution, complexes **1a**–**1g** react readily with O_2, as indicated by the disappearance of their characteristic absorption features in the UV–Vis region (Figure 11). For example, at 0 °C, the half-life of **1a** in toluene solution saturated with O_2 is ca. 20 min. Interestingly, while complexes **1b**–**1f** reacted with O_2 with a similar reaction profile to **1a**, the rates of the reactions varied with the substituents on the guanidinato ligand. Under the same conditions, the half-lives of the iridium(I) complexes increase in the order **1e** < **1d** < **1c** ≈ **1b** < **1a** < **1f** (Figure 11, Table 11).

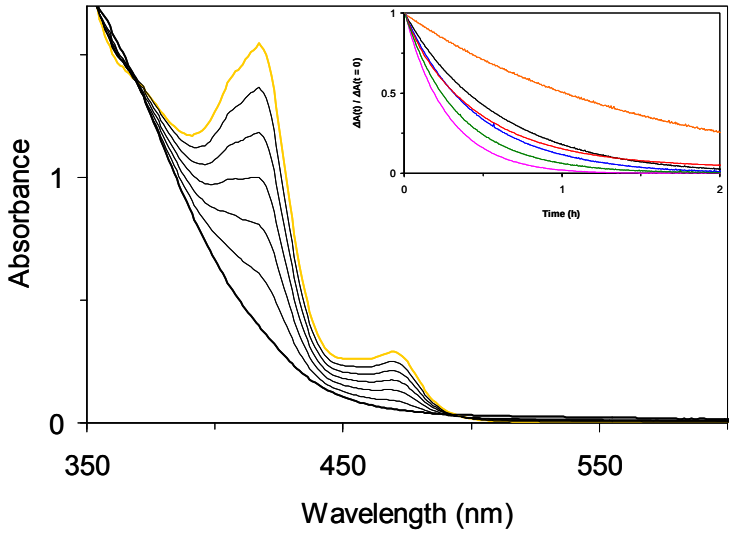

Figure 11. Reaction of 2 mM **1a** (orange line) in toluene with O_2 at 0 °C as monitored by electronic absorption spectroscopy (path length, 0.5 cm) Inset: Time courses for the reactions of **1a**–**1f** with O_2 in toluene. **1a**, black; **1b**, red; **1c**, blue; **1d**, pink; **1e**, green; **1f**, orange.

Thus, both methyl or methoxy substitution in *para* position of the benzene rings (**1c**−**1e**) and extension of the alkyl substituents of the NR_2 group (**1b**, **1d**) have an accelerating effect on the O_2 reaction, whereas methyl groups in *ortho* position of the benzene rings (**1f**) have a decelerating effect. Complex **1g** reacts with O_2 under these same conditions, but complete decay of the starting material was not observed. Also, the reaction was tried at a lower temperature (−25 °C), which increases the concentration of O_2 in solution, but complete decay of the starting material was still not observed.

Table 11. Half-lives from the reactions of **1a**–**1f** with O_2.

	1a	**1b**	**1c**	**1d**	**1e**	**1f**
$t_{1/2}$ **(s)**	1300	1100	1100	850	700	3600

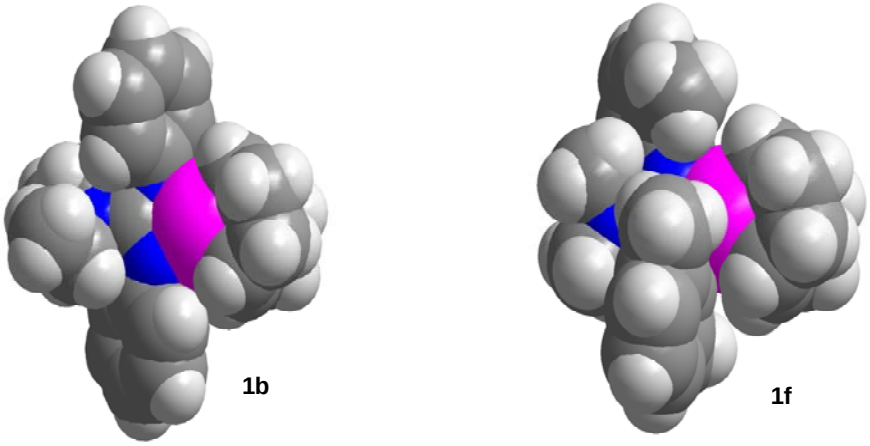

Figure 12. Space-filling representations of [Ir{PhNC(NEt_2)NPh}(cod)], **1b** (left), and [Ir{(2,6-MeC_6H_3)NC(NMe_2)N(2,6-MeC_6H_3)}(cod)], **1f** (right); color key: pink = Ir, blue = N, gray = C, light grey = H.

The higher reactivity of **1b**−**1e** compared to that of **1a** can be explained by increased electron donation from the guanidinato ligand to the iridium(I) center and consequent destabilization of the low oxidation state. In the case of **1f**, the steric

influences of the *ortho* methyl groups appear to exceed their electronic influences and may be responsible for the slower rate. Clearly, the iridium(I) centers in **1a**–**1e** are somewhat more exposed than those in **1f** and **1g**, and the alkyl groups of the latter may limit access to the metal center (Figure 12).

4.3.2 Formation and Characterization of (Alkene)peroxoiridium(III) Intermediates

Further insight into the reaction of the iridium(I) complexes with O_2 was obtained by NMR spectroscopy. When O_2 was added to a 20 mM solution of **1a** in benzene-d_6 at 20 °C, new ^{1}H resonance signals developed over the course of about 3 h as those of **1a** disappeared. In turn, the new signals disappeared within 9 h, indicating that the new intermediate, **5a**, is fairly unstable (Scheme 17).

Scheme 17. Generation of (Alkene)peroxoiridium(III) Intermediates **5a**–**5f**

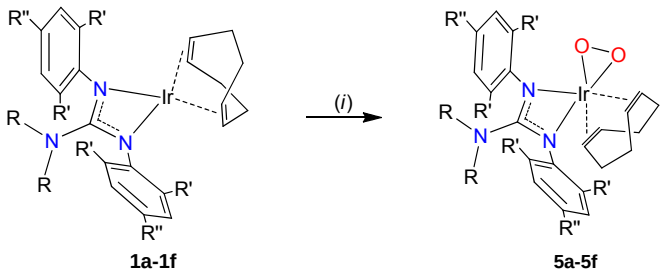

(*i*) O_2, 20 °C, benzene-d_6 or toluene

Along with the progression of the reaction, the bright yellow solution of **1a** turned first pale yellow (**5a**) and then dark green. The ^{1}H NMR spectrum of **5a**, shown in Figure 13, exhibits four distinct resonance signals in the alkene region between 4.0 and 4.8 ppm

and six broad multiplets attributable to CH_2 protons as well as a sharp singlet characteristic of the guanidinato NMe_2 group at 2.03 ppm and two sets of three signals in the aromatic region.

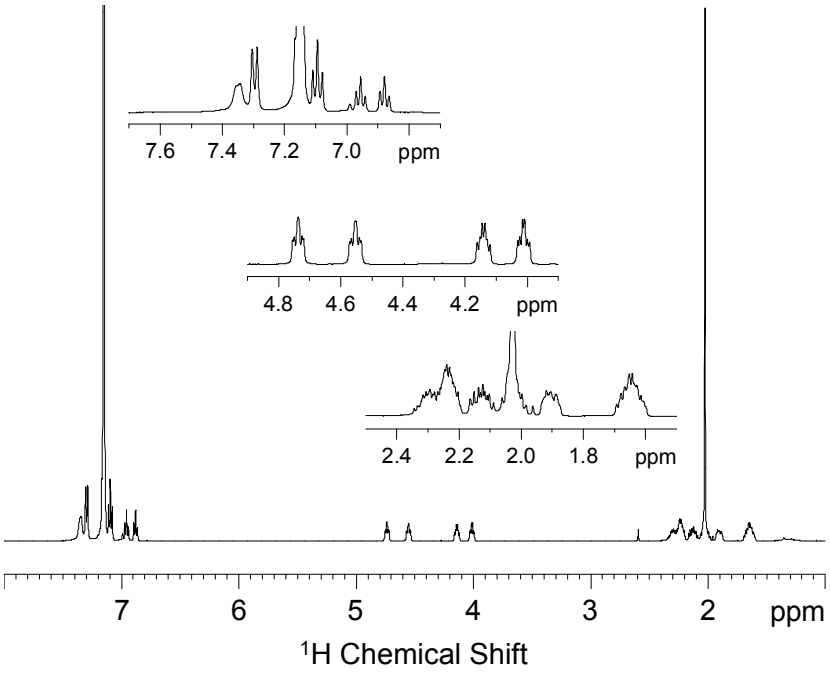

Figure 13. ^{1}H NMR spectrum of **5a** in benzene-d_6 (*ca*. 15 mM, 500 MHz, 20 °C). The resonance signal at 7.15 ppm partially overlaps with the residual solvent peak.

Detailed characterization of **5a** by two-dimensional NMR techniques revealed that the NMR data are consistent with a *cis*-[Ir{PhNC(NMe_2)NPh}(cod)X_2] complex rather than with a mixture of multiple products. In particular, ^{1}H,^{1}H correlated spectroscopy (COSY) data confirmed the presence of two inequivalent phenyl groups and established that the alkene and methylene proton resonances all belong to only one unique cod ligand (Figure 14).

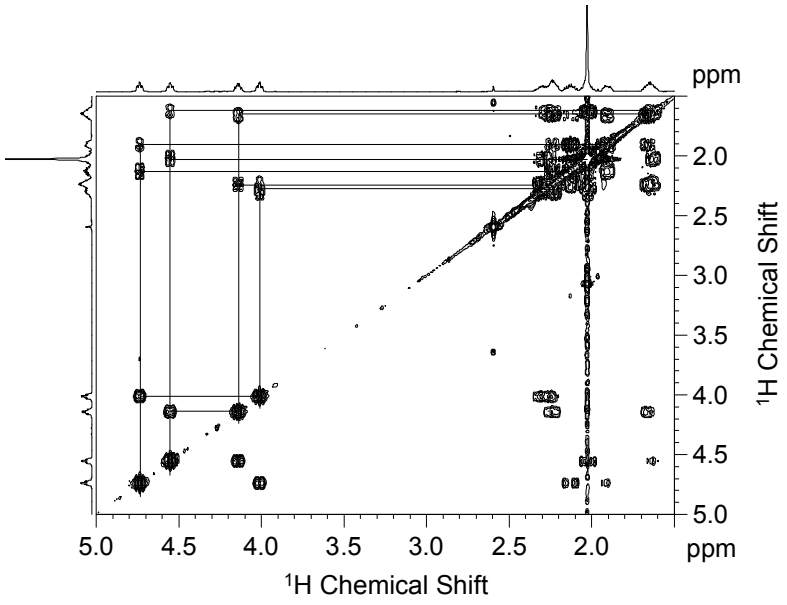

Figure 14. Part of the ^{1}H,^{1}H COSY spectrum of **5a** in benzene-d_6 (*ca*. 15 mM, 500 MHz, 20 °C). The solid lines indicate correlations among alkene proton resonances and between alkene and methylene proton resonances.

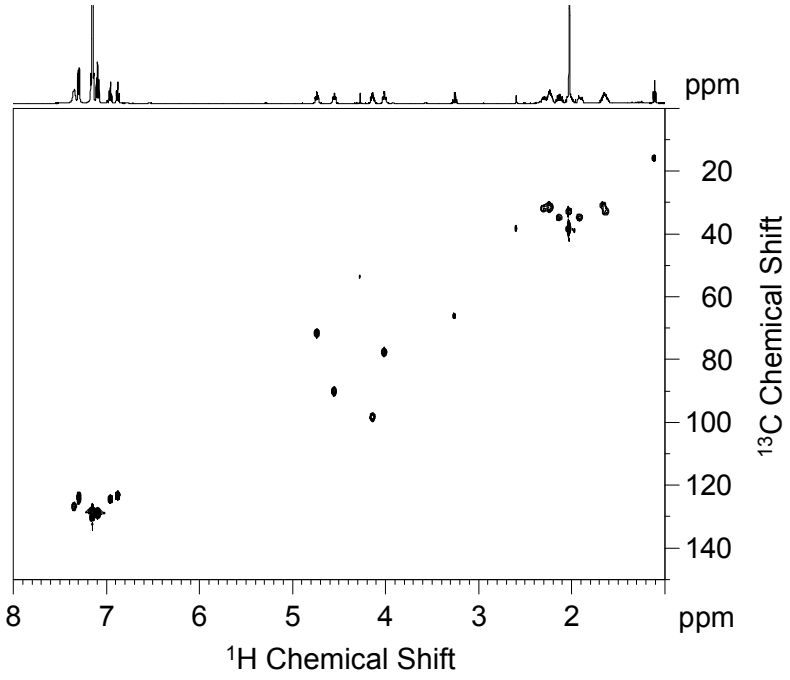

Figure 15. ^{1}H,^{13}C HSQC spectrum of **5a** in benzene-d_6 (*ca*. 15 mM, 500 MHz, 20 °C).

Table 12. ^{1}H and ^{13}C chemical shifts, δ (ppm), from the ^{1}H,^{13}C HSQC spectrum of **5a** in benzene-d_6.

Assignment		$\delta(^{1}H)$	$\delta(^{13}C)$
Ar	Group A	7.35	126.8
		7.15[a]	128.0[a]
		6.96	124.4
	Group B	7.30	123.9
		7.09	128.9
		6.88	123.3
=*CH*CH_2–	1-H, C-1	4.74	71.7
	2-H, C-2	4.01	77.7
	5-H, C-5	4.55	90.1
	6-H, C-6	4.14	98.3
=CH*CH_2*–	3-H_{ab}, C-3	2.31, 2.23	32.0
	4-H_{ab}, C-4	2.02, 1.63	32.8
	7-H_{ab}, C-7	2.23, 1.66	31.4
	8-H_{ab}, C-8	2.13, 1.91	34.8
NCH_3		2.03	38.1

[a] The resonance signals centered at $\delta(^{1}H)$ = 7.15 ppm and $\delta(^{13}C)$ = 128.0 ppm partially overlap with the residual solvent peaks.

Evidence for the incorporation of O_2 into **5a** was obtained by IR spectroscopy. Despite its limited stability, a solution of freshly prepared **5a** could be evaporated to dryness without noticeable decomposition. Three ^{18}O-isotope-sensitive bands were observed in the solid-state IR spectrum of **5a** at 865, 575 and 459 cm^{-1} (for **5a**-$^{18}O_2$, 813, 550 and 442 cm^{-1}; Figure 16, Table 13). The band at 865 cm^{-1} falls into the range expected for OO stretching vibrations (ν_{OO}) of (η^2-peroxo)iridium(III) complexes,[96-102] whereas the wavenumbers of the lower-energy bands are consistent with IrO stretching modes (ν_{IrO}).[102] The isotope shifts agree well with values calculated using harmonic oscillator models (calcd for **5a**-$^{18}O_2$, 816, 545 and 435 cm^{-1}).

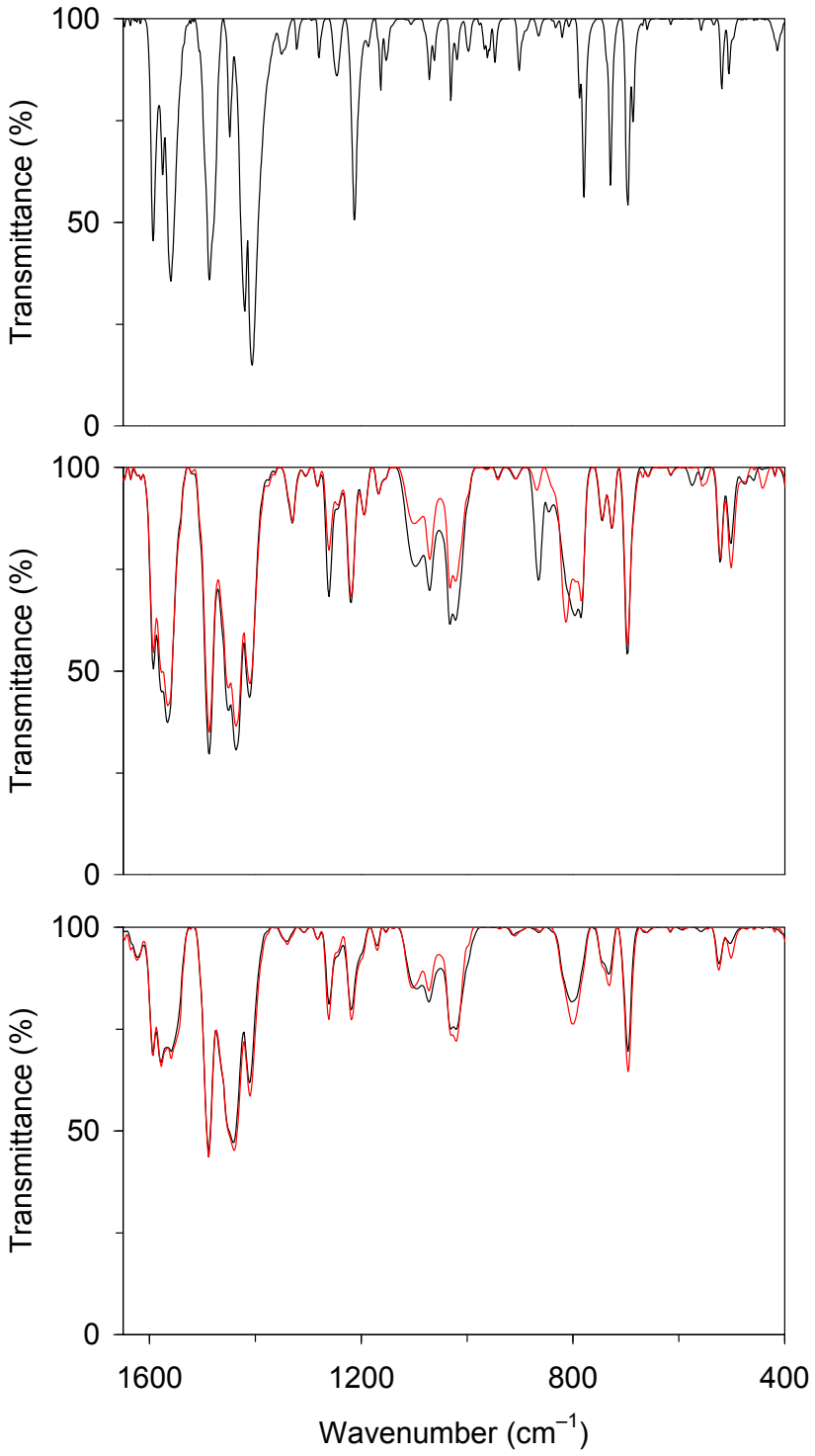

Figure 16. Top: IR spectra of **1a** (—, black); Middle: **5a** (—, black) and **5a**-$^{18}O_2$ (—, red); Bottom: IR spectra of the decay products of **5a** (—, black) and **5a**-$^{18}O_2$ (—, red).

Table 13. OO and IrO Stretching Frequencies, ν_{OO} and ν_{IrO} (cm^{-1}), of the (Alkene)peroxoiridium(III) Intermediates **5a**–**5e** and Mass-to-charge Ratios (*m*/*z*) from the Electrospray Ionization (ESI) Mass Spectra of the Decay Products of [Ir{ArNC(NR_2)NAr}(η^4-cod)(η^2-O_2)] (**5a**–**5f**).[a,b]

	ν_{OO} (cm^{-1})	ν_{IrO} (cm^{-1})	$\{LH + H\}^+$	$\{M - O_2H\}^+$	$\{M - OH\}^+$	$\{M - H\}^+$
5a	865	575, 459	240.2	538.3	554.2	570.1
5a-$^{18}O_2$	813	550, 442	240.2	538.4	556.3	574.3
5b	865	576, 459	268.1	566.2	582.1	598.1
5c	862	575, 459	268.1	566.2	582.1	598.1
5d	862	575, 458	296.2	594.2	610.1	626.1
5e	857	573, 457	300.2	598.3	614.2	630.1
5f			296.2	594.3	610.2	

[a] The reactions of **5a**–**5f** with O_2 were carried out as described in the Experimental Section 4.2.2 (2 mM in toluene at 0 °C or 15–20 mM in benzene-d_6 at 20 °C), and the resulting solutions were allowed to stand for at least 16 h at 20 °C. [b] LH = ArN=C(NR_2)NHAr. M refers to the [Ir{ArNC(NR_2)NAr}(η^4-cod)(η^2-O_2)] intermediates, **5a**–**5f**.

All three bands were absent from the IR spectra of **1a** and the decay products of **5a** and **5a**-$^{18}O_2$ (Figure 16). Thus, on the basis of our spectroscopic analysis, we formulate intermediate **5a** as the (η^4-diene)(η^2-peroxo) complex [Ir{PhNC(NMe_2)NPh}(η^4-cod)(η^2-O_2)]. While a symmetric dinuclear structure would also be consistent with the spectroscopic data, the mononuclear structure was corroborated by diffusion NMR experiments. Compounds **1a** and **5a** were found to have similar diffusion coefficients (*D*), 8.4 (±0.1) · 10^{-10} and 8.2 (±0.3) · 10^{-10} $m^2 \cdot s^{-1}$ **1a** and **5a**, respectively (Equation 1, where γ_X = gyromagnetic ratio of the X nucleus; δ = length of the gradient pulse; G = gradient strength; Δ = delay between the midpoints of the gradients; *D* = diffusion coefficient).

$$\ln(I/Io) = -\gamma_X^2 \delta^2 G^2 (\Delta - \delta/3) D \quad (1)$$

The plots in Figure 17 confirm the expected linear relationship between $\ln(I/I_0)$ and G^2. According to the established relationship between the diffusion coefficient and hydrodynamic radius,[103,104] these compounds are expected to have similar molecular sizes (Equation 2, where k = Boltzmann constant, T = temperature; η = viscocity of solvent (C_6D_6, 0.604 mPa·s)[105]).

$$r_H = kT/6\pi\eta D \quad (2)$$

The hydrodynamic radii (r_H) were calculated from D and determined to be approximately 4.1(1) Å for **1a** and 4.2(2) Å for **5a**. For **1a**, the r_H agrees well with the size estimated from the solid-state structures of the crystallographically characterized iridium(I) complexes (**1b**, **1d** and **1f**; Section 3.3.4). Because it is known **1a** is a mononuclear complex, it is possible to conclude that **5a** is also a mononuclear species.

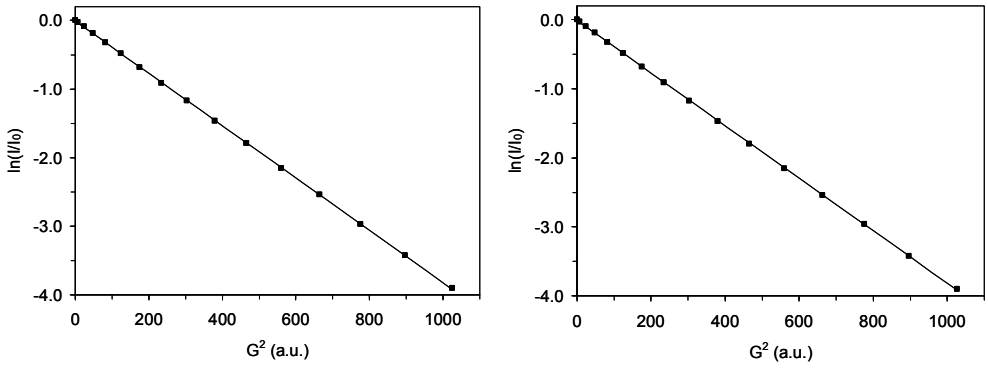

Figure 17. Plots of the natural logarithm of the intensity quotient, $\ln(I/I_0)$ *versus* the square of the gradient strength, G^2, for the NMe_2 resonance signal of **1a** (left, R^2 = 0.99996) and **5a** (right, R^2 = 0.99995).

Complexes **1b**−**1f** also react with O_2 to form analogous intermediates. When O_2 was added to 15–20 mM solutions of **1b**−**1f**, similar ^{1}H NMR peaks were formed within

3 h, and these resonances are assigned to intermediates **5b**−**5f**. For complex **1f**, an intermediate was observed as well, but full decay of the starting material was not observed, even at a lower reaction temperature (−25 °C) which increases the concentration of O_2 in solution. The formation rates of the intermediates follow a trend based on the electron donating strength of the guanidinato ligands (**1b**, 2.5 h; **1c**, 2.5 h; **1d**, 2.5 h; **1e**, 2 h), and all intermediates were fully decayed within 20 h after addition of O_2.

Intermediates **5b**−**5e** and their decay products were also analyzed by IR spectroscopy in a similar way as **5a**. Three bands were observed in the solid-state IR spectrum for each of these intermediates which disappear in the IR spectra of the decay products (Figures 18−22). The values for the OO stretching modes (ν_{OO}) are observed in the range of 857 – 865 cm^{-1}, while the values for IrO stretching modes (ν_{IrO}) are in the ranges of 573 – 576 and 457 – 459 cm^{-1} which all agree well with values for **5a** (Table 13).

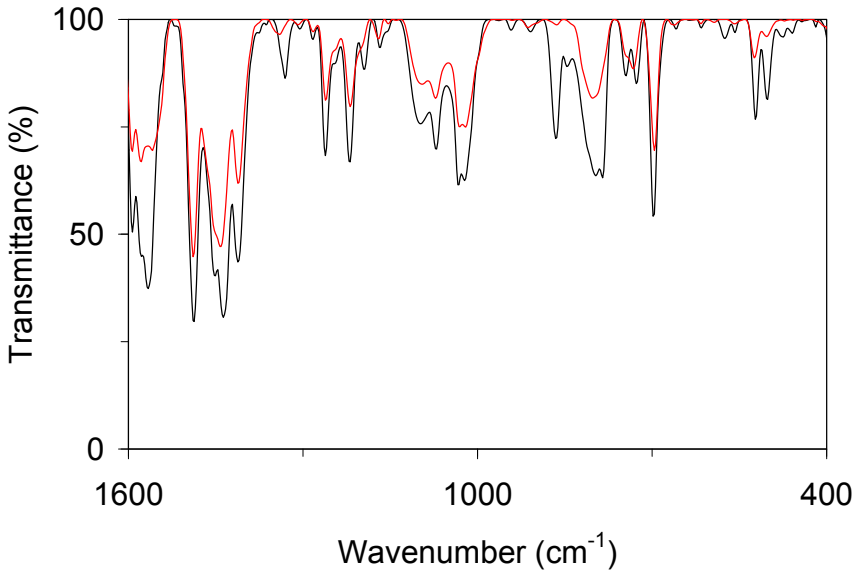

Figure 18. Solid-state IR (KBr) spectra of peroxo intermediate **5a** (—, black) and its decay products (—, red).

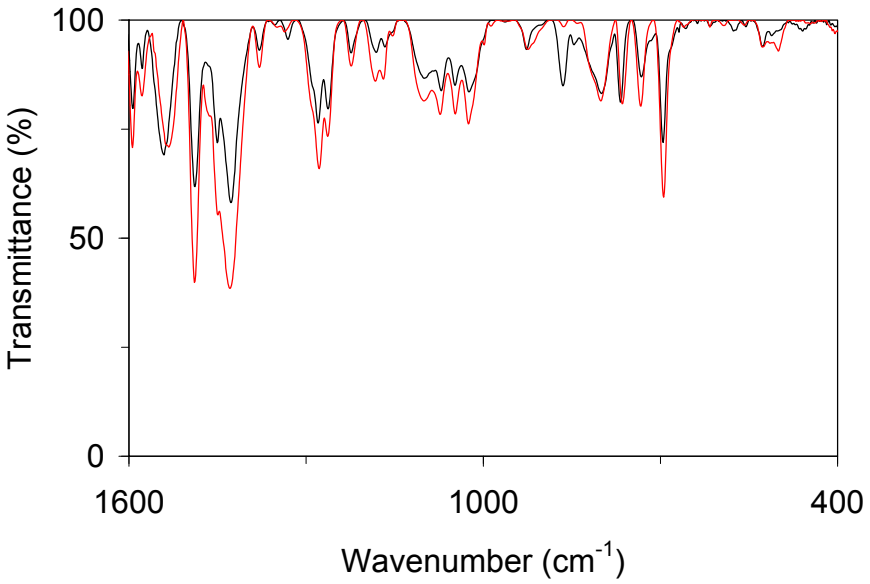

Figure 19. Solid-state IR (KBr) spectra of peroxo intermediate **5b** (—, black) and its decay products (—, red).

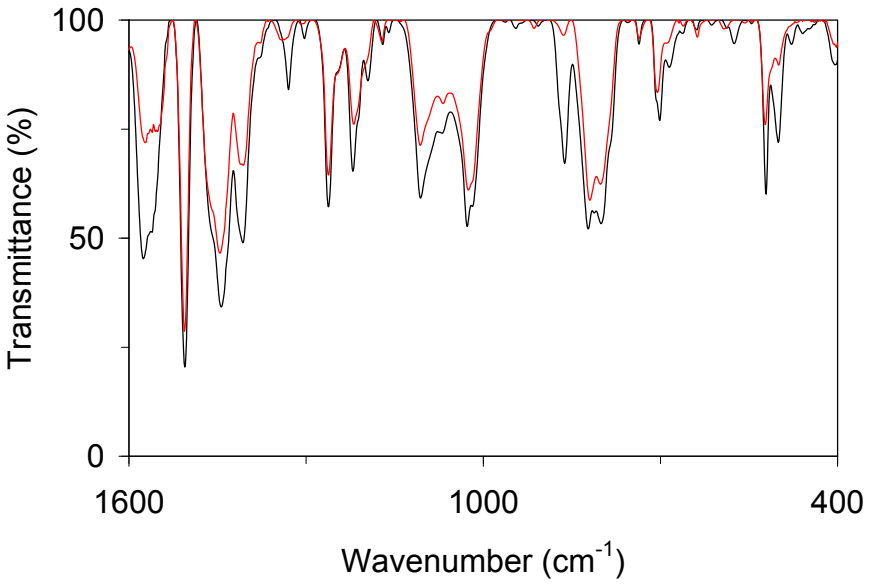

Figure 20. Solid-state IR (KBr) spectra of peroxo intermediate **5c** (—, black) and its decay products (—, red).

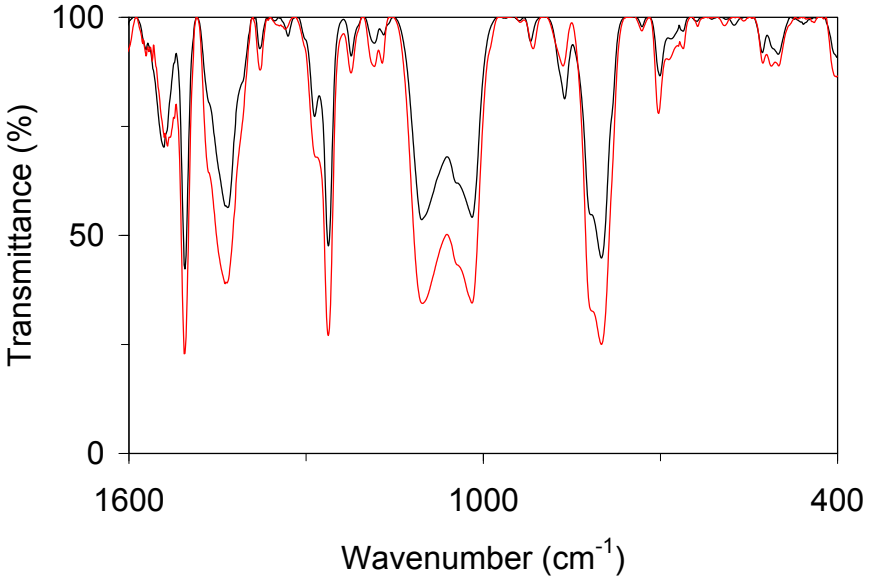

Figure 21. Solid-state IR (KBr) spectra of peroxo intermediate **5d** (—, black) and its decay products (—, red).

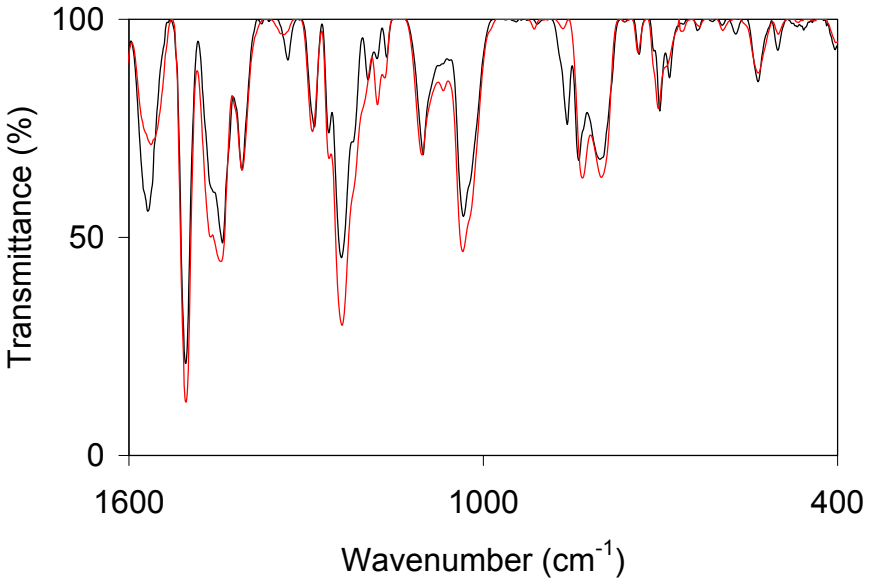

Figure 22. Solid-state IR (KBr) spectra of peroxo intermediate **5e** (—, black) and its decay products (—, red).

When comparing the OO stretching frequencies for intermediates **5a**–**5e**, a trend was observed that is related to the ligand donor strength of the guanidinato ligands. As the electron donating strength increases from **a** to **e**, the value for the OO stretching frequency shifts to lower energy in the IR spectra. This is due to the guanidinato ligand competing with the peroxo ligand for donation of electron density to the metal center, which allows for lower electron donation from the peroxo ligand to the metal center. The lower electron donation from the peroxo ligand causes a higher population of the peroxo π^* orbitals and thus weakens the bond of this ligand, thus causing a shift to lower energies in the IR spectra.

4.3.3 Reactivity of (Alkene)peroxoiridium(III) Intermediates and Their Decay Products

As expected, complex **5a** oxidizes PPh_3 to $OPPh_3$. Reaction of a deoxygenated solution of **5a** with an excess of PPh_3 (1.5 or 10 equiv with respect to Ir) yielded ca. 0.8 equiv of $OPPh_3$, as determined by ^{31}P NMR spectroscopy (Scheme 18). Taking into account the 75% accumulation of **5a**, the amount of $OPPh_3$ produced corresponds to the transfer of one oxygen atom from the peroxo group of **5a** to PPh_3.

Scheme 18. Reaction of (Alkene)peroxoiridium(III) Intermediate **5a** with PPh_3 and CO(*g*)

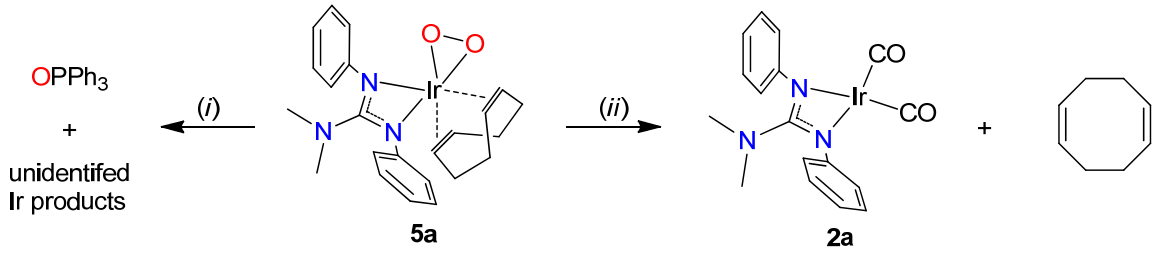

(*i*) 10 equiv of PPh_3, 20 °C, benzene-d_6; (*ii*) CO(*g*), 20 °C, benzene-d_6

The reaction of intermediate **5a** with CO was also investigated. Bubbling CO(*g*) through a solution of **5a** in benzene-d_6 at 20 °C causes a gradual reaction, with the peroxo intermediate decaying within ca. 1 d. Analysis of the reaction mixture by ^{1}H NMR spectroscopy showed formation of 0.3 equiv of unmodified cod and a similar amount of **2a** (Scheme 18). The formation of **2a** was also confirmed by IR spectroscopy in benzene-d_6 on the basis of the peaks observed at 2051 and 1976 cm^{-1} which are assigned to **2a**.

We also investigated the self-decay of **5a** in order to determine whether the coordinated alkene undergoes oxidation by the peroxo ligand. The electronic absorption spectrum of the dark green decay products of **5a** and the spectra of **1a** and **5a** are shown in Figure 23. We observe decay of the indicative peaks of the starting material (black line) to form the intermediate (solid red line) which has a featureless UV–Vis spectrum. Subsequent increase in the absorbance in the vis region is observed, indicating decay of the intermediate (decay products, blue line).

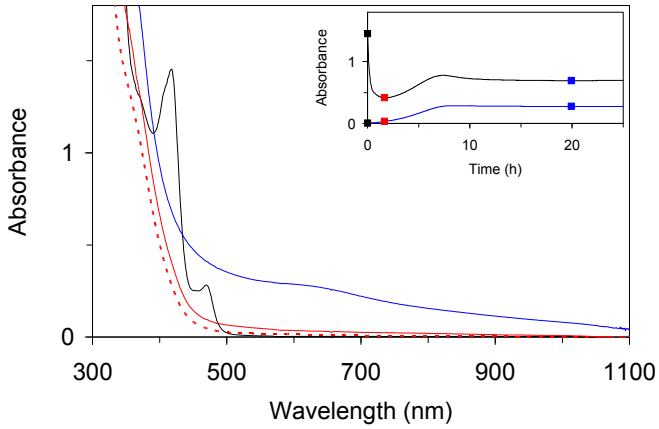

Figure 23. Electronic absorption spectra of 2 mM **1a** (—, black), **5a** (—, red) and the decay products of **5a** (—, blue) in toluene at 20 °C (path length, 0.5 cm). Also shown is the spectrum of a sample of **5a** generated by the reaction of 20 mM **1a** in benzene-d_6 with O_2 at 20 °C and subsequently diluted to a concentration of 2 mM (- - -, red) Inset: Time courses of the reaction of **5a** in toluene with O_2 at 20 °C [λ = 417 nm (—, black) and 630 nm (—, red)]. The squares indicate the reaction times associated with the spectra shown (black, **1a**; red, **5a**; and blue, decay products of **5a**).

To better understand the similarites between UV-Vis and NMR analysis of the reaction with O_2, an NMR experiment was done at 20 mM and upon formation of the peroxo intermediate was diluted to 2 mM (Figure 23, dashed red line). The similarities of the solid and dashed red lines shows that the the featureless UV–Vis spectrum is associated with the intermediate observed by NMR spectroscopy.

Examination of the product solution by mass spectrometry revealed the presence of several products, including mono- and dioxygenated complexes. On the basis of their masses and isotope distribution patterns, the peaks at m/z = 553 (EIMS) and m/z = 554 and 570 (ESI MS) can be assigned to $\{\mathbf{5a} - H_2O\}^{+\bullet}$, $\{\mathbf{5a} - OH\}^{+}$ and $\{\mathbf{5a} - H\}^{+}$, respectively (Table 13). Consistent with the presence of one or two oxygen atoms, these peaks showed the expected mass increases for samples prepared from isotope-enriched **5a**-$^{18}O_2$ [m/z = 555 (EIMS) and m/z = 556 and 574 (ESI MS)].

It was also determined that intermediates **5b**–**5f** have analogous peaks observed in the ESI MS analysis (Table 13) and because of this observation, it is believed that all the intermediates decay by a similar pathway. A plausible scenario for the decay of these intermediates is shown in Scheme 19 and involves alkene insertion into the Ir–O bond to give an iridadioxolane, [Ir(L)(η^2-$C_8H_{12}O_2$-κC,κO)] (**A**), followed by O–O bond cleavage and hydrogen migration to afford an (oxo-η^2-cyclooctenyl) complex, [Ir(L)(η^2-$C_8H_{11}O$-κC)(OH)] (**B**). Analogous species were reported to form from the reactions of other Ir^{I}(alkene) complexes with O_2, which were proposed to proceed through Ir^{III}(alkene)(O_2^{2-}) intermediates.[9,106] The two monooxygenated species observed by ESI and EI mass spectrometry may then be derived from the latter complex (**B**) by loss of OH^- or H_2O, respectively, whereas the dioxygenated species may be related to the former complex (**A**).

Scheme 19. Proposed Mechanism for the Decay of Intermediates **5a**–**5f**

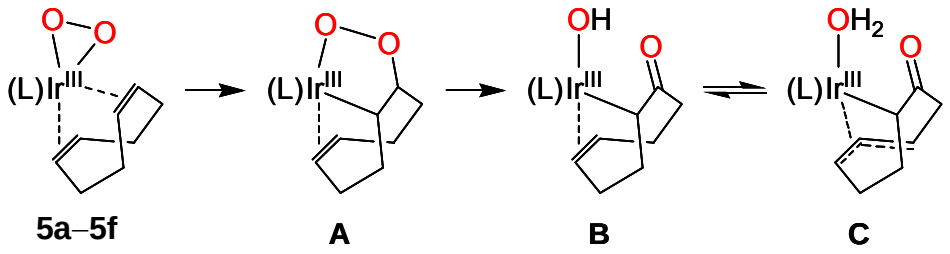

L = $\{ArNC(NR_2)NAr\}^-$

In an attempt to induce cleavage of the oxygenated alkene fragment from the iridium center, the decay products of **5a** were treated with an excess of cod. After 1 d at 70 °C, the color of the solution had turned orange and 4-cycloocten-1-one was identified by ^{1}H NMR spectroscopy and EI MS (*m*/*z* = 124) along with a small amount of **1a**. The analogous reaction using the decay products of **5a**-$^{18}O_2$ gave a peak shifted to *m*/*z* = 126, demonstrating that the oxygen atom in 4-cycloocten-1-one was in fact derived from the peroxo ligand in **5a**. When 2 equiv of cod was used (with respect to Ir), the reaction yielded 0.9 equiv of 4-cycloocten-1-one and ca. 0.3 equiv of **1a**. The oxygenated products could have been derived from the cod present in **5a** or, alternatively, from the added cod by alkene insertion into the Ir–OH bond[107,108] followed by *β*-hydrogen migration. To distinguish between these two possible pathways, the reaction with *cis*-cyclooctene (10 equiv) was investigated, and this reaction also produced 4-cycloocten-1-one, albeit in lower yield (0.2 equiv). This result suggests that the oxygenated product was derived from the cod present in **5a** rather than from alkene insertion into an Ir–OH bond. The latter mechanism would have led to cyclooctanone, which was not observed. As discussed in Section 2.2.2, a related example, a rhodaoxetane, prepared from a Rh^I(cod) complex and O_2, eliminated 4-cycloocten-1-one upon addition of PMe_3 or CO.[28,108]

To investigate any differences in the release of 4-cycloocten-1-one based on the guanidinato ligand, the decay products of intermediates **5c**, **5e** and **5f** were reacted with 2 equiv of cod under the same reaction conditions as the decay products of **5a**. Formation of 0.75 (**5c**) and 0.77 (**5e**) equiv of 4-cycloocten-1-one was observed by ^{1}H NMR spectroscopy after heating for 1 d at 70 °C. These results indicate there is no observable trend based on ligand donor strength. For **5f**, formation of 0.43 equiv of 4-cycloocten-1-one was observed. From these results, there is no increase in the reactivity of the decay products based on the sterics of the ligand. It should also be noted that formation of the iridium(I) starting material does occur for all three of these complexes (**5c**, 0.25 equiv; **5e**, 0.25; and **5f**, 0.12).

4.4 Conclusion

We have shown that a facile reaction with O_2 occurs with the iridium(I) guanidinato alkene complexes. It was observed that the $t_{1/2}$ of the reaction is significantly affected by the electronic and steric properties of the supporting ligand. Substitution in the *para* position of the aryl ring and extension of the NR_2 substituent has an accelerating effect while substitution in the *ortho* position on the aryl substituent has a decelerating effect. (Alkene)peroxoiridium(III) intermediates have been identified and characterized by ^{1}H NMR and IR spectroscopy in the reaction with O_2. It has been observed that intermediate **5a** is able to transfer oxygen to PPh_3 to form $OPPh_3$ and also react with CO to form some of the dicarbonyl complex, **2a**. Finally, the peroxo intermediates are able to undergo C−O formation and alkene oxidation upon decay. Addition of cod (or coe) to the solutions of the final products allows for release of an oxidized organic species, 4-cycloocten-1one, and reformation of some starting material can be observed.

CHAPTER 5
REACTION OF AN (ALKENE)(GUANIDINATO)IRIDIUM(I) COMPLEX WITH S_8: FORMATION OF AN (ALKENE)PERSULFIDOIRIDIUM(III) INTERMEDIATE

5.1 Introduction

In this chapter the reaction of [Ir{PhNC(NMe_2)NPh}(cod)] (**1a**, cod = 1,5-cyclooctadiene) with S_8 will be discussed. It was observed by ^{1}H NMR spectroscopy that the reaction of **1a** with S_8 forms an intermediate that is analogous to the (alkene)peroxoiridium(III) intermediate (**5a**) discussed in Section 4.3.2. Further investigation of this intermediate by two-dimensional NMR techniques (^{1}H,^{1}H COSY and ^{1}H,^{13}C HSQC) and IR spectroscopy provided evidence for the assignment of this intermediate as an (alkene)persulfidoiridium(III) species. This intermediate is fairly stable, much more stable than the (alkene)peroxoiridium(III) intermediate. The intermediate is able to transfer sulfur to PPh_3 and 2,6-dimethylphenyl isocyanide to form $SPPh_3$ and 2,6-dimethylphenyl isocyanate.

5.2 Experimental Section

Materials. All reagents and solvents were purchased from commercial sources and were used as received, unless noted otherwise. *n*-Pentane was dried over Na and distilled under N_2 prior to use.[59] Preparation and handling of air- and moisture-sensitive materials were carried out under an inert gas atmosphere by using either standard Schlenk and vacuum line techniques or a glovebox. [Ir{PhNC(NMe_2)NPh}(cod)] (**1a**) was synthesized as previously described in Section 3.2.3.[57,58] Isotope enriched $^{34}S_8$ (90 % ^{34}S) was purchased from ICON Isotopes, Summit NJ, USA.

Physical Methods. NMR spectra were recorded on a Bruker Avance MicroBay 300, Avance 400 or Avance 500 spectrometer at ambient temperature, unless noted otherwise. ^{1}H and ^{31}P chemical shifts are reported in parts per million (ppm) and were referenced to residual solvent peaks (for ^{1}H NMR spectra) or an external standard [H_3PO_4 (85%, δ = 0 ppm) for ^{31}P NMR spectra]. Two-dimensional correlated spectroscopy (COSY) and heteronuclear single-quantum coherence (HSQC) experiments were carried out on a Bruker Avance 500 spectrometer at 25 °C using the gradient versions of the COSY and HSQC pulse sequences, and the data were processed using the TopSpin 2.1 software package. For ^{1}H,^{1}H COSY, typical measurement parameters were as follows: time domain data points (TD), 2048 for TD and 512 for TD1; number of scans (NS), 8; and number of dummy scans (DS), 32. The data were processed with zero-filling to 4096 (TD) and 512 (TD1). For ^{1}H,^{13}C HSQC, typical measurement parameters were as follows: 2048 for TD and 256 for TD1; NS, 16; and DS, 16. The data were processed with zero-filling to 2048 (TD) and 1024 (TD1). The total measurement time for each experiment was approximately 2 h. Self-diffusion coefficients (*D*) were determined from stimulated-echo experiments using bipolar gradients acquired in two-dimensional mode (stebpgp1s). These experiments were performed on a Bruker Avance 400 spectrometer at 25 °C. Prior to each experiment, the diffusion time (delay between the midpoints of the gradients, Δ) and gradient length (δ) were optimized using the one-dimensional version of the pulse sequence (stebpgp1s1d). The data acquisition for each diffusion experiment took approximately 30 min. Data processing and analysis to determine *D* were carried out within the TopSpin 2.1 software package. IR spectra were recorded on a Bruker Vertex 70 Fourier-transform IR spectrometer using samples prepared by grinding the solid compound with KBr and pressing the mixture into a disk.

Generation and Characterization of [Ir{PhNC(NMe$_2$)NPh}(η^4-cod)(η^2-S$_2$)] (6a). In a typical experiment, a 15–20 mM solution of **1a** (4.0–5.4 mg, 0.0075–0.010 mmol) in 0.5 mL of C_6D_6 was placed in an NMR tube and a solution of 0.25 equiv of S_8

(0.48–0.64 mg, 0.015–0.020 mmol) in 0.50 μL C_6D_6 was added at 20 °C. The progress of the reaction was monitored by ^{1}H NMR spectroscopy. Under these conditions, **1a** converted into the intermediate, **6a**, nearly immediately and **6a** was typically fully decayed within 25 d after the addition of S_8 to **1a**. For quantification, 5 equiv of 1,2-dichloroethane (3.0–3.9 μL, 3.8–4.9 mg, 0.038–0.050 mmol) was added to the solution of **6a**, and the yield was estimated by comparing the integrations of the 1,2-dichloroethane (δ, 2.90 ppm) and alkene proton signals (ca. 70%). For IR spectroscopy, 0.15 mL of a solution of **6a** was mixed with KBr. The mixture was evaporated to dryness (20 °C, *in vacuo*) and pressed into a disk.

^{1}H NMR (500 MHz, C_6D_6, δ): 7.37 (d, J = 7.6 Hz, 2H, Ar H), 7.29 (br d, 2H, Ar H), 7.15 (Ar H; this signal partially overlaps with the residual solvent peak), 7.09 (t, J = 7.5 Hz, 2H, Ar H), 6.95–6.89 (m, 2H, Ar H), 4.45 (br dt, 1H, =C*H*CH_2–), 4.33 (br dt, 1H, =C*H*CH_2–), 4.03 (br dt, 1H, =C*H*CH_2–), 3.81 (br dt, 1H, =C*H*CH_2–), 2.35–2.27 (m, 1H, =CHC*H*$_2$–), 2.24–2.13 (m, 2H, =CHC*H*$_2$–), 2.07–1.92 (m, 2H, =CHC*H*$_2$–), 1.98 (s, 6H, NCH_3), 1.85–1.76 (m, 1H, =CHC*H*$_2$–), 1.68–1.60 (m, 1H, =CHC*H*$_2$–) 1.44–1.36 (m, 1H, =CHC*H*$_2$–). IR (KBr, cm^{-1}): 540 (ν_{ss}).

Reaction of 6a with Triphenylphosphine. A solution of **6a** in C_6D_6 was prepared as described above, then a solution of 0.075–0.100 mmol of PPh_3 (10 equiv with respect to Ir) in 0.2 mL of C_6D_6 was added. The progress of the reaction was monitored by ^{31}P NMR spectroscopy. The intermediate was fully decayed within 1 h. ^{31}P{^{1}H} NMR (121.5 MHz, C_6D_6, δ): 43.4 (s, $SPPh_3$), –4.3 (s, PPh_3).

Reaction of 6a with 2,6-Dimethylphenyl Isocyanide. A solution of **6a** in C_6D_6 was prepared as described above, then a solution of 0.075–0.100 mmol of 2,6-dimethylphenyl isocyanide (10 equiv with respect to Ir) in 0.1 mL of C_6D_6 was added. The progress of the reaction was monitored by ^{1}H NMR spectroscopy. The intermediate was fully decayed within 1 d. 2,6-Dimethylphenyl isocyanate was detected by ^{1}H NMR spectroscopy.

5.3 Results and Discussion

5.3.1 Formation and Characterization of an (Alkene)persulfidoiridium(I) Intermediate

Addition of 0.25 equiv S_8 to a 15–20 mM solution of **1a** in benzene-d_6 at 20 °C causes a nearly immediate color change to orange from bright yellow followed by a gradual color change to green over ca. 1 h. Over the same time period, the ^{1}H NMR signals of **1a** disappear along with the appearance of new peaks which are assigned to intermediate **6a** and a byproduct (Scheme 20). The peaks from the byproduct decay over 4 d while the signals from **6a** gradually decay over ca. 25 d. Intermediate **6a** is fairly stable under these reaction conditions and is significantly more stable in comparison to **5a** which decays within 12 h after addition of O_2.

Scheme 20. Generation of Intermediate **6a**

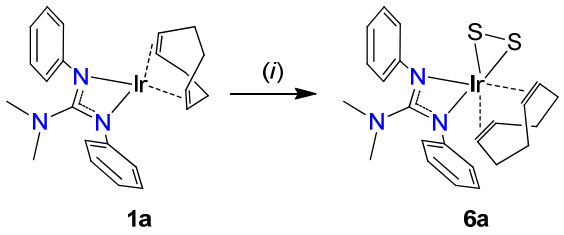

1a **6a**

(*i*) 0.25 equiv of S_8, 20 °C, benzene-d_6

The ^{1}H NMR spectrum of **6a**, shown in Figure 24, has two sets of three peaks for the aromatic protons, four multiplets for the alkene protons between 4.9 and 3.7 ppm along with a sharp singlet at 1.98 ppm for the NMe_2 protons and six broad multiplets for the CH_2 groups of the cod ligand.

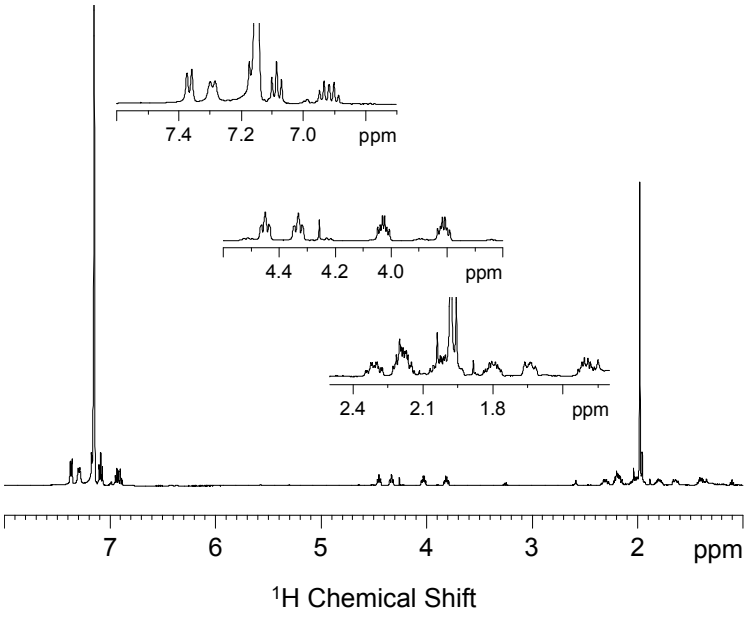

Figure 24. ^{1}H NMR spectrum of **6a** in benzene-d_6 (*ca*. 15 mM, 500 MHz, 20 °C). The resonance signal at 7.15 ppm partially overlaps with the residual solvent peak.

Further characterization of **6a** by two-dimensional NMR techniques revealed that the NMR data is consistent with a *cis*-[Ir{PhNC(NMe$_2$)NPh}(cod)X$_2$] complex and appears to be very similar to intermediate **5a**. The ^{1}H,^{1}H correlated spectroscopy (COSY) data, shown in Figure 25, confirms that two inequivalent phenyl rings are present and also shows that the alkene and methylene peaks can be assigned to one continuous cod ligand. The ^{1}H,^{13}C heteronuclear single-quantum coherence (HSQC) data, shown in Figure 26, confirms the assignment of the resonance signals and reveals that the four CH_2 groups of the cod ligand are correlated to four different ^{13}C resonances. The $\delta(^{13}C)$ values for the alkene carbon atoms obtained from the HSQC experiment fall in the range of 70–95 ppm and are greater than the corresponding values in **1a** (61.0 ppm), indicating decreased Ir-to-cod π back-bonding due to the increase in the oxidation state of iridium. With all observed resonances accounted for, **6a** was determined to accumulate in a yield of 70% by comparing the intensities of its alkene proton resonance signals to an internal standard (1,2-dichloroethane).

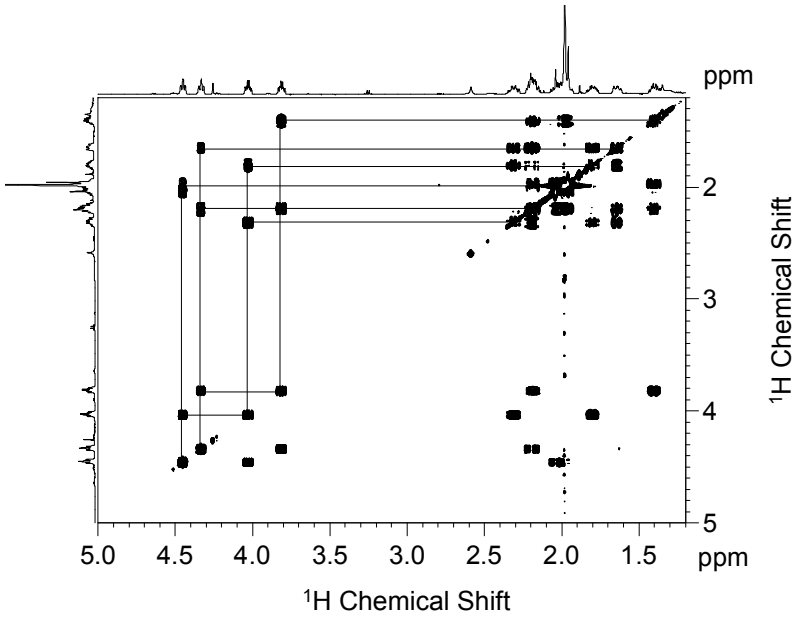

Figure 25. Part of the ^{1}H,^{1}H COSY NMR spectrum of **6a** in benzene-d_6 (*ca*. 15 mM, 500 MHz, 20 °C.). The solid lines indicate correlations among alkene proton resonances and between alkene and methylene proton resonances.

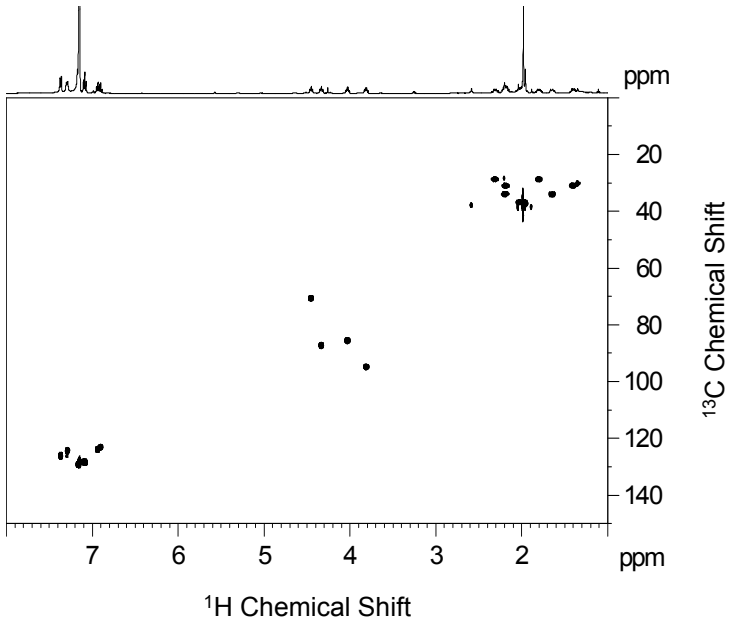

Figure 26. ^{1}H,^{13}C HSQC NMR spectrum of **6a** in benzene-d_6 (*ca*. 15 mM, 500 MHz, 20 °C).

The diffusion coefficient (D) of **6a** was determined to be 8.2 (±0.1) · 10^{-10} $m^2 \cdot s^{-1}$ which compares well with the values for **1a** (8.4 (±0.1) · 10^{-10} $m^2 \cdot s^{-1}$) and **5a** (8.2 (±0.3) · 10^{-10} $m^2 \cdot s^{-1}$) meaning **6a** has a similar hydrodynamic radius as these species and thus is a mononuclear species. The calculated values for the hydrodynamic radii (r_H) of these species are approximately 4.1(1) Å (**1a**), 4.2(2) Å (**5a**) and 4.2(1) Å (**6a**) (Section 4.3.2). The values of r_H show the peroxo and persulfido intermediates are nearly identical in size and, as expected, are slightly larger than the starting material. Figure 27 shows a plot of $\ln(I/I_0)$ vs. G^2 for the diffusion NMR data of **6a** with the expected linear relationship.

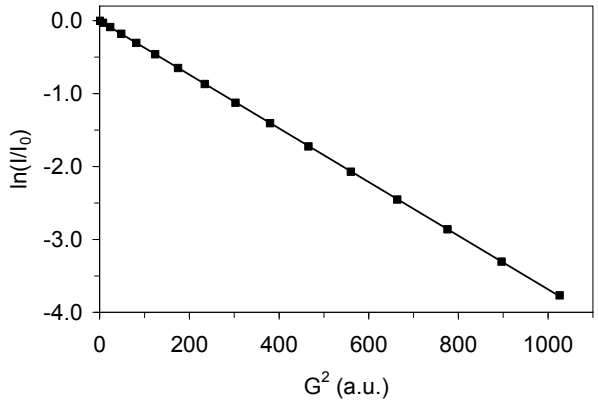

Figure 27 Plot of the natural logarithm of the intensity quotient, $\ln(I/I_0)$ *versus* the square of the gradient strength, G^2, for the NMe_2 resonance signal of **6a** (R^2 = 0.99998).

Evidence for the assignment of **6a** as an (alkene)persulfidoiridium(III) intermediate comes from IR spectroscopy. The solid-state (KBr) spectrum of **6a** has one weak signal at 540 cm^{-1} that is not present in the spectrum of a sample prepared using $^{34}S_8$. This band at 540 cm^{-1} falls in the range expected for SS stretching vibrations (ν_{SS}) of (η^2-persulfido)iridium(III) complexes.[110,111] Unfortunately, the shifted band for **6a**-$^{34}S_2$ (expected, 524 cm^{-1}) is masked by other signals in the spectrum and could not be observed. The band at 540 cm^{-1} is also absent from the IR spectra of **1a** and the decay

products of **6a** and **6a**-$^{34}S_2$. With the spectroscopic analysis that has been obtained and the similarities between **6a** and intermediate **5a**, we can formulate this intermediate as the (η^4-diene)(η^2-persulfido) complex [Ir{PhNC(NMe$_2$)NPh}(η^4-cod)(η^2-S$_2$)], **6a**. This is believed to be the first characterized (alkene)persulfidoiridium(III) complex and thus expands the information known for reactions with S_8 and also furthers our understanding of guanidinato complexes and their interesting reactivity.

5.3.2 Reactivity of the (Alkene)persulfidoiridium(I) Intermediate

We have investigated the reactions of this new (alkene)persulfidoiridium(III) intermediate with PPh_3 and 2,6-dimethylphenyl isocyanide. The reaction of **6a** with excess PPh_3 or 2,6-dimethylphenyl isocyanide, shown in Scheme 21, under mild reaction conditions shows the ability of this intermediate to transfer sulfur to simple organic substrates. The reactions of **6a** with PPh_3 and 2,6-dimethylphenyl isocyanide were monitored by NMR spectroscopy over 1 h (PPh_3) or 1 d (2,6-dimethylphenyl isocyanide) at 20 °C and the colors of the reaction mixtures turned from dark green to orange (PPh_3) or pale orange (2,6-dimethylphenyl isocyanide) during this time.

Scheme 21. Reaction of Intermediate **6a** with PPh_3 and 2,6-dimethylphenylisocyanide

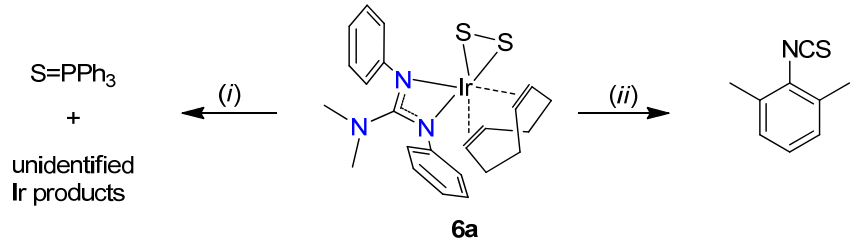

(*i*) 10 equiv of PPh_3, 20 °C, benzene-d_6; (*ii*) 10 equiv of 2,6-dimethylphenyl isocyanide, 20 °C, benzene-d_6

The reaction of **6a** with 10 equiv of PPh_3 yielded ca. 1.2 equiv of $SPPh_3$ within 1 h after addition, as determined by ^{31}P NMR spectroscopy. Taking into account the 70% yield of **6a**, this shows transfer of nearly two sulfur atoms per metal center and thus **6a** has the ability to transfer both sulfur atoms of the persulfido ligand to PPh_3. An analogous reaction with 10 equiv of 2,6-dimethylphenyl isocyanide was monitored by ^1H NMR spectroscopy showing formation of 2,6-dimethylphenyl isothiocyanate over 1 d. Using dichloroethane (5 equiv) as an internal standard, it was determined that ca. 0.6 equiv 2,6-dimethylphenyl isothiocyanate was formed showing that approximately one sulfur atom per metal center was transferred from the persulfido ligand.

It was discussed in Section 4.3.3 that intermediate **5a** reacts with carbon monoxide to release unmodified cod and form some of the dicarbonyl complex **2a**. Because of the similarities of these intermediates, the reaction of **6a** with CO was investigated. Purging CO(*g*) through a solution of **6a** at 20 °C for 10 min causes a gradual (7 h) color change to orange from green along with the formation of a small amount of orange precipitate. The reaction was monitored by ^1H NMR spectroscopy over 2 d with the release of unmodified cod being observed (0.4 equiv), but no formation of the dicarbonyl complex occurred. IR spectroscopy (benzene-d_6) was also taken after 2 d, with no peaks of any iridium(I) carbonyl species being observed. This experiment may suggest that the persulfido ligand in **6a** is bound more tightly to the iridium(III) metal center than the peroxo ligand in **5a**.

Intermediate **6a** is much more stable than the analogous (alkene)peroxoiridium(III) intermediate. The self-decay of this complex was investigated to determine if any C–S bond formation occurs. As intermediate **6a** decays, peaks from free cod along with peaks that are assigned to the unbound guanidine ligand can be observed which indicates decomposition of **6a**. The addition of excess cod to a solution of the decay products of **6a** shows no formation of any functionalized organic species even upon heating at 70 °C for 1 d. The decay products of the persulfido complex are

much less reactive than the decay products of the (alkene)peroxoiridium(III) intermediate and it appears that functionalization of any organic species is not possible under these reaction conditions.

5.4 Conclusion

In conclusion, a reactive (η^4-diene)(η^2-persulfido) intermediate was found to accumulate in high yield in the reaction of an Ir^{I}(cod) complex with S_8. Spectroscopic evidence shows this species is analogous to (η^4-diene)(η^2-peroxo) intermediates previously discussed in Section 4.3.2. This is believed to be the first characterized (alkene)persulfidoiridium(III) complex and thus expands the information known for reactions with S_8 and also furthers our understanding of our guanidinato complexes and their interesting reactivity. This complex has shown the ability to transfer up to two equiv of sulfur per metal center to simple organic reagents.

CHAPTER 6
SYNTHESIS, CHARACTERIZATION AND REACTIVITY OF IRIDIUM(I) COMPLEXES SUPPORTED BY AN AMIDINATO(1−) LIGAND

6.1 Introduction

This chapter includes the synthesis and characterization of $Ir^{I}(cod)$ and $Ir^{I}(CO)_2$ complexes supported by an amidinato ligand, $\{PhNC(Me)NPh\}^-$. These complexes have been synthesized to compare the ligand donor strength of the amidinato ligand to the guanidinato ligands and to compare the reactivity of an (alkene)(amidinato) complex toward O_2 to the guanidinato complexes discussed in Chapters 3 and 4. The carbonyl complexes with amidinato and guanidinato ligands exhibit structural differences that will be discussed. The cod complex reacts with O_2 and the corresponding (alkene)peroxoiridium(III) intermediate has been observed. The reactivity of the intermediate and its decay products are analogous to the guanidinato intermediates and formation of an oxidized organic species was also observed here.

6.2 Experimental Section

Materials. All reagents and solvents were purchased from commercial sources and were used as received, unless noted otherwise. Diethyl ether and toluene were deoxygenated by sparging with N_2 and purified by passage through two packed columns of molecular sieves under an N_2 pressure (MBraun solvent purification system). *n*-Pentane was dried over Na and distilled under N_2 prior to use.[59] Preparation and handling of air- and moisture-sensitive materials were carried out under an inert gas atmosphere by using either standard Schlenk and vacuum line techniques or a glovebox. Dioxygen was dried by passage through a short column of Drierite. Isotope-enriched $^{18}O_2$ (97% ^{18}O)

was purchased from Cambridge Isotope Laboratories, Andover, MA, USA. [{Ir(cod)}$_2$(μ-Cl)$_2$] was synthesized according to a published procedure (cod = 1,5-cyclooctadiene).[64] [{Ir(cod)}$_2$(μ-OMe)$_2$][65] was prepared from [{Ir(cod)}$_2$(μ-Cl)$_2$] and sodium methoxide in dichloromethane,[66] isolated by filtration and removal of the volatiles and used without further purification. The amidine PhN=C(Me)NHPh was synthesized from ethyl orthoacetate and aniline,[113] and the characterization matched data reported elsewhere.[114] Elemental analysis was performed by Atlantic Microlab, Inc., Norcross, GA, USA.

Physical Methods. NMR spectra were recorded on a Bruker Avance MicroBay 300, Avance 400 or Avance 500 spectrometer at ambient temperature, unless noted otherwise. ^{1}H, ^{13}C and ^{31}P chemical shifts are reported in parts per million (ppm) and were referenced to residual solvent peaks (for ^{1}H and ^{13}C NMR spectra) or an external standard [H_3PO_4 (85%, δ = 0 ppm) for ^{31}P NMR spectra]. Two-dimensional correlated spectroscopy (COSY) and heteronuclear single-quantum coherence (HSQC) experiments were carried out on a Bruker Avance 500 spectrometer at 25 °C using the gradient versions of the COSY and HSQC pulse sequences, and the data were processed using the TopSpin 2.1 software package. For ^{1}H,^{1}H COSY, typical measurement parameters were as follows: time domain data points (TD), 2048 for TD and 512 for TD1; number of scans (NS), 8; and number of dummy scans (DS), 32. The data were processed with zero-filling to 4096 (TD) and 512 (TD1). For ^{1}H,^{13}C HSQC, typical measurement parameters were as follows: 2048 for TD and 256 for TD1; NS, 16; and DS, 16. The data were processed with zero-filling to 2048 (TD) and 1024 (TD1). The total measurement time for each experiment was approximately 2 h. Self-diffusion coefficients (D) were determined from stimulated-echo experiments using bipolar gradients acquired in two-dimensional mode (stebpgp1s). These experiments were performed on a Bruker Avance 400 spectrometer at 25 °C. Prior to each experiment, the diffusion time (delay between the midpoints of the gradients, Δ) and gradient length (δ) were optimized using the one-dimensional version of the pulse sequence (stebpgp1s1d). The data acquisition for each

diffusion experiment took approximately 30 min. Data processing and analysis to determine *D* were carried out within the TopSpin 2.1 software package.

IR spectra were recorded on a Bruker Vertex 70 Fourier-transform IR spectrometer using solutions of the compounds in *n*-pentane or dimethyl sulfoxide-d_6 (5–15 mM) or solid samples. Solid samples were prepared by grinding the solid compound with KBr and pressing the mixture into a disk. Low-resolution mass spectral data were acquired on a quadrupole ion trap ThermoFinnigan LCQ Deca mass spectrometer using an electrospray ionization source or on a single quadrupole ThermoFinnigan Voyager mass spectrometer using an electron impact ionization source (equipped with a solids probe). High-resolution mass spectral data were acquired on a time-of-flight Waters GCT Premier mass spectrometer using an electron impact ionization source equipped with a solids probe. UV–Vis spectra were recorded on an HP 8453A diode array spectrophotometer (Agilent Technologies), which was equipped with a cryostat from Unisoku Scientific Instruments, Japan, for measurements at low temperature.

[Ir{PhNC(Me)NPh}(cod)] (7). Method A. A solution of 1.20 mmol of the *N*,*N*′-diphenylacetamidine and 1.1 equiv of methyllithium (1.6 M in Et_2O) in 15 mL of degassed diethyl ether was cooled to –40 °C under stirring. The resulting solution was allowed to warm to 20 °C and stirred for 1 h. Upon removal of the volatiles under reduced pressure, the Li^+ salt of the *N*,*N*′-diphenylacetamidinate anion, (Li{PhNC(Me)NPh}·Et_2O), was isolated as a colorless powder and stored under rigorous exclusion of moisture. The powder could also be recrystallized from a concentrated *n*-pentane solution at –30 °C to afford a microcrystalline solid.

In an N_2 atmosphere, a solution of 0.300 mmol of lithium amidinate in 10 mL of diethyl ether was added to a suspension of 100 mg (0.149 mmol) of [{Ir(cod)}$_2$(μ-Cl)$_2$] in 5 mL of diethyl ether under stirring at 20 °C. The color of the reaction mixture changed from orange to yellow–orange, accompanied by precipitation of a colorless solid. After 3

h, the solution was filtered and the solvent was removed under reduced pressure. The residue was recrystallized from *n*-pentane by preparing a concentrated solution at 20 °C and storing it at –30 °C. Yellow–orange single crystals were obtained after several recrystallizations. Yield (Method A): 102 mg (67%). Anal. Calcd for $C_{22}H_{25}IrN_2$: C, 51.84; H, 4.94; N, 5.50. Found: C, 52.29; H, 5.05; N, 5.69. ^{1}H NMR (300 MHz, C_6D_6, δ): 7.10 (t, J = 7.7 Hz, 4H, Ar H), 6.88 (t, J = 7.4 Hz, 2H, Ar H), 6.80 (d, J = 7.7 Hz, 4H, Ar H), 3.97 (br m, 4H, =C*H*CH_2–), 2.17 (br m, 4H, =CHC*H*$_2$–), 1.46 (s, 3H, CCH_3), 1.39 (m, 4H, =CHC*H*$_2$–). ^{1}H NMR (300 MHz, $CDCl_3$, δ): 7.26 (t, J = 7.9 Hz, 4H, Ar H), 7.02 (t, J = 7.4 Hz, 2H, Ar H), 6.91 (br, 4H, Ar H), 3.88 (br m, 4H, =C*H*CH_2–), 2.28 (br m, 4H, =CHC*H*$_2$–), 1.91 (s, 3H, CCH_3), 1.50 (m, 4H, =CHC*H*$_2$–). ^{13}C{^{1}H} NMR (75.5 MHz, $CDCl_3$, δ): 182.6 (N_2*C*CH_3), 144.6, 128.7, 123.9, and 123.6 (Ar), 63.3 (=*C*HCH_2–), 31.8 (=CH*C*H_2–), 17.4 (C*C*H_3). EIMS (70 eV) m/z: $M^{+\bullet}$ calcd for $C_{22}H_{25}IrN_2$, 510.2; found, 510.2. UV-Vis (toluene) λ_{max}, nm (ε): 349 (3300), 402 (1550), 440 (sh), 495 (sh).

Method B. In an N_2 atmosphere, a solution of 0.300 mmol of the *N*,*N*-dialkyl-*N*′,*N*″-diarylguanidine in 15 mL of diethyl ether was added to a suspension of 0.149 mmol of [{Ir(cod)}$_2$(μ-OMe)$_2$] in 5 mL of diethyl ether under stirring. The dark–orange mixture turned into a yellow–orange solution. After 3 h, the volatiles were removed under reduced pressure to afford a yellow–orange oil. The residue was recrystallized as described above (Method A). Yield: 118 mg (78%). The UV–Vis spectrum of this batch was identical to that of the product obtained from Method A.

[{Ir(CO)$_2$}$_2${μ-PhNC(Me)NPh-κN:$\kappa N'$}$_2$] (8). A steady stream of CO(*g*) was purged through a solution of 52.4 mg (0.103 mmol) of [Ir{PhNC(Me)NPh}(cod)] in 15 mL of diethyl ether for 15 min at 20 °C. The yellow–orange solution gradually turned purple over the first five minutes. Subsequently, the volatiles were removed under reduced pressure to afford a purple solid, which was recrystallized by preparing a concentrated solution in *n*-pentane at 20 °C and storing it at –30 °C. The solid obtained after several recrystallizations still contained minor impurities according to ^{1}H NMR

spectroscopy (approximate yield: 60%). ^{1}H NMR (300 MHz, $(CD_3)_2SO$, δ): 7.30 (br, 8H, Ar H), 7.23 (t, J = 7.7 Hz, 4H, Ar H), 7.15 (t, J = 7.3, 8H, Ar H), 1.73 (s, 6H, CCH_3). $^{13}C\{^1H\}$ NMR (75.5 MHz, $(CD_3)_2SO$, δ): 175.0 (IrCO), 170.7 (N_2CCH_3), 150.4, 128.8, 126.5 (br), and 125.1 (Ar), 19.3 (CCH_3). High-resolution EIMS (70 eV) m/z: $M^{+\bullet}$ calcd for $C_{32}H_{26}Ir_2N_4O_4$, 914.1190; found, 914.1196 ($M^{+\bullet}$), 886.1268 ($\{M - CO\}^{+\bullet}$), 858.1315 ($\{M - 2CO\}^{+\bullet}$), 830.1391 ($\{M - 3CO\}^{+\bullet}$), 802.1378 ($\{M - 4CO\}^{+\bullet}$), 458.0615 ($\{M/2\}^{+\bullet}$), 430.0697 ($\{M/2 - CO\}^{+\bullet}$), 402.0754 ($\{M/2 - 2CO\}^{+\bullet}$). IR (n-pentane, cm^{-1}): 2067, 2034 and 1992 (ν_{CO}). IR (dmso-d_6, cm^{-1}): 2058, 2025 and 1981 (ν_{CO}). IR (KBr, cm^{-1}): 2060, 2026 and 1982 (ν_{CO}). UV-Vis (toluene) λ_{max}, nm (ε): 400 (1050), 550 (2800).

Reactions of [Ir{PhNC(Me)NPh}(cod)] (7) with O_2. A 1 mM solution of **7** (0.001 mmol) in 1 mL of toluene was placed in a 0.5-cm UV–Vis cuvette, precooled to 0 °C and purged with O_2 (40 s). Kinetic data for the reaction of **7** with O_2 were obtained under pseudo-first-order conditions at –40 °C with complex concentrations in the range of 0.20 – 0.96 mM.

Generation and Characterization of [Ir{PhNC(Me)NPh}(Me)I] (9). To a 16.5 mM solution of [Ir{PhNC(NMe_2)NPh}(cod)] (4.2 mg, 0.0082 mmol) in 0.5 mL of C_6D_6 was added 0.0051 mL of a methyl iodide solution in C_6D_6 (1.2 mg, 0.0082 mmol). The resulting solution was allowed to stand for 1 d at 20 °C. The progress of the reaction was monitored by ^{1}H NMR spectroscopy. ^{1}H NMR (300 MHz, C_6D_6, δ): 7.20–7.07 (m, Ar H; these signals partially overlap with the residual solvent peak), 6.94 (t, J = 7.0 Hz, 2 H, Ar H), 5.02–4.90 (m, 2H, =C*H*CH_2–), 3.66–3.50 (m, 2H, =C*H*CH_2–), 3.07–2.94 (m, 2H, =CHC*H*$_2$–), 2.52 (s, 3H, $IrCH_3$), 1.90–1.72 (m, 2H, =CHC*H*$_2$–), 1.71–1.60 (m, 2H, =CHC*H*$_2$–), 1.37 (s, 3H, CCH_3) 1.04–0.97 (m, 2H, =CHC*H*$_2$–). EIMS (70 eV) m/z: $M^{+\bullet}$ calcd for $C_{23}H_{28}IrN_2I$, 652.1; found, 652.1.

Generation and Characterization of [Ir{PhNC(Me)NPh}(η^4-cod)(η^2-O_2)] (10). In a typical experiment, a 15–20 mM solution of **7** (3.8–5.1 mg, 0.0075–0.010 mmol) in 0.5 mL of C_6D_6 was placed in an NMR tube and purged with O_2(g) at 20 °C for

40 s. The progress of the reaction was monitored by ^{1}H NMR spectroscopy. Under these conditions, **7** (yellow−orange solution) converted into the intermediate, **10** (pale yellow solution), in about 15 min, and **10** was typically fully decayed (dark green solution) within 8 h after the addition of O_2 to **7**. For quantification, 5 equiv of 1,2-dichloroethane (3.0−3.9 μL, 3.8−4.9 mg, 0.038−0.050 mmol) was added to the solution of **10**, and the yield was estimated by comparing the integrations of the 1,2-dichloroethane (δ, 2.90 ppm) and alkene proton signals (ca. 75%). For IR spectroscopy, 0.15 mL of a solution of **10** was mixed with KBr. The mixture was evaporated to dryness (20 °C, *in vacuo*) and pressed into a disk. For labeling experiments, 5 mL (ca. 0.2 mmol) of $^{18}O_2$ (97% ^{18}O) was added to a 15−20 mM solution of **7** (0.0075−0.010 mmol) in 0.5 mL of C_6D_6.

^{1}H NMR (500 MHz, C_6D_6, δ): 7.37 (d, J = 7.8 Hz, 2H, Ar H), 7.12 (m, Ar H; this signal partially overlaps with the residual solvent peak), 7.08−7.04 (m, 4H, Ar H), 6.98 (t, J = 7.2 Hz, 1H, Ar H), 6.93 (t, J = 7.2 Hz, 1H, Ar H), 4.98−4.95 (m, 1H, =C*H*CH$_2$−), 4.83−4.79 (m, 1H, =C*H*CH$_2$−), 4.22−4.17 (m, 1H, =C*H*CH$_2$−), 3.97−3.93 (m, 1H, =C*H*CH$_2$−), 2.29−2.18 (m, 2H, =CHC*H*$_2$−), 2.04−1.88 (m, 2H, =CHC*H*$_2$−), 1.68−1.59 (m, 2H, =CHC*H*$_2$−), 1.34 (s, 3H, CCH$_3$), 1.29−1.12 (m, 2H, =CHC*H*$_2$−). ^{1}H NMR (300 MHz, $CDCl_3$, δ): 7.27 (d, J = 7.3 Hz, 2H, Ar H), 7.17−7.10 (m, Ar H; these signals partially overlap with the residual solvent peak), 7.06 (d, J = 8.5 Hz, 2H, Ar H), 6.94 (t, J = 7.2 Hz, 1H, Ar H), 4.95−4.88 (m, 1H, =C*H*CH$_2$−), 4.80−4.70 (m, 1H, =C*H*CH$_2$−), 4.17−4.07 (m, 1H, =C*H*CH$_2$−), 3.90−3.80 (m, 1H, =C*H*CH$_2$−), 2.68−2.55 (m, 1H, =CHC*H*$_2$−), 2.40−2.15 (m, 3H, =CHC*H*$_2$−), 2.08−1.93 (m, 2H, =CHC*H*$_2$−), 1.84 (s, 3H, CCH$_3$), 1.62−1.52 (m, 1H, =CHC*H*$_2$−), 1.39−1.23 (m, 1H, =CHC*H*$_2$−). IR (KBr, cm^{-1}): 860 and 843 (ν_{OO}), 574 and 467 (ν_{IrO}). IR of **10**-$^{18}O_2$ (KBr, cm^{-1}): 807 (ν_{OO}), 544 and 445 (ν_{IrO}).

Reaction of 10 with Triphenylphosphine. A solution of **10** in C_6D_6 was prepared as described above (ca. 15 min for the formation of **10**) and then purged with Ar for 5 min to remove excess O_2. A solution of 0.075−0.100 mmol of PPh_3 (10 equiv with respect to Ir) in 0.2 mL of C_6D_6 was added to the solution of **10**, and the progress of the

reaction was monitored by ^{31}P NMR spectroscopy. The intermediate was fully decayed within 40 min (pale orange solution). $^{31}P\{^{1}H\}$ NMR (121.5 MHz, C_6D_6, δ): 25.6 (s, $OPPh_3$), –4.5 (s, PPh_3), –6.9 (s).

Reaction of the Decay Products of 10 with 1,5-Cyclooctadiene. A 15–20 mM solution of **7** in C_6D_6 was purged with O_2 as described above, allowed to stand for at least 16 h, and then purged with Ar for 5 min to remove excess O_2. Alternatively, the solution was evaporated to dryness (20 °C, *in vacuo*), and the residue was dissolved in deoxygenated C_6D_6. After addition of 0.015–0.020 or 0.075–0.100 mmol of cod (2 or 10 equiv with respect to Ir), the solution was kept at 20 °C for 1 d and then heated at 70 °C for 1 d (NMR tube equipped with a J. Young valve). During this time the color of the solution changed from dark green to orange. 4-Cycloocten-1-one[23,109] and **7** were identified as products by ^{1}H NMR spectroscopy and EIMS. Quantifications (against 1,2-dichloroethane as a standard) were performed in triplicate. The average yields were 0.66 (±0.18) equiv of 4-cycloocten-1-one and 0.21 (±0.02) equiv of **7**. Data for 4-cycloocten-1-one were as follows: ^{1}H NMR (300 MHz, C_6D_6, δ): 5.65 (m, 1H, =C*H*CH_2–), 5.37 (m, 1H, =C*H*CH_2–), 2.66 (m, 1H, =CHC*H*$_2$–), 2.24 (m, 3H, =CHC*H*$_2$–), 2.10 (m, 2H, =CHC*H*$_2$–), 1.40–1.31 (m, 4H, =CHC*H*$_2$—). EIMS (70 eV) *m*/*z*: $M^{+\bullet}$ calcd for $C_8H_{12}O$, 124.1; found, 124.3 (the expected fragmentation pattern[95] was observed as follows: 109.3, 96.3, 81.3, 67.2, 54.2). For the reaction carried out using $^{18}O_2$, EIMS (70 eV) *m*/*z*: 126.3 ($M^{+\bullet}$; fragmentation pattern: 111.3, 96.3, 81.3, 67.2, 54.2).

6.3 Results and Discussion

6.3.1 Synthesis and Characterization of Alkene and Carbonyl Complexes Supported by an Amidinato Ligand

The neutral amidine PhN=C(Me)NHPh precursor was synthesized by a literature procedure and its characterization matches that of the published compound.[113,114] The amidinato Ir^{I}(cod) complex was synthesized by two different synthetic methods which are analogous to the synthesis of the guanidinato complexes discussed in Section 3.3.2 (Scheme 22).[58] Treatment of the neutral amidine with MeLi followed by transmetalation using [{Ir(cod)}$_2$(μ-Cl)$_2$][64] under an inert atmosphere furnished the yellow–orange iridium(I) complex [Ir{PhNC(Me)NPh}(cod)], **7**. The second method, shown in Scheme 22, is a one-step procedure where the neutral ligand is reacted with [{Ir(cod)}$_2$(μ-OMe)$_2$] under an inert atmosphere to give **7** (this method uses the internal base, MeO^-, for *in situ* deprotonation of the neutral ligand). Complex **7** is well soluble in low-polarity organic solvents such as toluene, diethyl ether, and *n*-pentane but only sparingly soluble in acetonitrile.

Scheme 22. Synthesis of (Cyclooctadiene)iridium(I) Complex **7**

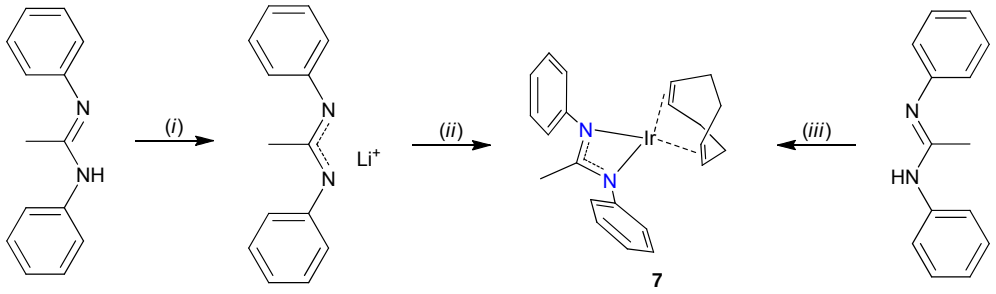

(*i*) MeLi, –78 °C → 20 °C, diethyl ether; (*ii*) [{Ir(cod)}$_2$(μ-Cl)$_2$], 20 °C, diethyl ether; (*iii*) [Ir{(cod)}$_2$(μ-OMe)$_2$], 20 °C, CH_2Cl_2

The ^{1}H NMR spectrum of **7**, shown in Figure 28, is consistent with an amidinato-κ^2N,N' and an η^4-cod ligand coordinated to a d^8 iridium(I) center in a square-planar environment. Analysis of **7** by EI MS shows a molecular ion peak for a mononuclear complex [Ir{PhNC(Me)NPh}(cod)] (*m*/*z* = 510). Based on ^{1}H NMR and EI MS analysis,

7 was identified as a mononuclear [Ir{PhNC(Me)NPh}(cod)] complex analogous to the guanidinato complexes previously discussed in Chapter 3.

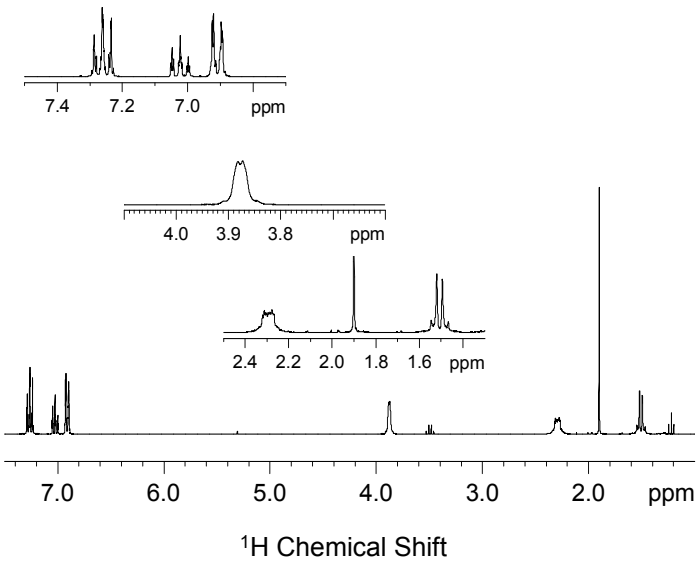

Figure 28. ^{1}H NMR spectrum of (cyclooctadiene)iridium(I) complex **7** in $CDCl_3$.

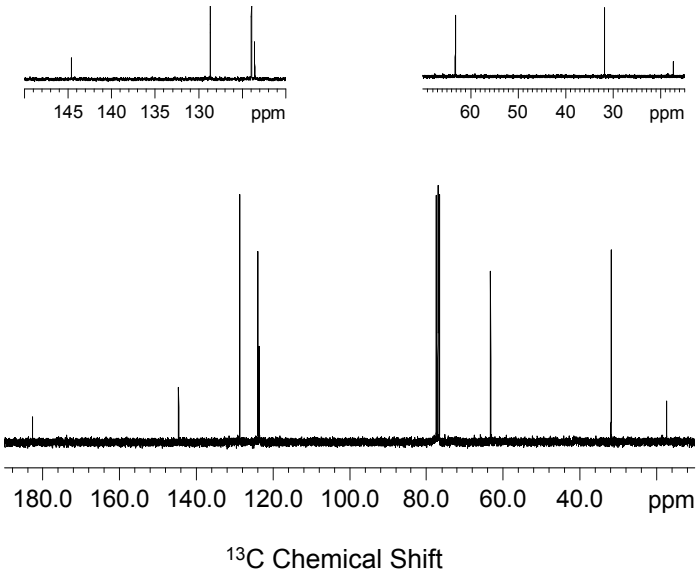

Figure 29. ^{13}C NMR spectrum of (cyclooctadiene)iridium(I) complex **7** in $CDCl_3$.

This complex was also characterized by ^{13}C NMR spectroscopy, and comparison of the donor strength of the amidinato ligand in **7** to the guanidinato ligands (in **1a**–**1g**) was done. Complex **7** exhibits a ^{13}C NMR resonance (Figure 29) for the alkene carbon atoms at 63.3 ppm which is significantly downfield shifted compared to the guanidinato complexes (58.7–61.0 ppm)[58] and indicates lower Ir-to-cod π back-bonding. This result indicates that the acetamidinato ligand is a less strongly donating ligand than the guanidinato ligands discuss in Chapter 3.

Scheme 23. Synthesis of Tetracarbonyldiiridium(I) Complex **8**

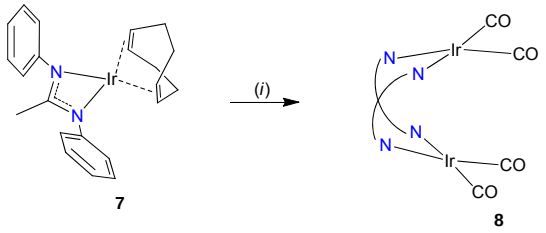

(*i*) CO(*g*), 20 °C, diethyl ether

We have previously synthesized the guanidinato $Ir^{I}(CO)_2$ complexes by a ligand substitution reaction using the Ir^{I}(cod) complexes as discussed in Section 3.3.3.[115] We have employed the same method here for the synthesis of the amidinato carbonyl complex. Bubbling CO(*g*) through a diethyl ether solution of **7** at 20 °C for 15 min causes a gradual (5 min) color change from yellow–orange to purple (Scheme 23). The reaction proceeded in a similar manner as for the guanidinato dicarbonyl complexes, but purification of the purple material obtained from the reaction was much more difficult. After several recrystallization attempts, the purple solid still contained some impurities, as observed in the ^{1}H NMR spectrum. Although somewhat impure, this purple material was characterized by NMR and IR spectroscopy and EI MS.

The ^{1}H NMR spectrum of **7** in dmso-d_6 shows three signals for the aromatic protons (one broad signal and two triplets) and one intense singlet for the CCH_3 protons along with some signals from impurities. High-resolution electron impact mass spectrometry (HREI MS) has a molecular ion peak at m/z = 916.1213 (calcd, m/z = 916.1208) which is consistent with the dinuclear tetracarbonyl complex, [{Ir(CO)$_2$}$_2${μ-PhNC(Me)NPh-κN:$\kappa N'$}$_2$], along with peaks from the loss of 1–4 CO ligands. Also observed is a peak at m/z = 458.0615 (calcd, m/z = 458.0607) which can be assigned to the mononuclear dicarbonyl species [Ir{PhNC(Me)NPh}(CO)$_2$], which is half of the dinuclear species. Peaks assigned to the loss of one and two CO ligands from this mononuclear species are also observed.

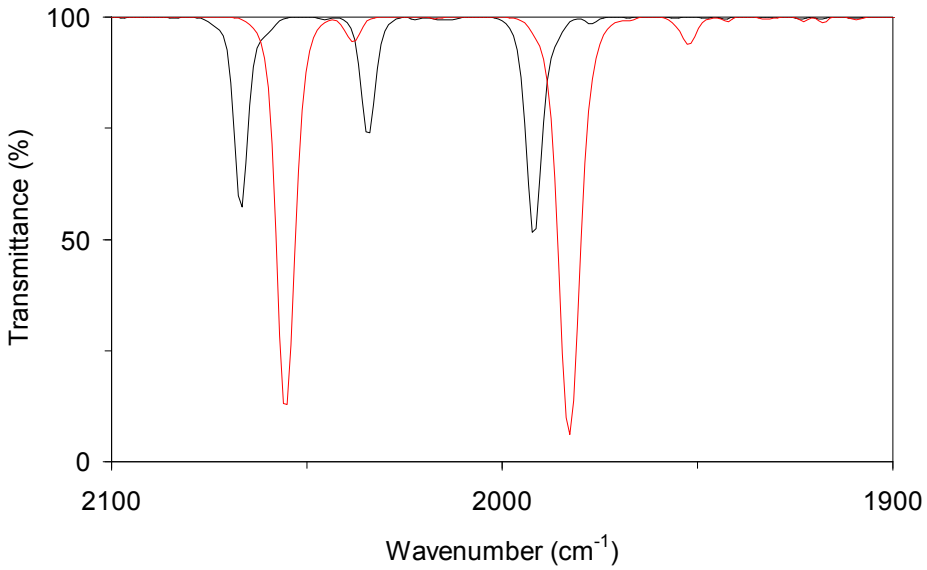

Figure 30. IR spectra of iridium carbonyl complexes **2a** (—, red) and **7** (—, black) in *n*-pentane.

The IR analysis, both solid- and solution-state, of this material shows three bands in the CO stretching region. The solid-state (KBr) IR spectrum has bands at 2060, 2026 and 1982 cm^{-1} while the solution-state (*n*-pentane) IR spectrum, shown in Figure 30, has

three bands at 2067, 2034 and 1992 cm^{-1} which are all assigned to CO stretching modes (ν_{CO}). This is different than the IR spectrum that was obtained for the guanidinato dicarbonyl complex, [Ir{PhNC(NMe_2)NPh}$(CO)_2$] **2a**, which is mononuclear and has only two bands in the CO stretching region at 2055 and 1983 cm^{-1} (Figure 30).[115] Further evidence of a dinuclear complex comes from determination of the diffusion coefficient (D) for **8**. A diffusion NMR experiment (dmso-d_6) to determine D for this complex was performed with the average from value three experiments being 2.2 (±0.1) · 10^{-10} $m^2 \cdot s^{-1}$ which is significantly lower than that for [Ir{PhNC(NMe_2)NPh}$(CO)_2$] (**2a**) (2.8 (±0.2) · 10^{-10} $m^2 \cdot s^{-1}$) in dmso-d_6 indicating **8** is significantly larger than **2a**. The plots in Figure 31 confirm the expected linear relationship between $\ln(I/I_0)$ and G^2. The hydrodynamic radii of these complexes were calculated from D and determined to be approximately 3.5(2) Å (**2a**) and 4.6(1) Å (**8**) (Section 4.3.2).[103,104] ^{1}H NMR and IR analysis of **8** was also performed at high concentrations (up to at least 40 mM in dmso-d_6) with no changes in the spectra being observed which indicates there is no monomer-dimer equilibrium occurring in solution for this concentration range. From the analysis discussed here, we have assigned **8** as the dinuclear tetracarbonyl complex [{Ir$(CO)_2$}$_2${μ-PhNC(Me)NPh-κN:$\kappa N'$}$_2$].

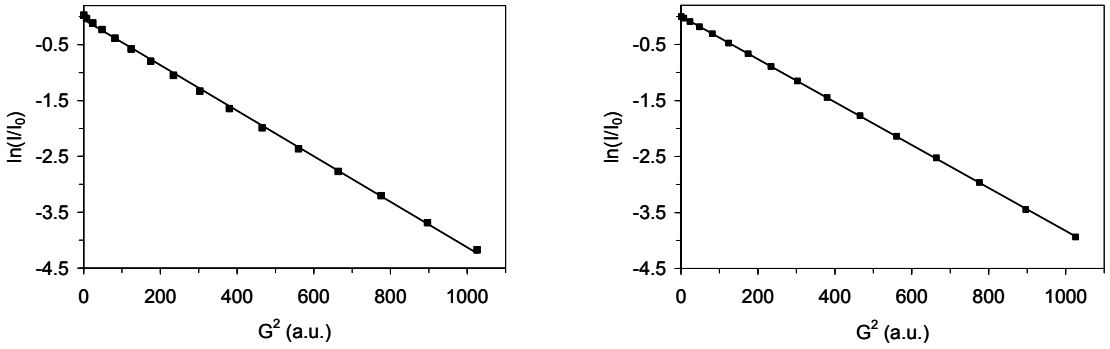

Figure 31. Plots of the natural logarithm of the intensity quotient, $\ln(I/I_0)$, *versus* the square of the gradient strength, G^2, for the NMe_2 or CCH_3 resonance signal of **2a** (left, R^2 = 0.99914) and **8** (right, R^2 = 0.99996).

6.3.2 Oxidative Addition of MeI to an Amidinato Cyclooctadiene Complex

Addition of 10 equiv of MeI to a 2 mM solution of **7** in toluene at 20 °C shows a slow decay of the characteristic UV-Vis peaks of **7** over ca. 20 h (Figure 32). Analysis of the reaction mixture by EI MS was done with a peak at m/z = 652 being observed, which may be assigned to the six-coordinate species [Ir{PhNC(Me)NPh}(cod)(Me)I], **9**. However, analysis of the reaction mixture by ESI MS shows no peaks that can be assigned to any interesting final complexes.

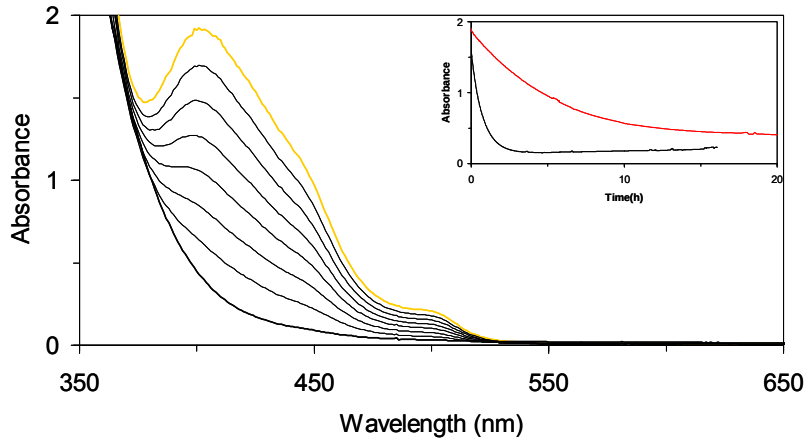

Figure 32. Reaction of 2 mM **7** (orange line) in toluene with 10 equiv of MeI at 20 °C as monitored by electronic absorption spectroscopy (path length, 0.5 cm). Inset: Time courses of the reactions of **1a** (black line; λ, 417 nm) and **7** (red line; λ, 402 nm) with 10 equiv MeI.

Investigation of a this reaction was done by ^{1}H NMR spectroscopy by the addition of 1 equiv of MeI to a 19 mM solution of **7** in benzene-d_6 at 20 °C. Decay of the peaks from the starting material and formation of peaks from a new species (**9**) and some byproduct are observed over ca. 1 d. The ^{1}H NMR and EI MS analysis shows that complex **9** is analogous to **3a** and can be assigned to [Ir{PhNC(Me)NPh}(cod)(Me)I]. It

is stable for at least 5 d at 20 °C, similar to the guanidinato complex **3a**. The yield of **9** was determined by addition of 1,2-dichloroethane (5 equiv) as an internal standard. Comparison of the alkene protons to that of the internal standard shows **9** accumulates in ca. 50% yield. The UV-Vis time courses of the reactions of **1a** and **7** with 10 equiv of MeI are shown in Figure 32. Interestingly, formation of **9** is much slower than formation of **3a**. This result is what one would expect based on ligand donor strength with the more strongly donating guanidinato ligand destabilizing the iridium(I) center to a larger extent than the amidinato ligand and thus causing an increase in the reactivity toward MeI.

The reaction of **7** with MeOTf was also attempted with formation of a number of different species being observed in the ^{1}H NMR spectrum upon addition of 1 equiv of MeOTf to a 20 mM solution of **7** in benzene-d_6 at 20 °C. Because of this result, no further reactions have been performed.

6.3.3 Identification and Characterization of an (Alkene)peroxoiridium(III) Intermediate in the Reaction with O_2

The reaction of **7** with O_2 was investigated by UV-Vis spectroscopy in a similar manner as for the guanidinato complexes. Addition of excess O_2 to a 1 mM solution of **7** at 0 °C in toluene shows decay of the characteristic peaks from the starting material to form a featureless spectrum (Figure 33). This reaction is very fast even at 0 °C with $t_{1/2}$ = 100 s, which is much faster than what was observed for the O_2 reactions of the guanidinato cod complexes. This can be observed from the time course of these reactions, as shown in Figure 33. Based on the lower electron donating ability of the amidinato ligand, it would be expected to have a much slower reaction in comparison to the guanidinato cod complexes. The unexpected results observed here can be explained by the difference in steric influence of the ligands. The Me group of the amidinato ligand is less sterically bulky than the NR_2 group of the guanidinato ligands and this allows the

benzene rings to rotate more in plane with the $MeCN_2Ir$ fragment and thus allows greater access to the metal center.

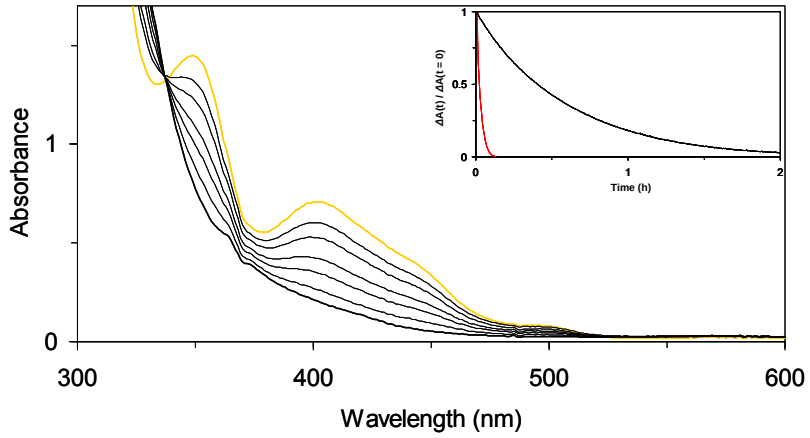

Figure 33. Reaction of 1 mM **7** (orange line) in toluene with O_2 at 0 °C as monitored by electronic absorption spectroscopy (path length, 0.5 cm). Inset: Time courses of the reactions of **1a** (—, black; λ, 417 nm) and **7** (—, red; λ, 402 nm) with O_2.

Scheme 24. Generation of (Alkene)peroxo Intermediate **10**

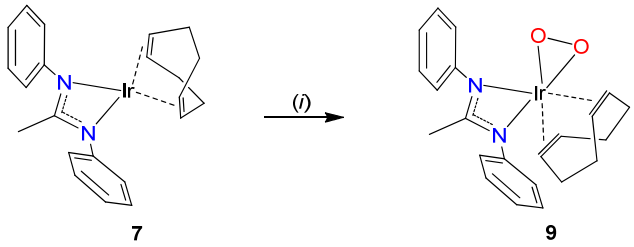

(*i*) O_2, 20 °C, benzene-d_6 or toluene

The kinetics of the reaction of **7** with O_2 was investigated under pseudo-first-order conditions at –40 °C, with concentrations of **7** between 0.20–0.96 mM. It was determined that the rate of the reaction is independent of the concentration of **7** under these conditions. The rate of the reaction was determined to be ca. five times slower when the

analogous set of experiments ([Ir], 0.20–0.91 mM, –40 °C) was performed with air, which is consistant with the five times lower concentration of O_2 in air. The overall reaction is second-order, first-order with respect to both iridium and O_2.

We have previously identified and characterized reactive (alkene)peroxoiridium(III) intermediates from the reaction of the guanidinato complexes with O_2.[57] We have also investigated the reaction of **7** with O_2 to determine if a similar intermediate can be observed for this complex. When O_2 was added to a 15−20 mM solution of **7** in benzene-d_6 at 20 °C (Scheme 24), the ^{1}H NMR signals of **7** disappear with signals from a new species developing over 15 min. These signals decay over ca. 8 h, indicating the newly formed intermediate, **10**, is fairly unstable.

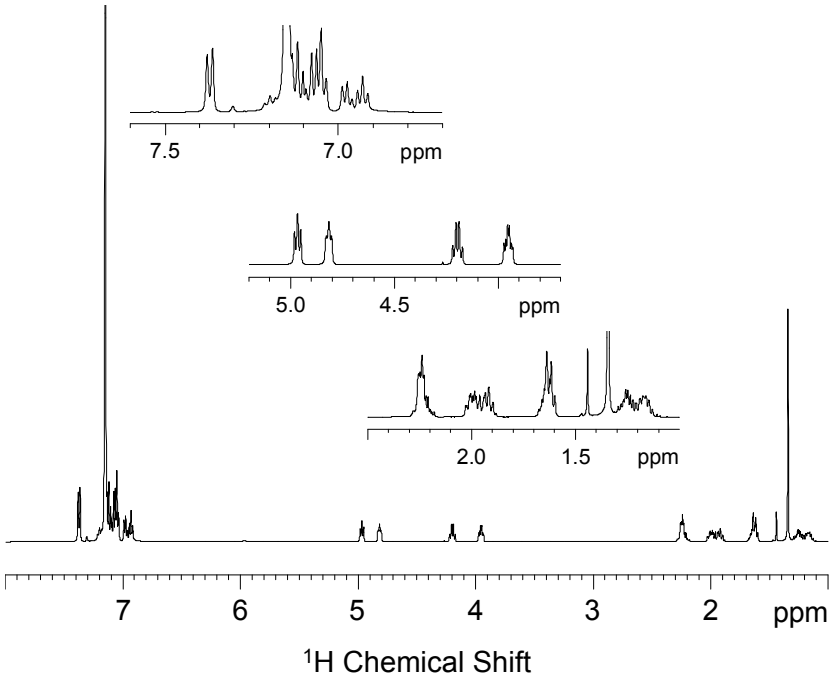

Figure 34. ^{1}H NMR spectrum of **10** in benzene-d_6 (*ca*. 15 mM, 500 MHz, 20 °C. The resonance signal at 7.15 ppm partially overlaps with the residual solvent peak.

The formation of this intermediate is significantly faster than that of the guanidinato intermediates, while the stability of the amidinato and guanidinato intermediates are similar. During the progression of the reaction, the yellow–orange solution of **7** turned pale yellow (**10**) and then dark green. The ^{1}H NMR spectrum of **10**, shown in Figure 34, is nearly analogous to that of the intermediates observed from the O_2 reaction of the guanidinato iridium(I) complexes (**5a**–**5f**). The NMR spectrum contains six broad multiplets for the CH_2 groups and four broad signals for the alkene protons of the cod ligand along with one intense singlet for the CCH_3 protons and two sets of three signals for the aromatic protons.

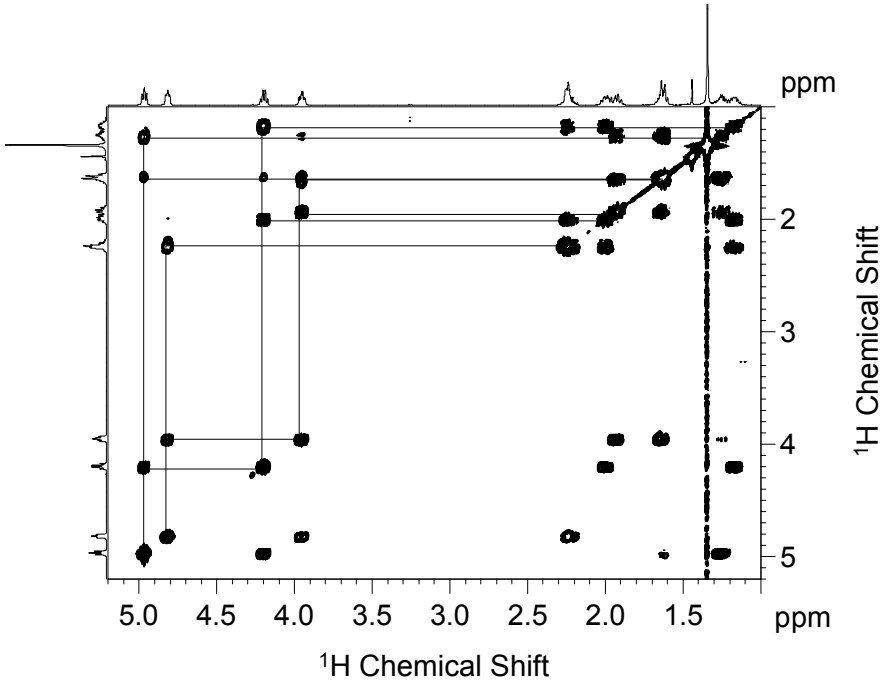

Figure 35. Part of the ^{1}H,^{1}H COSY spectrum of **10** in benzene-d_6 (*ca*. 15 mM, 500 MHz, 20 °C). The solid lines indicate correlations among alkene proton resonances and between alkene and methylene proton resonances.

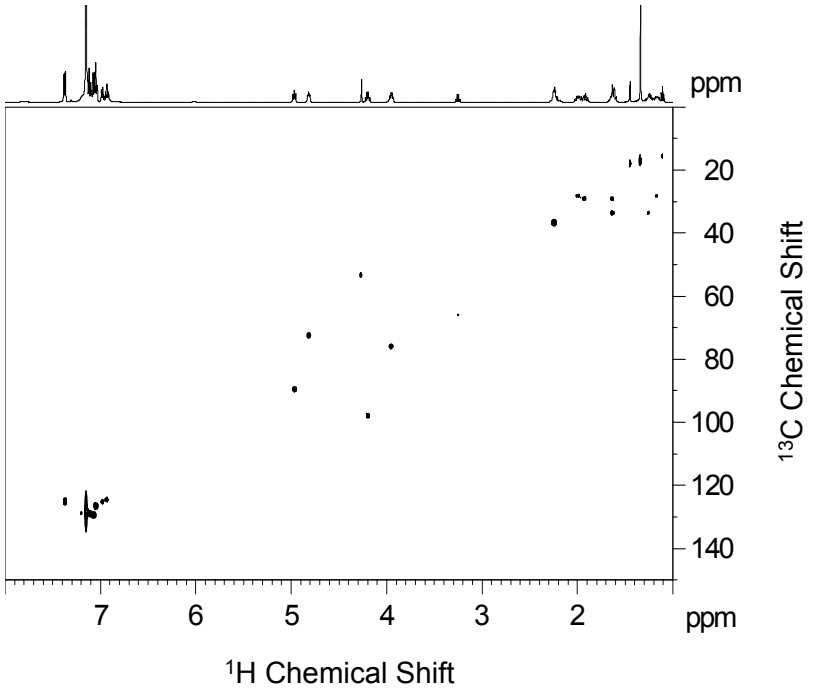

Figure 36. ^{1}H,^{13}C HSQC spectrum of **10** in benzene-d_6 (*ca*. 15 mM, 500 MHz, 20 °C).

Further characterization of **10** by two-dimensional NMR techniques gives more evidence for the formation of an (alkene)peroxoiridium(III) intermediate. ^{1}H,^{1}H COSY NMR data confirm the presence of two inequivalent phenyl groups and one unique cod ligand (Figure 35). The ^{1}H,^{13}C HSQC NMR data confirm the assignments for the multiplets in the range of 1.1–2.3 ppm to the CH_2 groups and revealed that each of the four groups correlate to four different ^{13}C resonances (Figure 36 and Table 14). The HSQC experiment gives the values for $\delta(^{13}C)$ for the alkene carbons which were observed in the range of 70–100 ppm and are greater than those of **7** (63.3 ppm) which indicates decreased Ir-to-cod π back-bonding due to the increase in the oxidation state of iridium. Comparison of the resonance signal of added 1,2-dichloroethane (5 equiv) to that of the alkene protons of the intermediate, it was determined that **10** accumulates in a yield of 75%.

Table 14. ^{1}H and ^{13}C chemical shifts, δ (ppm), from the ^{1}H,^{13}C HSQC spectrum of **10** in benzene-d_6.

Assignment		$\delta(^{1}H)$	$\delta(^{13}C)$
Ar	Group A	7.32	123.0
		7.12[a]	128.8
		6.93	124.4
	Group B	7.07	129.4
		7.06	126.5
		6.97	125.2
=*CH*CH$_2$–	1-H, C-1	4.20	97.8
	2-H, C-2	4.97	89.5
	5-H, C-5	3.95	75.8
	6-H, C-6	4.82	72.4
=CH*CH$_2$*–	3-H$_{ab}$, C-3	1.27, 1.64	33.6
	4-H$_{ab}$, C-4	1.64, 1.92	29.0
	7-H$_{ab}$, C-7	2.23[b]	36.6
	8-H$_{ab}$, C-8	1.15, 1.99	28.1
CH$_3$		1.34	17.1

[a] The resonance signals centered at $\delta(^{1}H)$ = 7.12 ppm and $\delta(^{13}C)$ = 128.0 ppm partially overlap with the residual solvent peaks. [b] The peak at 2.23 ppm corresponds to two H's on the same CH$_2$ group.

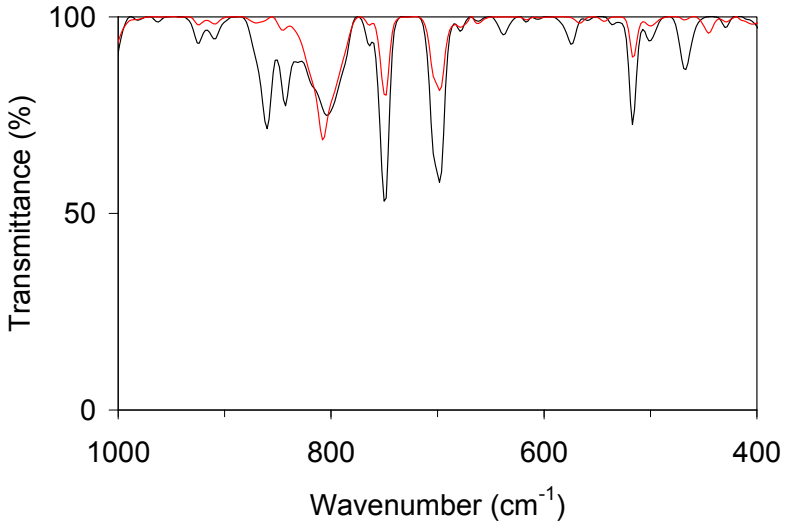

Figure 37. IR spectra of **10** (—, black) and **10**-$^{18}O_2$ (—, red).

Intermediate **10** was also characterized by IR spectroscopy with evidence for the incorporation of O_2 being obtained from experiments with $^{16}O_2$ and $^{18}O_2$. Intermediate **9** was evaporated to dryness with no observable decay to obtain the solid-state IR (KBr) spectra. The IR spectrum of **10** is somewhat more complex than that of the guanidinato intermediates with four ^{18}O-isotope-sensitive bands observed at 860, 843, 574, and 467 cm^{-1} (for **10**-$^{18}O_2$, 807, 544 and 445 cm^{-1}, Figure 37).

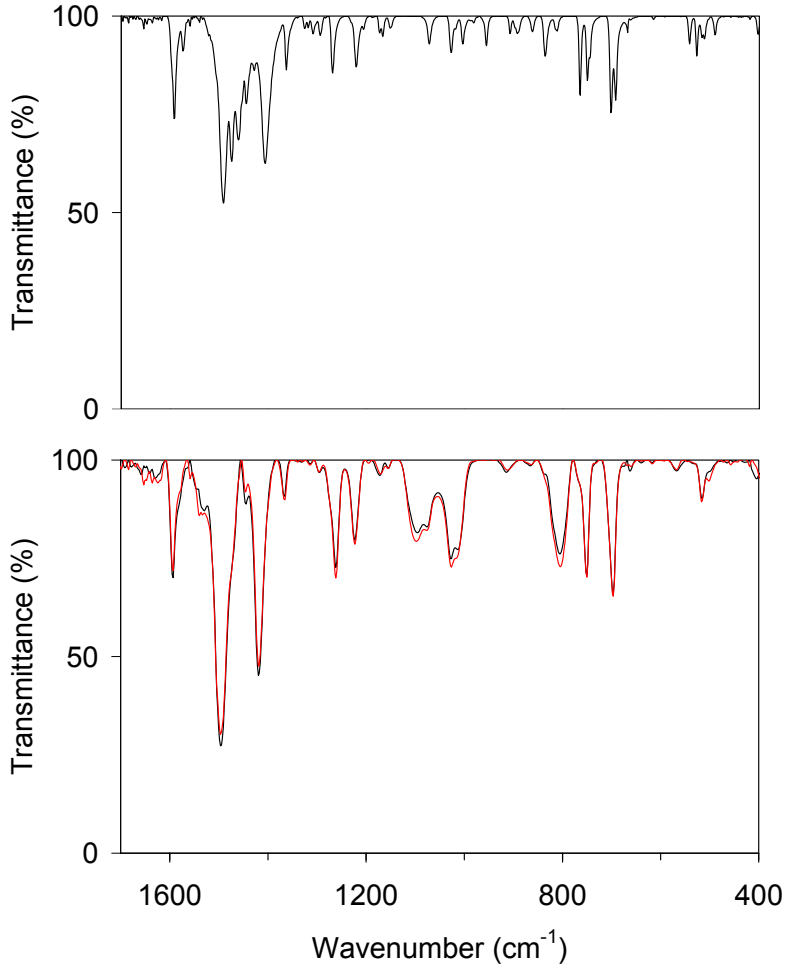

Figure 38. Top: IR spectrum of **7** (—, black). Bottom: IR spectra of the decay products of **10** (—, black) and **10**-$^{18}O_2$ (—, red).

The bands at 860 and 843 cm^{-1} fall in the range expected for OO stretching vibrations (ν_{OO}) of (η^2-peroxo)iridium(III) complexes,[96-102] whereas the lower-energy bands (574 and 467 cm^{-1}) are consistent with IrO stretching modes (ν_{IrO}).[102] The isotope shifts of the bands at 807, 544 and 445 cm^{-1} agree well with calculated values using harmonic oscillator models (calcd for **10**-$^{18}O_2$, 811, 544 and 442 cm^{-1}). The origin of the second band in the OO stretching region (843 cm^{-1}) is not clear, but may be caused by formation of a second isomer in the solid state that is not present in solution. The bands are all absent from the IR spectra of **7** and the decay products of **10** and **10**-$^{18}O_2$ (Figure 38). With the spectroscopic analysis obtained and the similarities to the guanidinato peroxo intermediates (**5a**–**5f**), intermediate **10** can be formulated as [Ir{PhNC(Me)NPh}(η^4-cod)(η^2-O_2)], Scheme 24.

Further confirmation of this intermediate as a monomer and not a symmetric dinuclear structure comes from the determination of the diffusion coefficient (D) of **10** and comparison to the value of D for **7**. It was determined that compounds **7** and **10** have very similar diffusion coefficients (**7**, 8.9 (±0.1) · 10^{-10}; **10**, 8.3 (±0.1) · 10^{-10} $m^2 \cdot s^{-1}$) and also the value of D for **10** is nearly identical to that of the guanidinato peroxo complex, [Ir{PhNC(NMe_2)NPh}(η^4-cod)(η^2-O_2)] (**5a**, 8.2 (±0.3) · 10^{-10} $m^2 \cdot s^{-1}$).[57]

The plots in Figure 39 confirm the expected linear relationship between $\ln(I/I_0)$ and G^2. The calculated values of the hydrodynamic radii (r_H) for **5a**, **7** and **10** are approximately 4.2(2) Å, 3.8(1) Å and 4.1(1) Å, respectively (Section 4.3.2).[103,104] The values for r_H show that the hydrodynamic radii of the peroxo intermediates **5a** and **10** are nearly identical to each other and the amidinato peroxo intermediate is slightly larger than the starting material, **7**.

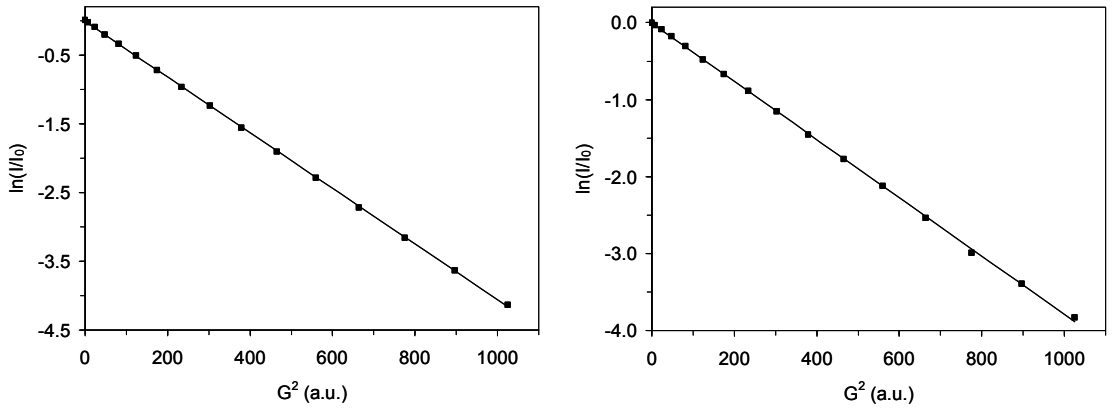

Figure 39. Plots of the natural logarithm of the intensity quotient, $\ln(I/I_0)$, *versus* the square of the gradient strength, G^2, for the CCH_3 resonance signal of **7** (left, $R^2 = 0.99991$) and **10** (right, $R^2 = 0.99970$).

6.3.4 Reactivity of the (Alkene)peroxoiridium(III) Intermediate and Its Decay Products

The peroxo intermediate **10** exibits the expected reactivity toward PPh_3. Reaction of a deoxygenated solution of **10** with 10 equiv of PPh_3 yielded ca. 1.2 equiv of $OPPh_3$, as determined by ^{31}P NMR spectroscopy. Taking into account the yield of 75% for **10**, the amount of $OPPh_3$ being produced corresponds to the transfer of more than one oxygen atom from the peroxo ligand of **10** to PPh_3.

We have also investigated the self-decay of **10** in order to determine whether oxidation of the coordinated alkene occurs. It was observed for the guanidinato peroxo intermediates that C–O bond formation and alkene oxidation occurs upon self-decay. With addition of cod or coe, release of 4-cycloocten-1-one was observed.[57] The electronic absorption spectra of **7**, **10** and the dark green decay products of **10** are shown in Figure 40. Also shown is the spectrum of an unknown intermediate (λ_{max} = 415 nm, blue line and square) that forms between intermediate **10** and the final decay products.

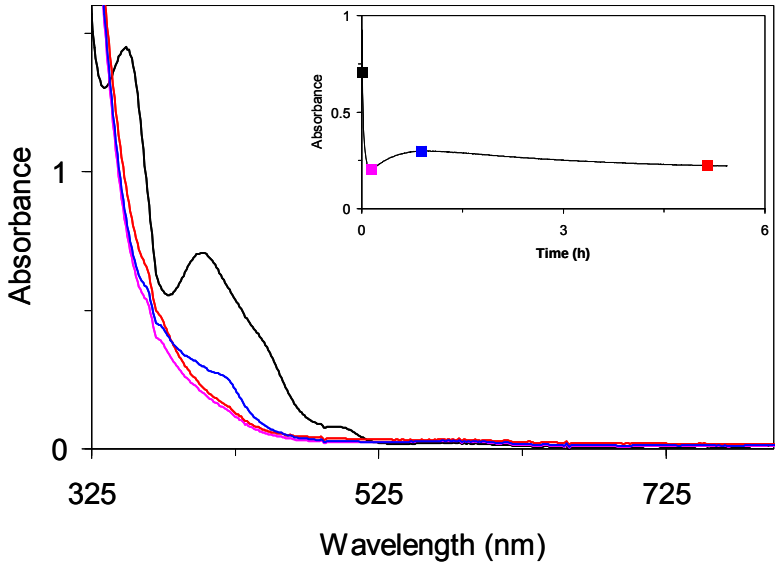

Figure 40. Electronic absorption spectra of 1 mM **7** (—, black), **10** (—, pink), unknown intermediate species (—, blue) and the decay products of **10** (—, red) in toluene at 20 °C (path length, 0.5 cm). Inset: Time course of the reaction of **7** in toluene with O_2 at 20 °C [λ = 402 nm (—, black)]. The squares indicate the reaction times associated with the spectra shown (black, **7**; pink, **10**; blue, unknown intermediate and red, decay products of **10**).

Analysis of the product solution by mass spectrometry reveals formation of several products, including mono- and dioxygenated complexes (Table 15). Based on their masses and isotope distribution patterns, the peaks at *m*/*z* = 524 (EI), 525 and 541 (ESI) can be assigned to $\{\mathbf{10} - H_2O\}^{+\bullet}$, $\{\mathbf{10} - OH\}^{+}$ and $\{\mathbf{10} - H\}^{+}$, respectively. Incorporation of oxygen from O_2 was confirmed by reactions with isotope-enriched **10**-$^{18}O_2$ with the expected shifts being observed [*m*/*z* = 526 (EI), 527 and 545 (ESI)]. Because of the peaks observed in the mass-spectrometric analysis, the amidinato peroxo intermediate is believed to decay by the same mechanism as the guanidinato peroxo intermediates.

Table 15. Mass-to-charge ratios (*m*/*z*) Obtained from the Electrospray Ionization (ESI) and Electron Impact (EI) Mass Spectra of the Decay Products of **10**.[a-c]

	ESI(+)MS				EIMS	
Complex	$\{LH + H\}^+$	$\{\mathbf{10} - O_2H\}^+$	$\{\mathbf{10} - OH\}^+$	$\{\mathbf{10} - H\}^+$	$\{\mathbf{10} - H_2O\}^{+\bullet}$	$\{IrL_3\}^{+\bullet}$
10	211.2	509.4	525.2	541.2	524.1397	820.2827
Calcd	211.1	509.2	525.2	541.2	524.1440	820.2866
10 ($^{18}O_2$)	211.3	509.5	527.4	545.4	526.3	820.4

[a] The reactions of **7** with O_2 were carried out as described above (1 mM in toluene at 0 °C or 15–20 mM in benzene-d_6 at 20 °C), and the resulting solutions were allowed to stand for at least 16 h at 20 °C. [b] LH = PhN=C(Me)NHPh. M refers to the [Ir(PhNC(Me)NHPh)(cod)] starting material, **7**. [c] High-resolution mass spectral data are reported with four decimal places.

To explore the possibility of alkene oxygenation, the decay products of **10** were treated with excess cod. After 1 d at 70 °C, the reaction mixture turned orange and 4-cycloocten-1-one was identified by ^{1}H NMR spectroscopy and EI MS (*m*/*z* = 124) along with formation of some **7**. The formation of 4-cycloocten-1-one was confirmed by a reaction using **10**-$^{18}O_2$, showing the expected shift in the EI MS to *m*/*z* = 126. This reaction also confirms that 4-cycloocten-1-one was formed from the oxygen atom of the peroxo ligand. When 2 equiv of cod was used (with respect to Ir), the reaction yielded 0.7 equiv of 4-cycloocten-1-one and 0.2 equiv of **7**. An analogous reaction with 10 equiv of *cis*-cyclooctene was performed with the formation of 0.2 equiv of 4-cycloocten-1-one and 0.1 equiv of **7**. The formation of the same products, albeit at lower yields, confirms the 4-cycloocten-1-one produced comes from the original cod in **7**.

6.4 Conclusion

The synthesis and characterization of alkene and carbonyl complexes supported by an amidinato ligand have been described. It was shown that the amidinato ligand functions as a weaker donor ligand than the structurally similar guanidinato ligands. An

(alkene)peroxoiridium(III) intermediate was observed to accumulate in a high yield in the reaction of the amidinato Ir^{I}(cod) complex with O_2. This intermediate is analogous to the guanidinato intermediates discussed in Chapter 4. Similar to the guanidinato intermediates, this peroxo intermediate was able to transfer oxygen to PPh_3 to form $OPPh_3$. Upon decay of this intermediate, C–O bond formation and alkene oxidation occurs and addition of cod causes release of 4-cycloocten-1-one and reformation of some of the iridium(I) starting material.

CHAPTER 7
SYNTHESIS, CHARACTERIZATION AND O_2 REACTIVITY Of RHODIUM(I) COMPLEXES SUPPORTED BY GUANIDINATO(1–) AND AMIDINATO(1–) LIGANDS

7.1 Introduction

The synthesis, characterization and O_2 reactivity of three rhodium alkene complexes will be discussed in this chapter. Two of the rhodium complexes, [Rh{PhNC(NMe$_2$)NPh}(cod)] (**11a**) and [Rh{PhNC(Me)NPh}(cod)] (**12**), were synthesized by reaction of the lithium guanidinato (Li{PhNC(NMe$_2$)NPh}·Et$_2$O) or amidinato (Li{PhNC(Me)NPh}·Et$_2$O) precursor and [{Rh(cod)}$_2$(μ-Cl)$_2$] (cod = 1,5-cyclooctadiene). The third rhodium complex, [{Rh(nbd)}$_2${μ-PhNC(NMe$_2$)NPh-κN:$\kappa N'$}$_2$] (**13a**), was synthesized from the reaction of the lithium guanidinato precursor (Li{PhNC(NMe$_2$)NPh}·Et$_2$O) and [{Rh(nbd)$_2$}$_2$(μ-Cl)$_2$] (nbd = norbornadiene or bicyclo[2.2.1]hepta-2,5-diene). These complexes have been characterized by a variety of spectroscopic techniques and single-crystal X-ray crystallography. The comparison of the nuclearity of complexes with different supporting and alkene ligands will be discussed along with the reactivity of these complexes toward O_2. A major difference in the reactivity of these complexes toward O_2 has been observed in comparison to the iridium(I) complexes (**1a** and **7**).

7.2 Experimental Section

Materials. All reagents and solvents were purchased from commercial sources and were used as received, unless noted otherwise. Diethyl ether and toluene were deoxygenated by sparging with N_2 and purified by passage through two packed columns

of molecular sieves under an N_2 pressure (MBraun solvent purification system). *n*-Pentane was dried over Na and distilled under N_2 prior to use.[59] Preparation and handling of air- and moisture-sensitive materials were carried out under an inert gas atmosphere by using either standard Schlenk and vacuum line techniques or a glovebox. Dioxygen was dried by passage through a short column of Drierite. [{Rh(cod)}$_2$(μ-Cl)$_2$] and [{Rh(nbd)}$_2$(μ-Cl)$_2$] were synthesized according to published procedures (cod = 1,5-cyclooctadiene, nbd = norbornadiene or bicyclo[2.2.1]hepta-2,5-diene).[116,117] The guanidine PhN=C(NMe$_2$)NHPh was synthesized as described previously in Chapter 3.[58] The amidine PhN=C(Me)NHPh was synthesized from ethyl orthoacetate and aniline as described,[117] and the characterization matched data published elsewhere.[118] Elemental analyses were performed by Atlantic Microlab, Inc., Norcross, GA, USA.

Physical Methods. NMR spectra were recorded on a Bruker Avance MicroBay 300 spectrometer at ambient temperature. ^{1}H and ^{13}C chemical shifts are reported in parts per million (ppm) and were referenced to residual solvent peaks. Mass spectral data were acquired on a quadrupole ion trap ThermoFinnigan LCQ Deca mass spectrometer using an electrospray ionization source or on a single quadrupole ThermoFinnigan Voyager mass spectrometer using an electron impact ionization source (equipped with a solids probe). UV–Visible spectra were recorded on an HP 8453A diode array spectrophotometer (Agilent Technologies).

General Procedure for the Synthesis of [Rh{PhNC(NMe$_2$)NPh}(cod)] (11a), [Rh{PhNC(Me)NPh}(cod)] (12) and [{Rh(nbd)}$_2${μ-PhNC(NMe$_2$)NPh-κN:$\kappa N'$}$_2$] (13a). The Li^+ salts of the guanidinate and amidinate anions were prepared as described in the section on Ir^I(cod) complexes in Chapter 3 and 6 (*vide supra*). In an N_2 atmosphere, a solution of 0.30 mmol of lithium guanidinate or lithium amidinate in 10 mL of diethyl ether was then added to a suspension of 74 mg (0.15 mmol) of [{Rh(cod)}$_2$(μ-Cl)$_2$] or 69 mg (0.15 mmol) of [{Rh(nbd)}$_2$(μ-Cl)$_2$] in 5 mL of diethyl ether under stirring at 20 °C. The color of the reaction mixture changed from orange to

yellow–orange or red, accompanied by precipitation of a colorless solid. After 3 h, the solution was filtered and the solvent was removed under reduced pressure. The residue was recrystallized from *n*-pentane by preparing a concentrated solution at 20 °C and storing it at –30 °C. Yellow (**11a**), yellow–orange (**12**) or red single (**13a**) crystals of X-ray diffraction quality were typically obtained within two days.

[Rh{PhNC(NMe$_2$)NPh}(cod)] (11a). Yield: 96 mg (71%). Anal. Calcd for $C_{23}H_{28}N_3Rh$: C, 61.47; H, 6.28; N, 9.35. Found: C, 61.66; H, 6.24; N, 9.31. ^{1}H NMR (300 MHz, $CDCl_3$, δ): 7.18 (t, J = 7.3 Hz, 4H, Ar H), 6.86 (t, J = 7.3 Hz, 2H, Ar H), 6.71 (d, J = 7.3 Hz, 4H, Ar H), 3.84 (br m, 4H, =C*H*CH$_2$–), 2.46 (s, 6H, NCH$_3$), 2.35 (br m, 4H, =CHC*H*$_2$–), 1.68 (m, 4H, =CHC*H*$_2$–). ^{13}C{^{1}H} NMR (75.5 MHz, $CDCl_3$, δ): 148.8, 128.7, 121.7, and 120.8 (Ar), 77.6 (d, J_{RhC} = 13.2 Hz, =*C*HCH$_2$–), 38.8 (NCH$_3$), 30.7 (=CH*C*H$_2$–). EIMS (70 eV) *m/z*: M$^{+\bullet}$ calcd for $C_{23}H_{28}N_3Rh$, 449.1; found, 449.1. UV-Vis (toluene) λ_{max}, nm (ε): 353 (4000), 390 (2400).

[Rh{PhNC(Me)NPh}(cod)] (12). Yield: 90 mg (71%). Anal. Calcd for $C_{22}H_{25}N_2Rh$: C, 62.86; H, 5.99; N, 6.66. Found: C, 63.04; H, 6.08; N, 6.75. ^{1}H NMR (300 MHz, $CDCl_3$, δ): 7.22 (t, J = 7.8 Hz, 4H, Ar H), 6.98 (t, J = 7.4 Hz, 2H, Ar H), 6.85 (d, 7.4 Hz, 4H, Ar H), 4.01 (br m, 4H, =C*H*CH$_2$–), 2.45 (br m, 4H, =CHC*H*$_2$–), 1.86 (s, 3H, CCH$_3$) 1.73 (m, 4H, =CHC*H*$_2$–). ^{13}C{^{1}H} NMR (75.5 MHz, $CDCl_3$, δ): 146.5, 128.6, 123.9, and 122.7 (Ar), 78.8 (d, J_{RhC} = 12.8 Hz, =*C*HCH$_2$–), 30.7 (=CH*C*H$_2$–), 15.7 (C*C*H$_3$). EIMS (70 eV) *m/z*: M$^{+\bullet}$ calcd for $C_{22}H_{25}N_2Rh$, 420.1; found, 419.5. UV-Vis (toluene) λ_{max}, nm (ε): 370 (3000).

[{Rh(nbd)}$_2${μ-PhNC(NMe$_2$)NPh-κ*N*:κ*N*′}$_2$] (13a). Yield: 84 mg (64%). Anal. Calcd for $C_{46.5}H_{54}N_6Rh_2$ (**11** + 0.50 C_5H_{12}): C, 61.86; H, 6.03; N, 9.31. Found: C, 62.25; H, 6.09; N, 9.19. ^{1}H NMR (300 MHz, C_6D_6, δ): 8.30 (br, 4H, Ar H), 7.57 (d, J = 7.2 Hz, 2H, Ar H), 7.39 (t, J = 7.8 Hz, 4H, Ar H), 7.30 (t, J = 7.5 Hz, 2H, Ar H), 6.97–6.90 (m, 4H, Ar H), 6.82 (t, J = 7.3 Hz, 2H, Ar H), 6.14 (d, J = 7.4 Hz, 2H, Ar H), 4.18–4.13 (m, 4H, =C*H*CH–), 3.97 (br, 2H, =C*H*CH–), 3.85 (br, 2H, =C*H*CH–), 3.71 (br, 2H,

=CHC*H*–), 3.44 (br, 2H, =CHC*H*–), 1.83 (br, 6H, NCH_3), 1.32–1.24 (m, 10H, guanidinato NCH_3 and nbd $CHCH_2CH$). $^{13}C\{^1H\}$ NMR (75.5 MHz, $CDCl_3$, δ): 164.9 (CN_3), 152.2, 152.0, 128.6, 128.4, 127.3, 127.0, 125.9, 124.7, 121.2, 120.9, and 119.5, 61.1, 61.0, 60.8, 60.7, 54.3 (d, J_{RhC} = 10.5 Hz, =*C*$CHCH_2$–), 53.7 (d, J_{RhC} = 10.5 Hz, =*C*$CHCH_2$–), 51.4, 51.4, 50.7, 50.7 49.4, 49.4, 49.3, 49.2, 49.2, 49.1. EIMS (70 eV) *m/z*: $M^{+\bullet}$ calcd for $C_{22}H_{24}N_3Rh$, 433.1; found, 433.2. UV-Vis (toluene) λ_{max}, nm (ε): 456 (1200), 524 (2150).

Reactions of 11a, 12 and 13a with O_2. A 1 mL solution of [Rh{PhNC(NMe_2)NPh}(cod)] (**11a**), [Rh{PhNC(Me)NPh}(cod)] (**12**) or [{Rh(nbd)}$_2${μ-PhNC(NMe_2)NPh-κN:$\kappa N'$}$_2$] (**13a**) in toluene was placed in a 0.5-cm UV–Vis cuvette and the solution was purged with O_2 (40 s) at 20 °C.

X-ray Crystallographic Analyses. A single crystal of each compound was coated with Paratone N oil and mounted on a glass capillary for data collection at 200(2) or 150(2) K on a Nonius KappaCCD diffractometer using Mo *K*α radiation (graphite monochromator). The temperature was controlled by an Oxford Cryostream Cooler (700 series, N_2 gas). Data collection, data reduction, and absorption correction were carried out following standard CCD techniques using the software packages Collect and HKL-2000.[73,74] Final cell constants were calculated from 4564 (**11a**) or 8194 (1**2**) reflections from the complete data set. The space groups *P*1 (**11a**) and *P*-1 (**12**) were determined based on systematic absences and intensity statistics. The structures were solved by direct methods and refined by full-matrix least-squares minimization and difference Fourier methods (SHELXTL v.6.12).[75,76] All non-hydrogen atoms were refined with anisotropic displacement parameters. All hydrogen atoms were placed in ideal positions and refined as riding atoms with relative isotropic displacement parameters, with the exception of the alkene hydrogen atoms (=C*H*), which were located in the difference Fourier map and refined with a restrained C–H distance (1.00 Å) and relative isotropic displacement parameters (1.2 times the equivalent isotropic value of the bonded carbon atom). For **11a**,

the final full-matrix least-squares refinement converged to $R1$ = 0.0757 and $wR2$ = 0.1223 (F^2, all data). For **12**, the final full-matrix least-squares refinement converged to $R1$ = 0.0388 and $wR2$ = 0.0711 (F^2, all data). Table 16 contains additional crystal and refinement information. Selected distances and angles are summarized in Tables 17-22.

7.3 Results and Discussion

7.3.1 Synthesis and Characterization of Guanidinato and Amidinato Alkene Complexes

The rhodium(I) alkene complexes, [Rh{PhNC(NMe$_2$)NPh}(cod)] (**11a**), [Rh{PhNC(Me)NPh}(cod)] (**12**) and [{Rh(nbd)}$_2${μ-PhNC(NMe$_2$)NPh-κN:$\kappa N'$}$_2$] (**13a**) have been synthesized using the corresponding lithium guanidinato (Li{PhNC(NMe$_2$)NPh}·Et$_2$O) or amidinato (Li{PhNC(Me)NPh}·Et$_2$O) precursor which were described in Chapter 3 and 6.

Scheme 25. Synthesis of [Rh{PhNC(NMe$_2$)NPh}(cod)], **11a**, [Rh{PhNC(Me)NPh}(cod)], **12**, and [{Rh(nbd)}$_2${μ-PhNC(NMe$_2$)NPh-κN:$\kappa N'$}$_2$], **13a**

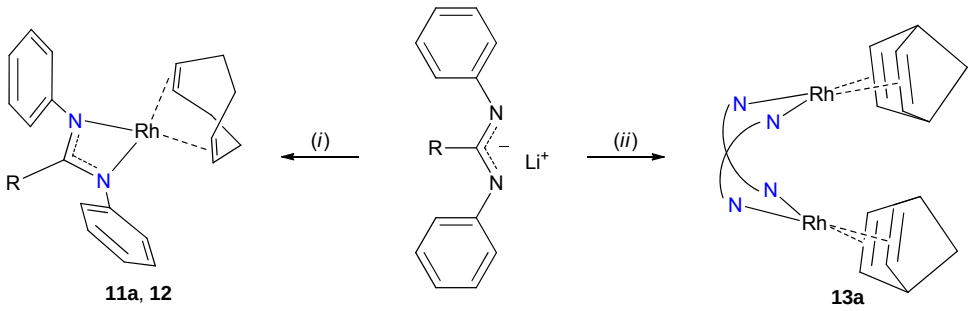

11a, **12** **13a**

11a, R = N(CH$_3$)$_2$; **12**, R = CH$_3$; **13a**, R = N(CH$_3$)$_2$; N–N = {PhNC(NMe$_2$)NPh}$^-$

(*i*) [{Rh(cod)}$_2$(μ-Cl)$_2$], 20 °C, diethyl ether; (*ii*) [{Rh(nbd)}$_2$(μ-Cl)$_2$], 20 °C, diethyl ether

As shown in Scheme 25, the complexes are synthesized in an analogous manner as the iridium(I) complexes with the neutral ligands being treated with MeLi at low temperature, followed by transmetalation with $[\{Rh(cod)_2\}_2(\mu\text{-}Cl)_2]$ (**11a** and **12**) or $[\{Rh(nbd)_2\}_2(\mu\text{-}Cl)_2]$ (**13a**).

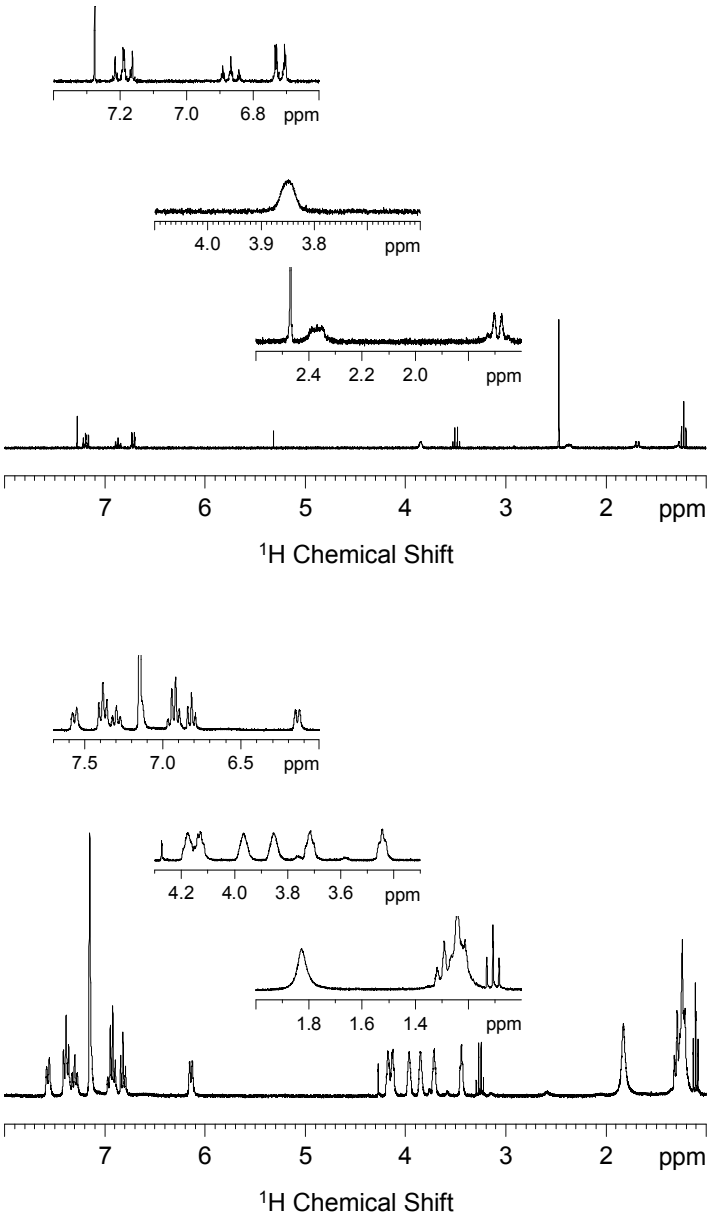

Figure 41. ^{1}H NMR spectra of the (alkene)rhodium(I) complexes **11a** (top) and **13a** (bottom) in $CDCl_3$.

Complexes **11a**, **12** and **13a** have been characterized by a variety of analytical techniques including ^{1}H and ^{13}C NMR spectroscopy, EI MS and elemental analysis. Also, X-ray quality single-crystals of **11a** (yellow) and **12** (yellow−orange) were obtained from crystallization of these complexes from concentrated *n*-pentane solutions stored at −30 °C (discussed in Section 7.3.2). These complexes are well soluble in low-polarity organic solvents such as toluene, diethyl ether, and *n*-pentane but only sparingly soluble in acetonitrile.

The ^{1}H NMR spectra of **11a** (Figure 41) and **12** (Figure 42) are analogous to those of the iridium(I) complexes (**1a** and **7**) with three signals (two triplets and one doublet) for the aromatic protons, one broad signal for the alkene protons, two broad multiplets for the CH_2 groups of the cod ligand and one intense singlet for the $N(CH_3)_2$ or CCH_3 protons. The ^{1}H NMR spectra of **11a** and **12** were investigated at a variety of concentrations (up to at least 75 mM), and no changes were observed in the spectra which indicates there is no monomer-dimer equilibrium occurring in solution for this concentration range.

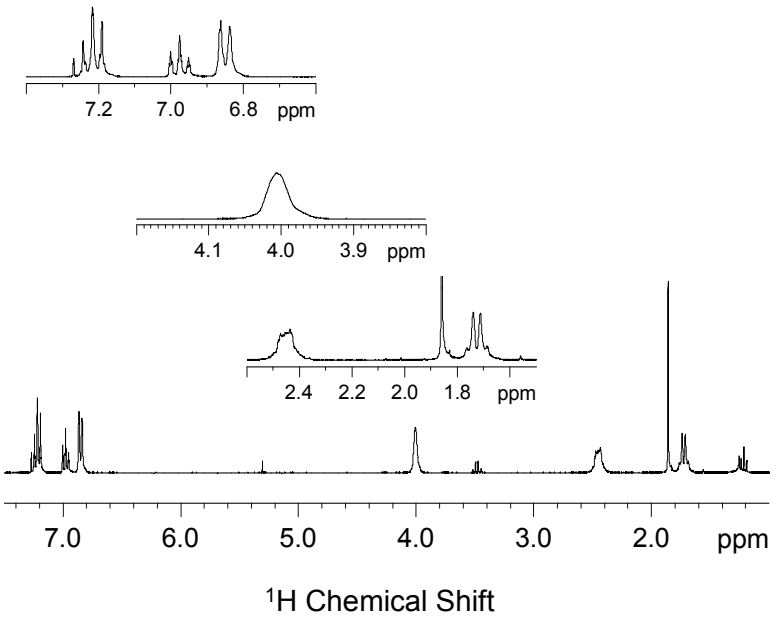

Figure 42. ^{1}H NMR spectrum (cyclooctadiene)rhodium(I) complex **12** in $CDCl_3$.

The EI MS of these complexes was obtained and the spectra show peaks at m/z = 449 and 420 for complexes **11a** and **12**, respectively. These peaks are assigned to the mononuclear complexes [Rh{PhNC(NMe_2)NPh}(cod)], **11a**, and [Rh{PhNC(Me)NPh}(cod)], **12**. No peaks were observed at higher m/z values that could be attributed to dinuclear species. Based on the ^{1}H NMR and EI MS analysis of **11a** and **12**, the complexes can be assigned as mononuclear d^8 rhodium(I) complexes with the nitrogen-donor ligand binding in an *N*,*N*'-chelating mode and an μ^4-cod ligand. There are examples in the literature of rhodium(I) complexes bearing structurally similar guanidinato and amidinato ligands that have been characterized with the nitrogen-donor ligands binding in an (η^5-cyclohexadienyl) fashion to the Rh^I(cod) fragment.[120] These complexes have been synthesized under similar reaction conditions as **11a** and **12** but have been obtained in relatively low yields. They were thermally isomerized to complexes having the more common *N*,*N*′-chelating mode by heating them at 80 °C for 5 h. Our complexes have been synthesized in high yield and no intermediate species have been observed.

The ^{13}C NMR spectra of **11a** and **12** were obtained with observation of doublets for the peaks assigned to the alkene carbons on the cod ligands (Figure 43). These doublets were observed at 77.6 and 78.9 ppm for **11a** and **12**, respectively. The multiplicity arises from ^2J coupling to the NMR-active rhodium nucleus. Comparison in ligand donor strength of **11a** and **12** to other Rh^I(cod) complexes in the literature shows that the trend observed in the Ir^I(cod) and $Ir^I(CO)_2$ complexes holds for other metal centers. As observed for the iridium(I) complexes (Chapters 3 and 6), the complex of the weaker amidinato ligand has a $\delta(^{13}C_{C=C})$ peak shifted downfield from the peak in the complex of the more strongly donating guanidinato ligand. Also, the rhodium(I) complexes bearing κ^2-Tp (79.1 and 81.1 ppm)[122] or β-diiminate ligands (78.8 and 79.8 ppm)[121] have downfield shifted peaks and are thus weaker donating ligands than the guanidinato and amidinato ligands. Upfield shifted peaks are observed for Rh^I(cod)

complexes with κ^3-Tp (73.3 ppm)[122] and Cp ligands (62.1 ppm), indicating that the ligands on these complexes are more strongly donating.[123] The ^{13}C NMR data for the Rh^{I}(cod) complexes help support the idea of the guanidinato ligands being more strongly donating than other common bidentate nitrogen-donor ligands in the literature.

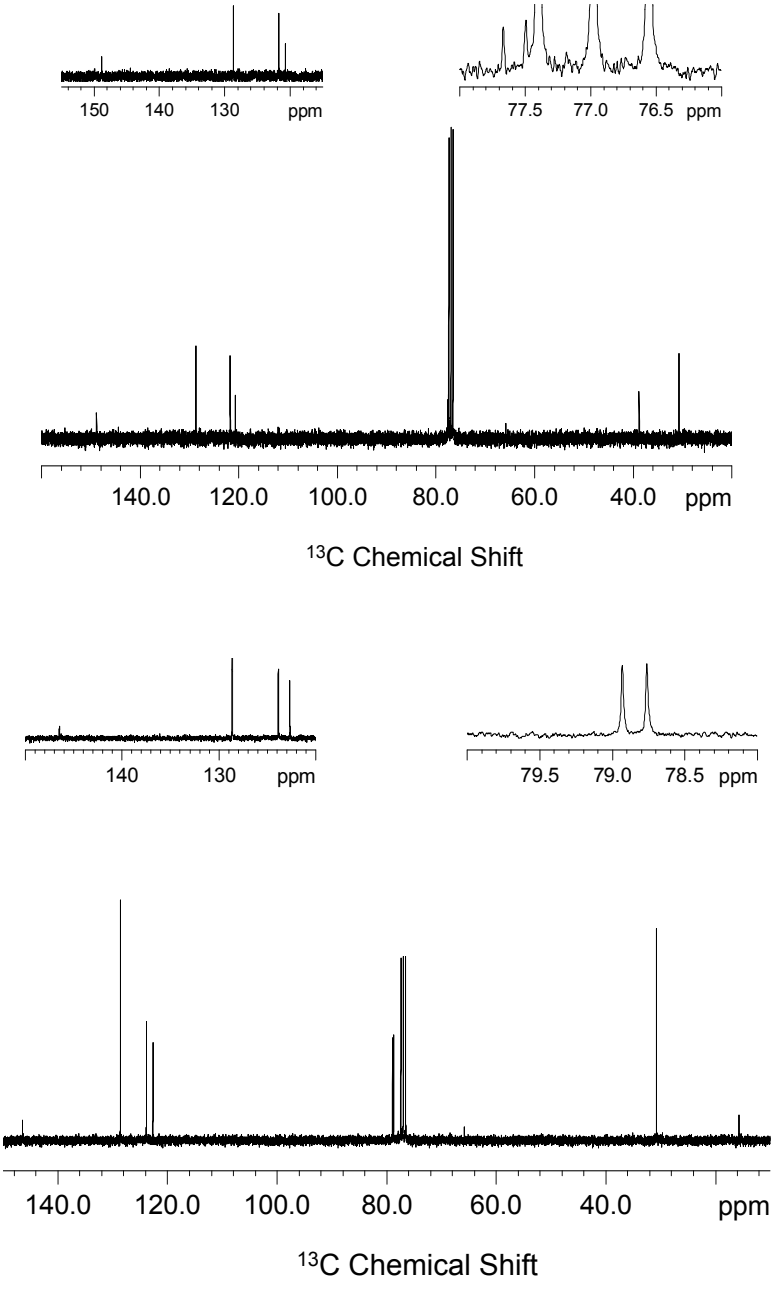

Figure 43. ^{13}C NMR spectra of (alkene)rhodium(I) complexes **11a** (top) and **12** (bottom) in $CDCl_3$.

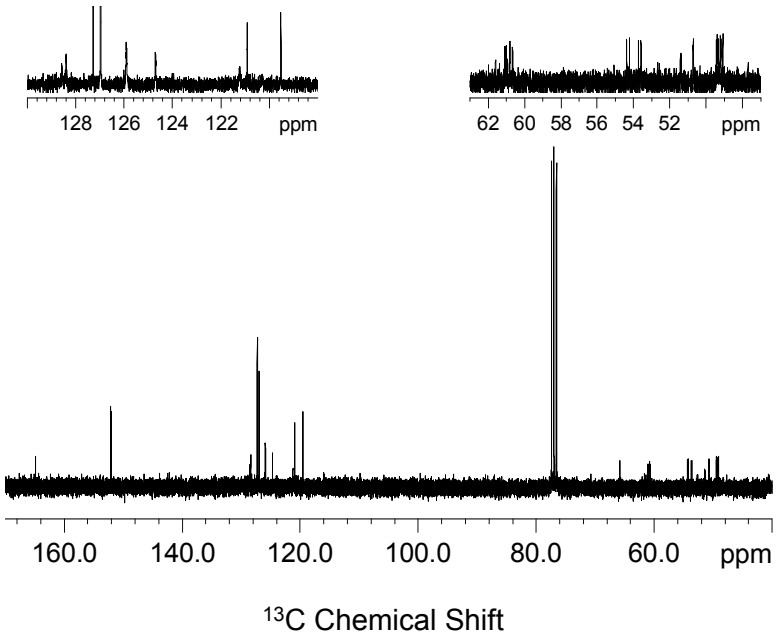

Figure 44. ^{13}C NMR spectrum of (alkene)rhodium(I) complex **13a** in $CDCl_3$.

The analysis of the nbd complex **13a** is very different from that of the cod complexes and indicates a different nuclearity based on the analytical techniques used. The ^{1}H NMR spectrum of **13a** is much more complex than that of the guanidinato cod complex with more than twice as many signals observed, shown in Figure 41. The ^{1}H NMR spectrum of **13a** has six signals which are assigned to the alkene protons, thus indicating a dinuclear species is formed. The ^{13}C NMR spectrum also has more than twice as many peaks than the mononuclear complexes **11a** and **12** (Figure 44). Interestingly, the EI MS of this complex shows a peak at m/z = 433 which corresponds to a mononuclear nbd complex, [Rh{PhNC(NMe$_2$)NPh}(nbd)], and no peak at the expected value (m/z = 866) for the dinuclear complex was observed. Presumably the dinuclear complex breaks up under the conditions of the EI MS experiment.

As observed here, both mono- and dinuclear rhodium(I) complexes bearing structurally similar guanidinato and amidinato ligands have been reported. Literature

examples of both mononuclear and dinuclear rhodium(I) complexes with structurally similar nitrogen-donor ligands exist. The Rh^{I}(cod) complex bearing a less sterically bulky triazenide ligand, [{Rh(cod)}$_2$(μ-1,3-PhN$_3$Ph)$_2$],[124,125] was characterized as a dinuclear species, whereas complexes with bulkier ligands such as [Rh{(2,6-^{i}PrC$_6$H$_3$)NC(R)N(2,6-^{i}PrC$_6$H$_3$)}(cod)] (where R = ^{t}Bu, N^{i}Pr$_2$, NCy$_2$)[120] are mononuclear. Also, a few mononuclear Rh^{I}(nbd) complexes with bulky tris(1-pyrazolyl)borate ligands [Rh(Tp$^{R,R'}$)(nbd)] (where R, R' = H, Me; Me, Me; or ^{i}Pr, Br),[122] are known. Based on the examples in the literature and here, the formation of mononuclear and dinuclear rhodium(I) complexes is influenced by both the nitrogen-donor ligand and also by the coordinated alkene ligand.

7.3.2 Crystal Structures

Yellow (**11a**) and yellow−orange (**12**) crystals were grown from concentrated *n*-pentane solutions upon standing at –30 °C. The solid-state molecular structures of both compounds were determined from crystallographic analyses and confirm the mononuclear nature of **11a** and **12** (Figure 45 and Tables 17-22). For **12**, two crystallographically independent molecules were found in the asymmetric unit. The Rh–N and Rh–C distances are in the ranges of 2.084(2)–2.113(2) Å and 2.104(2)–2.126(2) Å, respectively, which agree well with values of related complexes.[77,120,121] Due to the acute bite angles of the chelating guanidinato and amidinato ligands (N1–Rh–N2, 63.8(2)° for **11a**; 62.89(7)° and 62.65(7)° for **12**), the metal centers adopt a distorted square-planar coordination geometry.

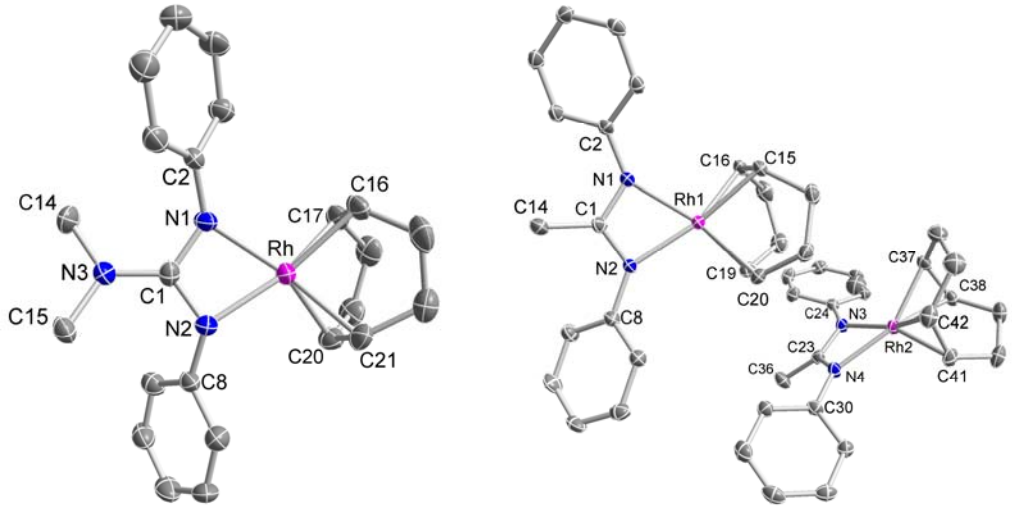

Figure 45. Molecular structures of [Rh{PhNC(NMe$_2$)NPh}(cod)], **11a**, and [Rh{PhNC(Me)NPh}(cod)], **12**; displacement ellipsoids are drawn at 50% probability level; hydrogen atoms have been omitted for clarity.

Other structural features for complex **11a** compare well with the crystallographicaly characterized guanidinato iridium(I) complexes with the C–N distances in the planar CN_3 core of the guanidinato complex being nearly identical, 1.343(6)–1.355(6) Å. The N3 atoms adopt a trigonal-planar geometry with bond angle sum of 359.9(4)° while the N2 atom is more pyramidalized with bond angle sums of 347.1(4) and 352.6(4)°. The C–N2–C and N–C1–N planes are still slightly twisted with respect to each other 17.1(6)°. The parameters obtained for the (alkene)rhodium(I) complexes are very similar to what was observed for the (cyclooctadiene)iridium(I) complexes (**1b**, **1d**, **1f**; Section 3.3.4).

Table 16. Crystallographic data and structure refinement for [Rh{PhNC(NMe$_2$)NPh}(cod)], **11a**, and [Rh{PhNC(Me)NPh}(cod)], **12**.

	11a	**12**
Empirical formula	$C_{23}H_{28}N_3Rh$	$C_{22}H_{25}N_2Rh$
Formula weight	449.40	420.35
Crystal habit, color	blade, colorless	prism, yellow
Crystal size	0.20 x 0.06 x 0.015 mm^3	0.25 x 0.22 x 0.11 mm^3
Temperature, T	200(2) K	150(2) K
Wavelength, λ	0.71073 Å	0.71073 Å
Crystal system	triclinic	triclinic
Space group	$P1$	$P\bar{1}$
Unit cell dimensions	a = 7.7164(15) Å	a = 10.0477(11)
	b = 11.535(2) Å	b = 13.2777(14)
	c = 12.052(2) Å	c = 14.2606(15)
	α = 79.03(3)°	α = 103.910(5)
	β = 83.94(3)°	β = 100.863(5)
	γ = 72.33(3)°	γ = 90.363(5)
Volume, V	1002.1(1) Å^3	1811.0(3) Å^3
Z	1	4
Calculated density	1.489 Mg·m^{-3}	1.542 Mg·m^{-3}
Absorption coefficient, μ	0.864 mm^{-1}	0.949 mm^{-1}
F(000)	464	864
θ range for data collection	3.10 to 27.93°	2.94 to 27.85°
Limiting indices	$-10\leq h\leq 10$, $-15\leq k\leq 15$, $-15\leq l\leq 15$	$-13\leq h\leq 13$, $-17\leq k\leq 17$, $-18\leq l\leq 18$
Reflections collected / unique	9114 / 4777 [R(int) = 0.0438]	16148 / 8558 [R(int) = 0.0189]
Completeness to θ	99.4 % (θ = 27.93°)	99.2 % (θ = 27.85°)
Max. and min. transmission		0.9028 and 0.7973
Refinement method	Full-matrix least-squares on F^2	Full-matrix least-squares on F^2
Data / restraints / parameters	4777 / 4 / 258	8558 / 8 / 477
Goodness-of-fit on F^2	1.144	1.076
Final R indices [I>2sigma(I)]	$R1$ = 0.0523, $wR2$ = 0.1223	$R1$ = 0.0291, $wR2$ = 0.0660
R indices (all data)	$R1$ = 0.0757, $wR2$ = 0.1303	$R1$ = 0.0388, $wR2$ = 0.0711
Largest diff. peak and hole	1.348 and –0.585 e.A^{-3}	1.164 and –0.812 e.A^{-3}

Table 17. Selected interatomic distances (Å) for [Rh{PhNC(NMe$_2$)NPh}(cod)], **11a**.[a]

Distances (Å)		Distances (Å)	
Rh–N1	2.093(4)	N1–C1	1.354(6)
Rh–N2	2.084(4)	N1–C2	1.403(6)
Rh–C16	2.111(5)	N2–C1	1.343(6)
Rh–C17	2.121(5)	N2–C8	1.407(6)
Rh–C20	2.109(5)	N3–C1	1.355(6)
Rh–C21	2.109(6)	N3–C14	1.458(6)
C20–C21	1.400(9)	N3–C15	1.457(6)
C24–C25	1.406(9)		

[a] Numbers in parentheses are standard uncertainties in the last significant figures. Atoms are labeled as indicated in Figure 45.

Table 18. Selected angles (°) for [Rh{PhNC(NMe$_2$)NPh}(cod)], **11a**.[a]

Angles (°)		Angles (°)	
N1–Rh–N2	63.8(2)	C1–N1–C2	127.3(4)
N1–Rh–C16	103.0(2)	C1–N1–Rh	92.6(3)
N1–Rh–C17	105.0(2)	C2–N1–Rh	132.7(3)
N1–Rh–C20	153.3(2)	C1–N2–C8	125.9(4)
N1–Rh–C21	159.9(2)	C1–N2–Rh	93.3(3)
N2–Rh–C20	99.9(2)	C8–N2–Rh	127.9(3)
N2–Rh–C21	104.3(2)	C1–N3–C14	122.5(4)
N2–Rh–C16	157.4(2)	C1–N3–C15	123.0(4)
N2–Rh–C17	158.0(2)	C15–N3–C14	114.4(4)
C16–Rh–C17	38.6(2)	N1–C1–N2	109.9(4)
C21–Rh–C20	38.9(2)	N1–C1–N3	124.5(4)
C20–Rh–C16	98.5(2)	N2–C1–N3	125.6(4)
C21–Rh–C17	91.2(2)		
C20–Rh–C17	82.4(2)		
C21–Rh–C16	82.3(2)		

[a] Numbers in parentheses are standard uncertainties in the last significant figures. Atoms are labeled as indicated in Figure 45.

Table 19. Selected dihedral angles (°) for [Rh{PhNC(NMe_2)NPh}(cod)], **11a**.[a,b]

Dihedral Angles (°)			
N1–C1–N2 / N1–Rh–N2	7.3(5)	C14–N3–C15 / N1–C1–N2	17.1(6)
N1–Rh–N2 / C16–Rh–C17	86.9(3)	(N1,C1,N2,N3) / (C2→C7)[b]	52.4(2)
N1–Rh–N2 / C20–Rh–C21	83.9(3)	(N1,C1,N2,N3) / (C8→C13)[b]	56.1(2)
C16–Rh–C17 / C20–Rh–C21	87.9(3)		

[a] Numbers in parentheses are standard uncertainties in the last significant figures. Atoms are labeled as indicated in Figure 45. [b] Angle between the least-squares planes of the guanidinate atoms (N1, C1, N2, and N3) and the aryl ring atoms (*e.g.*, C2, C3, C4, C5, C6, and C7).

Table 20. Selected interatomic distances (Å) for [Rh{PhNC(Me)NPh}(cod)], **12**.[a]

Distances (Å)			
Rh1–N1	2.110(2)	Rh2–N3	2.102(2)
Rh1–N2	2.102(2)	Rh2–N4	2.113(2)
Rh1–C15	2.126(2)	Rh2–C37	2.107(2)
Rh1–C16	2.104(2)	Rh2–C38	2.127(2)
Rh1–C19	2.126(2)	Rh2–C41	2.123(2)
Rh1–C20	2.118(2)	Rh2–C42	2.126(2)
N1–C1	1.342(3)	N3–C23	1.334(3)
N1–C2	1.398(3)	N3–C24	1.398(3)
N2–C1	1.326(3)	N4–C23	1.327(3)
N2–C8	1.410(3)	N4–C30	1.409(3)
C15–C16	1.402(3)	C37–C38	1.402(3)
C19–C20	1.402(3)	C41–C42	1.397(4)

[a] Numbers in parentheses are standard uncertainties in the last significant figures. Atoms are labeled as indicated in Figure 45.

Table 21. Selected angles (°) for [Rh{PhNC(Me)NPh}(cod)], **12**.[a]

Angles (°)			
N1–Rh1–N2	62.89(7)	N3–Rh2–N4	62.65(7)
N1–Rh1–C15	106.17(8)	N3–Rh2–C37	99.76(8)
N1–Rh1–C16	100.94(8)	N3–Rh2–C38	106.40(8)
N1–Rh1–C19	157.88(8)	N3–Rh2–C41	158.71(9)
N1–Rh1–C20	156.73(9)	N3–Rh2–C42	156.41(9)
N2–Rh1–C19	105.16(8)	N4–Rh2–C41	103.80(9)
N2–Rh1–C20	102.94(8)	N4–Rh2–C42	105.62(9)
N2–Rh1–C15	160.95(9)	N4–Rh2–C37	152.71(9)
N2–Rh1–C16	153.23(8)	N4–Rh2–C38	160.79(9)
C15–Rh1–C16	38.69(9)	C37–Rh2–C38	38.68(9)
C20–Rh1–C19	38.57(9)	C41–Rh2–C42	38.37(10)
C19–Rh1–C15	89.99(9)	C41–Rh2–C37	98.39(10)
C20–Rh1–C16	98.54(10)	C42–Rh2–C38	89.99(9)
C19–Rh1–C16	82.11(10)	C41–Rh2–C38	81.38(9)
C20–Rh1–C15	81.60(9)	C42–Rh2–C37	82.31(10)
C1–N1–C2	124.76(19)	C23–N3–C24	126.17(19)
C1–N1–Rh1	92.39(14)	C23–N3–Rh2	93.13(14)
C2–N1–Rh1	142.38(14)	C24–N3–Rh2	140.68(15)
C1–N2–C8	123.72(19)	C23–N4–C30	123.70(19)
C1–N2–Rh1	93.18(13)	C23–N4–Rh2	92.85(13)
C8–N2–Rh1	142.26(15)	C30–N4–Rh2	142.59(15)
N1–C1–N2	110.85(19)	N3–C23–N4	110.85(19)
N1–C1–C14	124.3(2)	N3–C23–C36	124.5(2)
N2–C1–C14	124.5(2)	N4–C23–C36	124.3(2)

[a] Numbers in parentheses are standard uncertainties in the last significant figures. Atoms are labeled as indicated in Figure 45.

Table 22. Selected dihedral angles (°) for [Rh{PhNC(Me)NPh}(cod)], **12**.[a,b]

Dihedral Angles (°)			
N1–C1–N2 / N1–Rh1–N2	9.1(3)	N3–C23–N4 / N3–Rh2–N4	7.9(3)
N1–Rh1–N2 / C15–Rh1–C16	82.8(1)	N3–Rh2–N4 / C37–Rh2–C38	80.6(1)
N1–Rh1–N2 / C19–Rh1–C20	86.6(1)	N3–Rh2–N4 / C41–Rh2–C42	86.6(1)
C15–Rh1–C16 / C19–Rh1–C20	87.0(1)	C37–Rh2–C38 / C41–Rh1–C42	87.0(1)
(N1,C1,N2,C14) / (C2→C7)[b]	47.1(1)	(N3,C23,N4,C36) / (C24→C29)[b]	44.6(1)
(N1,C1,N2,C14) / (C8→C13)[b]	59.4(1)	(N3,C23,N4,C36) / (C30→C35)[b]	56.7(1)

[a] Numbers in parentheses are standard uncertainties in the last significant figures. Atoms are labeled as indicated in Figure 45. [b] Angle between the least-squares planes of the amidinate atoms (N1, C1, N2, and C14) and the aryl ring atoms (*e.g.*, C2, C3, C4, C5, C6, and C7).

7.3.3 Reactivity of (Alkene)rhodium(I) Complexes toward O_2

The reactivity of these rhodium(I) complexes toward O_2 was investigated in a similar manner as for the iridium(I) complexes discussed in Chapters 4 and 6. A 2 mM solution of **11a** in toluene was treated with excess O_2 at 20 °C in a UV-Vis experiment, but no changes were observed in the spectrum. The complex was also treated with O_2 at a variety of other reaction conditions (high and low temperature; varying concentrations) with no changes being observed. In contrast, **12** was found to react with O_2. A 2 mM solution of this complex in toluene reacts with O_2 at 20 °C with a $t_{1/2}$ of ca. 2 d. The final reaction products were characterized by ESI MS with the observation of peaks at m/z = 437 and 453. These peaks are assigned to the mono- and dioxygenated species $\{M + O + H\}^+$ and $\{M + 2O + H\}^+$. Complex **13a** also reacted with O_2 very slowly under the same reaction conditions with a $t_{1/2}$ of ca. 1 d. The final products of this reaction were also analyzed by ESI MS and similar mono- and dioxygenated species were observed at m/z =

450 and 466 and assigned as $\{0.5\ M + O + H\}^+$ and $\{0.5\ M + 2O + H\}^+$. The rhodium(I) complex **12** reacts much more slowly than the analogous iridium(I) complex **7**, and the different peaks observed in the ESI MS of the final reaction mixtures indicate that different mechanisms are at work for these complexes. As mentioned in Section 4.2.2, the iridium(I) complex **1a** reacts with O_2 to form an interesting (alkene)peroxoiridium(III) complex, while the analogous rhodium(I) complex **11a** does not react with O_2 at all. These differences in reactivity shows that the rhodium(I) complexes are less reactive than the analgous iridium(I) complexes.

There is a literature example of a rhodium(I) complex, $[\{Rh(cod)\}_2(\mu\text{-}1,3\text{-}PhN_3Ph)\}_2]$ that reacts with O_2 to form a dinuclear bis(metallaoxetane) species, $[\{Rh(\mu\text{-}1,3\text{-}PhN_3Ph)(C_8H_{12}O)\}_2]$.[108] Analysis of the reaction products by MS shows peaks for the dinuclear complex and also a peak assigned to half of the dinuclear complex. The monooxygenated species observed in the ESI MS from the reaction of **12** and **13a** with O_2 could be assigned to a protonated metallaoxetane species. Keeping this in mind and also the observation of the (alkene)peroxo intermediates in the reaction of the Ir^I(cod) complexes with O_2, further investigation of the reactions of **12** and **13a** with O_2 was performed by NMR spectroscopy. Monitoring of the reaction of these complexes with O_2 at 20 °C in benzene-d_6 by NMR spectroscopy shows only decay of the starting material with no accumulation of any intermediates being observed. This indicates that neither a metallaoxetane nor an (alkene)peroxo complex accumulate in observable yields under these reaction conditions. In general, the reactivity of these complexes toward O_2 is much lower than that of the iridium(I) complexes and indicates that the rhodium(I) complexes are much more stable than the corresponding iridium(I) complexes.

7.4 Conclusions

In this chapter, the synthesis, characterization and O_2 reactivity of some (alkene)rhodium(I) complexes has been discussed. These complexes have been characterized by a variety of analytical techniques including single-crystal X-ray crystallography. It was shown that formation of both mono- and dinuclear complexes may occur with these ligands. The trends in ligand donor strength was observed to be analogous to the iridium(I) complexes and supports the idea of the guanidinato ligands being more strongly donating than similar nitrogen-donor ligands in the literature. Also, the reactivity of these complexes toward O_2 is significantly different compared to the iridium(I) complexes and shows that the rhodium(I) complexes are much less reactive toward O_2. It was also shown that different peaks are observed by ESI MS analysis of the O_2 reaction mixtures which indicates that different mechanisms are at work for the rhodium(I) and iridium(I) complexes.

CHAPTER 8

SUMMARY AND CONCLUSION

Mononuclear iridium(I) complexes coordinated by bidentate guanidinato(1−) ligands were prepared and characterized. These complexes add to the limited number of low-valent metal complexes supported by guanidinato ligands. Spectroscopic analysis of these complexes indicates that the *N*,*N*-dialkyl-*N*′,*N*″-diarylguanidinates used here function as more strongly donating ligands than other monoanionic nitrogen-donor ligands such as κ^2-binding tris(1-pyrazolyl)borates, amidinates and β-diketiminates.

Identification and characterization of (alkene)peroxo- and (alkene)persulfidoiridium(III) intermediates has been achieved in the reactions of the Ir^{I}(cod) complexes with O_2 and S_8. The (alkene)peroxoiridium(III) intermediates add to a limited number of characterized (alkene)peroxo complexes known in the literature. The (alkene)persulfidoiridium(III) intermediate is the first characterized example known for these types of complex. It has been shown that these intermediates are reactive and transfer of oxygen or sulfur to simple organic molecules such as PPh_3 was observed. The metastable (alkene)peroxoiridium(III) intermediates undergo C–O bond formation and oxidation of the alkene ligand upon decay, and with addition of cod release of 4-cycloocten-1-one was observed along with reformation of some starting material.

Synthesis and characterization of alkene and carbonyl complexes supported by an amidinato ligand has been achieved. It was observed that changing to a less bulky supporting ligand causes formation of a dinuclear tetracarbonyl complex rather than the mononuclear dicarbonyl complexes observed for the guanidinato ligands. The alkene complex reacts with O_2 in a similar, but faster, manner than the guanidinato complexes and formation of an analogous (alkene)peroxoiridium(III) intermediate was observed. This intermediate and its decay products also react in an analogous manner as the guanidinato complexes.

Synthesis and characterization of rhodium(I) guanidinato and amidinato complexes has been done. It was observed that substitution of a smaller alkene ligand has a major affect on the nuclearity of the metal complex. The ligand donor strength of the guanidinato and amidinato rhodium(I) cod complexes was investigated and confirms that the guanidinato ligands function as stronger donors than other bidentate monoanionic nitrogen-donor ligands in the literature. The reaction of these complexes with O_2 was determined to be much slower than for the iridium(I) complexes, and spectroscopic evidence shows that different products are formed.

There are a number of different aspects of this project that deserve further investigation. One part where further investigation is needed is developing a stoichiometric cycle for the reaction of the iridium(I) cod complexes with O_2. This may provide more information about the mechanism of this reaction and give improved understanding of what is necessary to achieve the goal of catalytic alkene oxidation with O_2. Once a stoichiometric cycle is achieved, investigation of catalytic reactions with these complexes could be done. This may lead to a very interesting set of catalysts that can achieve alkene oxidation with O_2.

Another part of this project that may be further investigated is the reactions of the rhodium(I) alkene complexes with O_2. We observed very sluggish reactivity with these complexes thus far, but further investigation into different reaction conditions may be helpful. The use of light to activate these complexes may help in the reaction with O_2 and would be something that could be investigated. Also, the use of more electron donating guanidinato ligands may increase the reactivity of these complexes with O_2 by further destabilizing the rhodium(I) center.

Further investigation of the reaction of these guanidinato and amidinato complexes with S_8 should be done. We have already obtained a reactive (alkene)persulfidoiridium(III) intermediate which is the first of its kind. Investigating

more of the Ir^{I}(cod) complexes and also the rhodium(I) alkene complexes could provide a more reactive complex that may be able to perform C–S bond formation.

Further modification of the guanidinato supporting ligand is something to further investigate. The guanidinato ligands provide the ability to make changes to the steric and electronic properties of the complex and these differences may provide for the synthesis of optimized complexes that can perform interesting reactions with O_2 and S_8 and possibly other small inert molecules. Tetraalkyl guanidinato ligands may provide these differences in steric and electronic properties that are needed to optimize these reactions. We know that tetraalkyl guanidinato ligands have the potential to be more electron donating than the dialkyldiaryl guanidinato ligands that have been used in this work and this may help with optimization of the metal complex being used for these reactions.

REFERENCES

1. Bailey, P. J.; Pace, S. *Coord. Chem. Rev.* **2001**, *214*, 91.
2. Duncan, A. P.; Mullins, S. M.; Arnold, J.; Bergman, R. G. *Organometallics* **2001**, *20*, 1808.
3. Mullins, S. M.; Duncan, A. P.; Bergman, R. G.; Arnold, J. *Inorg. Chem*. **2001**, *40*, 6952.
4. Bazinet, P.; Wood, D.; Yap, G. P. A.; Richeson, D. S. *Inorg. Chem*. **2003**, *42*, 6225.
5. Soria, D. B.; Grundy, J.; Coles, M. P.; Hitchcock, P. B. J. *Organomet. Chem*. **2005**, *690*, 2278.
6. Wilder, C. B.; Reitfort, L. L.; Abboud, K. A.; McElwee-White, L. *Inorg. Ch*em. **2006**, *45*, 263.
7. Rische, D.; Baunemann, A.; Winter, M.; Fischer, R. A. *Inorg. Chem*. **2006**, *45*, 269.
8. Hill, C. L.; Weinstock, I. A. *Nature* **1997**, *388*, 332.
9. de Bruin, B.; Budzelaar, P. H. M.; Gal, A. W. *Angew. Chem., Int. Ed*. **2004**, *43*, 4142.
10. Punniyamurthy, T.; Velusamy, S.; Iqbal, J. *Chem. Rev*. **2005** *105*, 2329.
11. Tejel, C.; Ciriano, M. A. *Top. Organomet. Chem.*, **2007**, *22*, 97.
12. Stahl, S. S. Angew. *Chem., Int. Ed*. **2004**, *43*, 3400.
13. Cornell, C. N.; Sigman, M. S. *Inorg. Chem*. **2007**, *46*, 1903.
14. Muzart, J. *Tetrahedron* **2007**, *63*, 7505;
15. Keith, J. A.; Henry, P. M. *Angew. Chem., Int. Ed*. **2009**, *48*, 9038.
16. van Santen, R. A.; Kuipers, H. P. C. E. *Adv. Catal*. **1987**, *35*, 265.
17. Serafin, J. G.; Liu, A. C.; Seyedmonir, S. R. *J. Mol. Catal. A: Chem*. **1998**, *131*, 157.
18. Monnier, J. R. *Appl. Catal*., *A* **2001**, *221*, 73.
19. Barteau, M. A. *Top. Catal*. **2003**, *22*, 3.
20. James, B. R. *Adv. Chem. Ser*. **1980**, *191*, 253.
21. Mimoun, H. *Pure Appl. Chem*. **1981**, *53*, 2389.
22. Drago, R. S.; Zuzich, A.; Nyberg, E. D. *J. Am. Chem. Soc*. **1985**, *107*, 2898.
23. Faraj, M.; Martin, J.; C. Martin, C.; Bregeault, J.-M.; Mercier, J. *J. Mol. Catal*. **1985**, *31*, 57.

24. Read, G. *J. Mol. Catal*. **1988**, *44*, 15.

25. de Bruin, B.; Peters, T. P. J.; Wilting, J. B. M.; Thewissen, S.; Smits, J. M. M.; Gal, A. W. *Eur. J. Inorg. Chem*. **2002**, 2671.

26. Day, V. W.; Klemperer, W. G.; Lockledge, S. P.; Main, D. J. *J. Am. Chem. Soc*. **1990**, *112*, 2031.

27. Tejel, C.; Ciriano, M. A.; Sola, E.; del Rio, M. P.; Rios-Moreno, G.; Lahoz, F. L.; Oro, L.A. Angew. *Chem. Int., Ed*. **2008**, *47*, 2502.

28. Tejel, C.; del Rio, M. P.; Lopez, J. A.; Ciriano, M. A. *Chem. Eur. J*. **2010**, *16*, 11261.

29. Day, V. W.; Eberspacher, T. A.; Klemperer, W. G.; Zhong, B. *J. Am. Chem. Soc*. **1994**, *116*, 3119.

30. Krom, M.; Coumans, R. G. E.; Smits, J. M. M.; Gal, A. W. *Angew. Chem., Int Ed*. **2001**, *40*, 2106.

31. Krom, M.; Peters, T. P. J.; Coumans, R. G. E.; Sciarone, T. J. J.; Hoogboom, J.; ter Beek, S. I.; Schelbos, P. P. J.; Smits, J. M. M.; de Gelder, R.; Gal, A. W. *Eur. J. Inorg. Chem*. **2003**, 1072.

32. Dauth, A.; Love, J. *A. Chem. Rev*. **2011**, *111*, 2010.

33. van Gaal, H.; Cuppers, H. G. A. M.; van der Ent, A. *J. Chem. Soc. D: Chem. Commun*., **1970**, 1694.

34. van der Ent, A.; Onderdelinden, A. L. *Inorg. Chim. Acta* **1973**, *7*, 203.

35. Louw, W.; Gerber, J. T. I. A.; de Waal, D. J. A. *J. Chem. Soc., Chem. Commun*. **1980**, 760.

36. de Waal, D. J. A.; Gerber, T. I. A.; Louw, W. J.; van Eldik, R. *Inorg. Chem*. **1982**, *21*, 2002.

37. Vigalok, A.; Shimon, L. J. W.; Milstein, D. *Chem. Commun*. **1996**, 1673.

38. Brown, J. M.; John, R. A.; Lucy, A. R. *J. Organomet. Chem*. **1985**, *279*, 245.

39. Trofimenko, S. *Chem. Rev*. **1993**, *93*, 943.

40. Trofimenko, S. *Polyhedron* **2004**, *23*, 197.

41. Bourget-Merle, L.; Lappert, M. F.; Severn, J. R. *Chem. Rev*. **2002**, *102*, 3031.

42. Roesky, P. W. *Chem. Soc. Rev*. **2000**, *29*, 335.

43. Barker, J.; Kilner, M. *Coord. Chem. Rev*. **1994**, *133*, 219.

44. Edelmann, F. T. *Coord. Chem. Rev*. **1994**, *137*, 403.

45. Gantzel, P.; Walsh, P. J. *Inorg. Chem*. **1998**, *37*, 3450.

46. Hauber, S.-O.; Niemeyer, M. *Inorg. Chem*. **2005**, *44*, 8644.

47. Bailey, P. J.; Bone, S. F.; Mitchell, L. A.; Parsons, S.; Taylor, K. J.; Yellowlees, L. J. *Inorg. Chem*. **1997**, *36*, 867.

48. Bailey, P. J.; Bone, S. F.; Mitchell, L. A.; Parsons, S.; Taylor, K. J.; Yellowlees, L. J. *Inorg. Chem*. **1997**, *36*, 5420.

49. Cotton, F. A.; Murillo, C. A.; Wang, X.; Wilkinson, C. C. *Inorg. Chem*. **2006**, *45*, 5493.

50. Irwin, M. D.; Abdou, H. E.; Mohamed, A. A.; Fackler, J. P., Jr. *Chem. Commun*. **2003**, 2882.

51. Mohamed, A. A.; Mayer, A. P.; Abdou, H. E.; Irwin, M. D.; Perez, L. M.; Fackler, J. P., Jr. *Inorg. Chem*. **2007**, *46*, 11165.

52. Coyle, J. P.; Monillas, W. H.; Yap, G. P. A.; Barry, S. T. *Inorg. Chem*. **2008**, *47*, 683.

53. Fandos, R.; Otero, A.; Rodriguez, A.; Terreros, P. *Collect. Czech. Chem. Commun*. **2007**, *72*, 579.

54. Ogata, K.; Oka, O.; Toyota, A.; Suzuki, N.; Fukuzawa, S.-I. *Synlett* **2008**, 2663.

55. Jones, C.; Mills, D. P.; Rose, R. P.; Stasch, A. *Dalton Trans*. **2008**, 4799.

56. Rohde, J.-U.; Lee, W.-T. *J. Am. Chem. Soc*., **2009**, *131*, 9162.

57. Kelley, M. R.; Rohde, J-U. *Chem Commun*, **2012**, *48*, 2876.

58. Rohde, J.-U.; Kelley, M. R.; Lee, W-T. *Inorg. Chem*. **2008**, *47*, 11461.

59. Armarego, W. L. F.; Chai, C. *Purification of Laboratory Chemicals*, 5th ed.; Butterworth Heinemann: Oxford, U.K., 2003.

60. Kresze, G.; Hatjiissaak, A. *Phosphorus Sulfur Relat. Elem.* **1986**, *29*, 41.

61. Ramadas, K.; Srinivasan, N. *Tetrahedron Lett.* **1995**, *36*, 2841.

62. Srinivasan, N.; Ramadas, K. *Tetrahedron Lett.* **2001**, *42*, 343.

63. Ramadas, K.; Janarthanan, N.; Pritha, R. *Synlett* **1997**, 1053.

64. Herde, J. L.; Lambert, J. C.; Senoff, C. V. *Inorg. Synth*. **1974**, *15*, 18.

65. Uson, R.; Oro, L. A.; Cabeza, J. A. *Inorg. Synth*. **1985**, *23*, 126.

66. Wanninger Weib, C.; Wagenknecht, H.-A. *Eur. J. Org. Chem*. **2008**, *1*, 64.

67. Schmidt, H.-J.; Schäfer, H. J. *Angew. Chem., Int. Ed.* **1979**, *18*, 68.

68. Zepik, H. H.; Benner, S. A. *J. Org. Chem.* **1999**, *64*, 8080.

69. Natarajan, A.; Guo, Y.; Arthanari, H.; Wagner, G.; Halperin, J. A.; Chorev, M. *J. Org. Chem*. **2005**, *70*, 6362.

70. Yang, D.; Chen, Y.-C.; Zhu, N.-Y. *Org. Lett.* **2004**, *6*, 1577.

71. Noor, A.; Glatz, G.; Muller, R.; Kaupp, M.; Demeshko, S.; Kempe, R. *Z. Anorg. Allg. Chem*. **2009**, *635*, 1149.

72. Ge, S.; Meetsma, A.; Hessen, B. *Organometallics*, **2008**, *27*, 3131.

73. Hooft, R. W. W. *Collect*; Nonius BV: Delft, The Netherlands, 1998.

74. Otwinowski, Z.; Minor, W. *Methods Enzymol.* **1997**, *276*, 307.

75. *SHELXTL: Program Library for Structure Solution and Molecular Graphics*, version 6.12; Bruker Analytical X-Ray Systems, Inc.: Madison, WI, 2001.

76. Sheldrick, G. M. *Acta Crystallogr., Sect. A: Found. Crystallogr.* **2008**, *A64*, 112.

77. Lahoz, F. J.; Tiripicchio, A.; Tiripicchio Camellini, M.; Oro, L. A.; Pinillos, M. T., *J. Chem. Soc., Dalton Trans.* **1985**, 1487.

78. Cotton, F. A.; Poli, R., *Inorg. Chim. Acta* **1986,** *122*, 243.

79. Kanematsu, N.; Ebihara, M.; Kawamura, T., *Inorg. Chim. Acta* **1999,** *292*, 244.

80. Albinati, A.; Bovens, M.; Rüegger, H.; Venanzi, L. M. *Inorg. Chem.* **1997**, *36*, 5991.

81. Bernskoetter, W. H.; Lobkovsky, E.; Chirik, P. J. *Organometallics* **2005**, *24*, 6250.

82. Dzik, W. I.; Smits, J. M. M.; Reek, J. N. H.; de Bruin, B. *Organometallics* **2009**, *28*, 1631.

83. Gussenhoven, E. M.; Olmstead, M. M.; Fettinger, J. C.; Balch, A. L. *Inorg. Chem.*, **2007**, *47*, 4570.

84. Green, S. P.; Jones, C.; Stasch, A. *Science* **2007**, *318*, 1754.

85. Robinson, S. D.; Sahajpal, A.; Steed, J. *Inorg. Chim. Acta* **2000**, *303*, 265.

86. Bailey, P. J.; Grant, K. J.; Mitchell, L. A.; Pace, S.; Parkin, A.; Parsons, S. *J. Chem. Soc., Dalton Trans.* **2000**, 1887.

87. Coles, M.P.; Hitchcock, P. B. *Organometallics* **2003**, 22, 5201.

88. Sowa, J. R.; Angelici, R. J. *J. Am. Chem. Soc.* **1991**, *113*, 2537.

89. Elliott, P. I. P.; Haslam, C. E.; Spey, S. E.; Haynes, A. *Inorg. Chem.*, **2006**, *45*, 6269.

90. Blais, M. S.; Rausch, M. D. *J. Organomet. Chem.*, **1995**, *502*, 1.

91. Theron, M.; Grobbelaar, E.; Purcell, W.; Basson, S. S. *Inorg. Chim. Acta* **2005**, *358*, 2457.

92. Janka, M.; Atesin, A.; Fox, D. J.; Flaschenriem, C.; Brennessel, W. W.; Eisenberg, R. *Inor. Chem.* **2006**, *45*,6559.

93. Calimano, E.; Tilley, T. D. *Dalton Trans*. **2010**, *39*, 9250.

94. del Rio, M. P.; Ciriano, M. A.; Tejel. C. *Angew. Chem. Int. Ed.* 2008, *47*, 2502.

95. NIST/EPA/NIH Mass Spectral Library, data version NIST 98 [CD-ROM]; National Institute of Standards and Technology, U.S. Department of Commerce: Washington, DC, 1998.

96. Choy, V. J.; O'Connor, C. J. *Coord. Chem. Rev.* **1972**, *9*, 145.

97. Valentine, J. S.*Chem. Rev.* **1973**, *73*, 235.

98. Vaska, L. *Acc. Chem. Res.* **1976**, *9*, 175.

99. Williams, D. B.; Kaminsky, W.; Mayer, J. M.; Goldberg, K. I. *Chem. Commun.* **2008**, 4195.

100. Lebel, H.; Ladjel, C.; Belanger-Gariepy, F.; Schaper, F. *J. Organomet. Chem.* **2008**, *693*, 2645.

101. Dutta, D. K.; Deb, B.; Sarmah, B. J.; Woollins, J. D.; Slawin, A. M. Z.; Fuller, A. L.; Randall, R. A. M. *Eur. J. Inorg. Chem.* **2011**, 835.

102. Penner, A.; Braun, T. *Eur. J. Inorg. Chem.* **2011**, 2579.

103. Pregosin, P. S.; Kumar, P. G. A.; Fernandez, I. *Chem. Rev.* **2005**, *105*, 2977.

104. Macchioni, A.; Ciancaleoni, G.; Zuccaccia. C.; Zuccaccia, D. *Chem. Soc. Rev.* **2008**, *37*, 479.

105. Matsuo, S; Makita, T. *Int. J. Thermophysics*, **1993**, *14*, 67.

106. Tejel, C.; Ciriano, M. A. *Top. Organomet. Chem.* **2007**, *22*, 97.

107. Woerpel, K. A.; Bergman, R. G. *J. Am. Chem. Soc.* **1993**, *115*, 7888.

108. Ritter, J. C. M.; Bergman, R. G. *J. Am. Chem. Soc.*, **1997**, *119*, 2580.

109. del Rio, M. P.; Ciriano, M. A.; Tejel, C. *Angew. Chem., Int. Ed.* **2008**, *47*, 2502.

110. Ginsberg, A. P.; Lindsell, W. E. *J. Chem. Soc. D: Chem Commun*, **1971**, 232.

111. Mague, J. T.; Davis, E. J. *Inorg. Chem.* **1977**, *16*, 131.

112. Ginsberg, A. P.; Batlogg, H. B.; Osborne, J. H.; Sprinkle, C.R. *Inorg. Chem*. **1985**, *24*, 4192.

113. Taylor, E. C.; Ehrhart, W. A. *J. Org. Chem*. **1963**, *28*, 1108.

114. Forsberg, J. H. *et al*. *J. Org. Chem*. **1987**, *52*, 1017.

115. Kelley, M. R.; Rohde, J.-U. Manuscript in Perparation.

116. Giordano, G.; Crabtree, R. H. *Inorg*. *Synth*. **1990**, *28*, 88.

117. Abel, E. W.; Bennett, M. A.; Wilkinson, G. *J. Chem*. *Soc*. **1959**, 3178.

118. Taylor, E. C.; Ehrhart, W. A. *J. Org*. *Chem*. **1963**, *28*, 1108.

119. Forsberg, J. H. *et al*. *J. Org*. *Chem*. **1987**, *52*, 1017.

120. Jones, C.; Mills, D. P.; Stasch, A. *Dalton Trans*. **2008**, 4799.

121. Budzelaar, P. H. M.; Moonen, N. N. P.; de Gelder, R.; Smits, J. M. M.; Gal, A. W. *Eur. J. Inorg. Chem.* **2000**, 753.

122. Bucher, U. E.; Currao, A.; Hesper, R.; Ruegger, H.; Venanzi, L. M.; Younger, E. *Inorg. Chem.*, **1995**, *34*, 66.

123. Axelson, D. E.; Holloway, C.E.; Oliver, A. J. *Inorg. Nucl. Chem. Letters* **1973**, *9*, 885.

124. Knoth W. H. *Inorg. Chem.* **1973**, *12*, 38.

125. Tejel, C.; Ciriano, M. A.; Sola, E.; del Rio, M. P.; Rios-Moreno, G.; Lahoz, R. J.; Oro, L. A. *Angew. Chem. Int. Ed.* **2005**, *44*, 3267.